# Total body photon irradiation with a modified cobalt-60 unit

Renée-Xavière Larouche
Medical Physics Unit
McGill University, Montréal
December 2002

A Thesis submitted to the
Faculty of Graduate Studies and Research
in partial fulfilment of the
requirements for the degree of
Masters of Science
in
Medical Physics

*Your file Votre référence*
*ISBN: 0-612-88241-1*
*Our file Notre référence*
*ISBN: 0-612-88241-1*

# Abstract

Following a departmental expansion, an isocentric cobalt-60 external beam teletheraphy unit was modified to produce a large fixed field for total body irradiation. The sourcehead was separated from the gantry and installed at a distance of 251.2 cm from the floor. The collimator was removed and replaced with a custom built secondary collimator projecting a 277×132.6 $cm^2$ radiation field at floor level. The work presented in this thesis describes the measurements performed to bring the unit into clinical use for total body irradiation. A custom flattening filter was placed below the secondary collimator to flatten the beam to within ±3% of the central axis dose as measured at 10 cm in water. Percent depth dose, tissue-phantom-ratios, surface dose and absolute output were measured in the radiation field. The effects of inhomogeneities were studied and the thickness of lead used for lung attenuators was determined. Verification of treatment planning and delivery was performed with an Alderson-Rando anthropomorphic phantom and showed dose uniformity within ±10% of the prescribed dose when a lead attenuator was used over the lung.

# Résumé

Suivant une expansion départementale, une unité d'irradiation externe isocentrique de cobalt-60 fut modifiée pour produire un large champ fixe pour l'irradiation pan-corporelle. La tête-de-source fut séparée du bras support et installée à 251.2 cm du plancher. Le collimateur fut retiré et remplacé par un collimateur secondaire projetant au sol un champ d'irradiation de 277×132.6 $cm^2$. Le travail présenté dans cette thèse décrit les mesures prises afin de préparer l'appareil pour son utilisation en clinique pour les traitements d'irradiation pan-corporelle. Un filtre compensateur installé sous le collimateur secondaire assurait un champ d'irradiation plat, mesuré à une profondeur de 10 cm dans l'eau à une variation de moins de ±3%. Le rendement en profondeur, le ratio-tissue-fantôme, la dose en surface et la dose absolue furent mesurés. Les effets d'inhomogénéités furent étudiés et l'épaisseur d'un atténuateur en plomb pour les poumons fut déterminée. Vérification de la planification et de la livraison du traitement se réalisa avec un fantôme anthropomorphique Alderson-Rando. Cela démontra une uniformité à l'intérieur de ±10% de la dose prescrite lorsqu'un atténuateur de plomb était utilisé au-dessus du poumon.

# Acknowledgements

I would like to first extend my appreciation and endless gratitude to my supervisor, Michael Evans, for his support, guidance and advice given throughout the course of this work.

I would also like to extend my appreciation and gratitude to my co-supervisor, Dr. Ervin B. Podgorsak, for the support and the educational opportunity he has provided.

I would like to thank Pierre Léger, Joe Larkin and Vlad Bobes for the modifications brought to the cobalt-60 unit and for the many explanations provided of the different mechanisms present in the unit. Also, I would like to thank Shoukry Aboulehaf and Robin Van Gils for machining the various parts which were added to the modified cobalt-60 unit.

I would especially like to thank Marina Olivares for the work done with the TLD measurements and for showing me how to perform TLD measurements myself.

I would also like to thank Frank Paolino for his help in manufacturing the lead compensators used throughout this work.

I would also like to thank Yanic Bercier, Dr. Robert Corns, François Deblois, Caroline Gauvreau and Margery Knewstubb for their help in various aspects along the way.

Finally, I wish to thank my fellow students for their encouragement; Maurice Chacron for his love, and my mother, Paule Larouche, for always encouraging me to attain my goals.

# Table of Contents

# Chapter 1

# Development of methods for total body irradiation



## 1.1 INTRODUCTION

On any given week, an average of 2 579 Canadians [1] will be diagnosed with cancer. Cancer is not one disease, but the name given to a host of diseases which share the characteristic of an uncontrolled growth of abnormal cells. In general, total body photon irradiation (TBI) is not the first choice of treatment, since to avoid lethal complications, TBI must be followed by bone marrow transplantation and alternative treatments are preferred. Cancers that may benefit from TBI include acute lymphocytic leukaemia, acute non-lymphocytic leukaemia, chronic myeloid leukaemia, non-Hodgkin's lymphoma, Hodgkin's lymphoma, multiple myeloma and neuroblastoma. Other types of disease which are not malignant, i.e. not cancerous in nature, but where treatment with TBI may be successful, include aplastic

anaemia, thalassemia and some inborn errors of metabolism [2]. In these cases, TBI may be used as a precursor to bone marrow transplantation.

Total body photon irradiation aims to deliver a high dose of radiation (between 6 and 15 Gy) to the entire body. Doses in this range can cause serious damage to the hematopoietic system (blood forming organs). The hematopoietic prodromal syndrome, which arises following a total body dose of greater than 2 Gy is a syndrome characterised by a reduction in the levels of white blood cells, lymphocytes and platelets. Symptoms appear a few weeks after irradiation, when the white blood cells, lymphocytes and platelets die off and are not replaced. With the depression of blood elements, symptoms such as an onset of chills, fatigue, petechial haemorrhages in the skin (subcutaneous haemorrhage occurring in minute spots), ulceration of the mouth and epilation may occur. Following a depression of the blood platelets, common symptoms are infections and fever and a general impairment of the immune mechanisms, as well as bleeding and anaemia caused by haemorrhage [3]. The gravity of the symptoms increases with dose and may become deadly. The purpose of TBI is to condition the patient prior to receiving bone marrow transplantation by killing their affected bone marrow. The transplanted bone marrow then produces white blood cells, lymphocytes and platelets to avoid the severe symptoms of the prodromal syndrome. Other conditioning regimes exist (i.e. with chemotherapy), but the advantages of conditioning the patient with TBI are a suppression of the immune system, and in the case of malignant disease, the killing of so-called sanctuary or hidden malignant cells. Radiation therapy rests on the principle that some malignant tumours are more radiosensitive than healthy tissues and therefore have a higher probability of being lethally damaged by radiation than surrounding healthy tissue. The cancers mentioned above exhibit this radiosensitivity.

Delivery of a TBI treatment is not trivial. Generally, the International Commission of Radiation Units and measurements (ICRU) has recommended that the deposited dose be known with an accuracy of ± 5% [4]. However, non-uniformities in dose deposition of up to ± 10% are tolerated for TBI if the prescribed dose is below normal tissue toxicity [5, 6]. These non-uniformities are due to the patient contour and tissue inhomogeneities present in the body. Different methods are used to deliver dose in a uniform fashion throughout the body and the steps taken to achieve this are presented in this chapter.

## 1.2 SCIENTIFIC BREAKTHROUGHS

Radiation as applied to medicine dates back to the late 1890's and fundamental research was conducted in parallel with the development of clinical applications. The work led by such renowned physicists as Röentgen, Becquerel, Henri, and Marie Curie laid the foundation for the use of radiation in the treatment of disease. The first example of radiation therapy with x-ray photons occurred in January 1896 with Emil Herman Grubbé (1875-1960) treating a 55-year-old patient suffering from recurrent breast cancer with a fractionated irradiation schedule [7]. A primitive x-ray tube was initially used as a radiation generator, however, with the discovery of radium and then of artificial radioactivity, radioactive isotopes which produce higher photon energies replaced the use of x-ray tubes for radiation therapy.

## 1.3 BLOOD-RELATED COMPLICATIONS

The effects of radiation on the human body such as the hematopoietic prodromal syndrome previously discussed were not well known at first and hampered early attempts at TBI. In order to limit the immune suppression of the patient, the dose was limited to 3 Gy in one fraction. Beyond this dose, the effects of the radiation on the hematopoietic system were found to be lethal [8]. This limitation was overcome after safe bone marrow transplantation was available, and the first successful bone marrow transplantation was performed in 1959 between identical twins in Cooperstown, NY, USA [9]. After this milestone, rapid development of TBI techniques followed.

## 1.4 INITIAL DEVELOPMENT OF TOTAL BODY IRRADIATION

### *1.4.1 First total body irradiation*

Frederic Dessauer in 1905 is credited with the design of a system capable of delivering TBI with x-ray tubes. He designed a cascade transformer that permitted higher voltages to be applied to the x-ray tube. Two years later, Adalar Eifer in Hungary used this arrangement to treat patients with leukaemia [8]. X-ray production before the invention of the Coolidge x-ray tube in 1913 was difficult since the original x-ray tubes were very inefficient at producing x-rays and could not produce radiation reliably for long periods of time due to overheating. In

1923, the idea of using large fields reappeared in the literature. Chaoul and Lange published in Germany the results for a treatment of lymphogranulomatosis (Hodgkin's disease) using large fields of radiation. Their method consisted of four x-ray fields positioned around the patient. In 1927, Teschendorf reported in Germany that he had irradiated the entire body of patients diagnosed with various forms of leukaemia and malignant granuloma [10].

### 1.4.2 First total body irradiation in North America

The work of Chaoul, Lange and Teschendorf led to the study of TBI at the Memorial Hospital in New York (NY, USA) under the direction of Heublein [11]. A special "lead lined ward" was prepared in 1931 in which a Coolidge x-ray tube could work continuously. A "cut-out" switch was linked to the door and stopped the exposure of the patients when nurses came into the ward. Furthermore, to improve the dose uniformity received by the patients, their beds were located far from the x-ray tube. Depending on the bed a patient was lying in, the delivery of 25 per cent of a so-called erythema dose necessitated either 149 or 278 hours of irradiation. Erythema dose was known to be related to the reddening of the skin due to dose deposition and was equal to 750 R (where R was historically defined as a roentgen [12]). Heublein noted the toxic effects of dose beyond a certain limit due to the hematopoietic prodromal syndrome. Until this dose limit could be safely increased, no new advances in the delivery of TBI were noted.

## 1.5 DEDICATED TOTAL BODY IRRADIATION TECHNIQUES

### 1.5.1 Introduction

The original TBI techniques used low output, low energy x-ray beams. Consequently, the duration of the treatment was relatively long (on the order of several hundred hours) and dose uniformity was poor. Research on TBI in the United States led to the use of higher energy photon beams using cesium-137 (0.662 MeV) and cobalt-60 (1.25 MeV) isotopes. The use of radioactive isotopes was favoured over x-ray tubes used by the pioneers since they had the advantage of both a higher output and high beam energy. It was still assumed that the dose deposition needed to be simultaneous across the whole body and as a consequence, dedicated irradiators were built as the solution to the homogeneous dose distribution problem.

### 1.5.2 Irradiators

The concept of a total body irradiator is to have a number of radioactive sources move into position and form a uniform radiation field with which to treat a patient. In the 1950's and 1960's, dedicated irradiators were built in government and military laboratories in the United States. The first TBI installation (1953) in the United States based on radioactive isotopes was at the Naval Medical Research Institute in Bethesda, MD, and was mainly used for research. It consisted of 60 tubes placed in a circular fashion around an opening for a patient. Co-60 slugs were moved into each tube by a pneumatic system. This installation had high maintenance costs and was not used elsewhere [10].

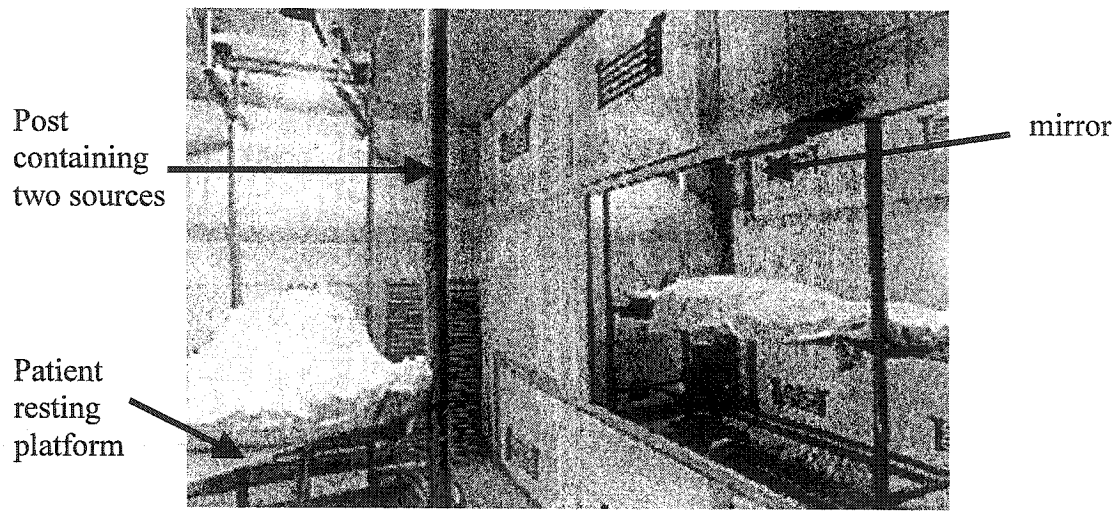


*Figure 1.1* View of a patient lying on a resting platform between 4 bed posts as well as the reflected view from a mirror on the right wall of the Oak Ridge Associated Universities Medium exposure total body irradiation facility.

A different model of irradiator was built at the Oak Ridge Associated Universities (Oak Ridge, TE, USA) and at the City of Hope Medical Centre (Duarte, CA, USA) in 1960 [10]. The medium exposure TBI facility consisted of eight cesium-137 sources. The sources were placed inside the posts of a four poster bed, two sources per post. They were raised from a shielded position below the floor to an irradiation position with sources above and below the patient resting platform (see *Figure 1.1*).

### 1.5.3 Parallel-opposed techniques

The cost of multiple source total body irradiators was prohibitive for conventional hospital institutions and alternative techniques using fewer sources were considered. At the Mary Imogene Bassett Hospital (Cooperstown, NY, USA), Sahler developed a technique whereby two cobalt-60 photon beams were arranged to intersect at the patient [13]. They were parallel to one another in a lateral-type orientation; producing a parallel-opposed source arrangement. Treatment set-ups with this technique could be either anterior-posterior, posterior-anterior (AP-PA) parallel-opposed when the beams cross perpendicular to the chest wall or laterally parallel-opposed when the beams enter parallel to the chest. The design of the room at the Mary Imogene Bassett Hospital allowed for up to 3 meters between the patient and each source, thereby allowing a field large enough to accommodate the patient. Following the development of large field irradiation, TBI techniques became available in hospital based facilities.

## 1.6 CURRENT TBI TECHNIQUES

### 1.6.1 Introduction

Due to the high costs of building and maintaining a dedicated room with equipment for TBI, most hospitals did not offer this treatment. As the usefulness of TBI treatments was demonstrated [14, 15], medical physicists came to be involved in developing unique solutions for providing larger fields, while maintaining a uniform dose delivery. It was realised that the final dose deposition needed to be homogeneous throughout the body, but that there were no requirements on how this dose was delivered. To accomplish TBI, both patient and source movement was considered and as a result, new techniques to provide TBI were developed.

### 1.6.2 Translational beam technique

The translational beam technique consisted in using the motion of the source of radiation to produce a large field. Only part of the patient is in the beam of radiation at any one time. This technique was used at the Princess Margaret Hospital (PMH) in Toronto, ON, Canada, between 1960 and 1974. The cobalt-60 source was housed in a Picker C-3000 teletherapy unit

suspended from a carriage running on rails fastened to the ceiling. The unit moved along 185 cm rails. This technique is dynamic in nature and consequently not easy to implement in radiotherapy clinics [16]. This particular unit was also routinely used for regular clinical work.

Conventional linear accelerators which are isocentrically gantry mounted are not easily adaptable to this technique. The corollary to the translational beam technique is to have the patient move under a stationary beam, whereby a motorised couch translates the patient under the radiation source (see *Figure 1.2*). The motion of the couch can be controlled to increase dose homogeneity delivered to the patient [17]. The disadvantage with this technique is that a special couch and moving apparatus are needed and these added components increase the complexity of treatment delivery and dosimetry.

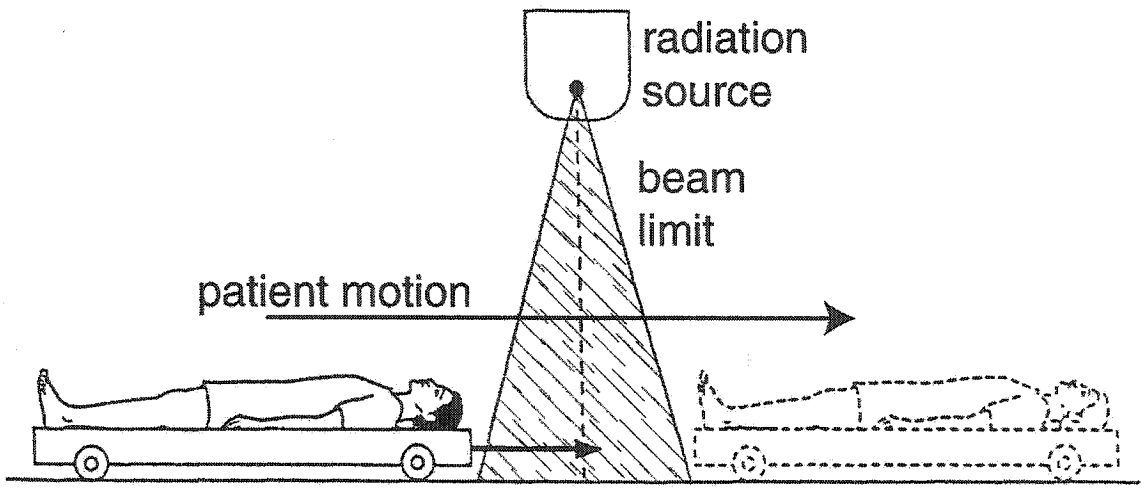


*Figure 1.2* Translating couch moves under a source of radiation to irradiate the entire body. [Figure from "Special Techniques in Radiotherapy" in *The Modern Technology of Radiation Oncology: A compendium for Medical Physicists and Radiation Oncologists*, Medical Physics Publishing: Madison, WI, USA, p. 649, 1999.]

### *1.6.3 Sweeping beam*

Another method using the motion of a limited area radiation beam to irradiate the whole patient is one which takes advantage of the rotational motion of the linear accelerator head (head swivel). With this method, known as the sweeping beam technique, a large field is effectively produced to deliver TBI (see *Figure 1.3*). In 1983, the McGill University Health Centre (MUHC) in Montréal, QC, Canada, developed a technique using a 4 MV column

mounted linear accelerator [18] to produce a sweeping beam. Following the development of the McGill technique, similar techniques were also reported using a cobalt-60 source instead [19].

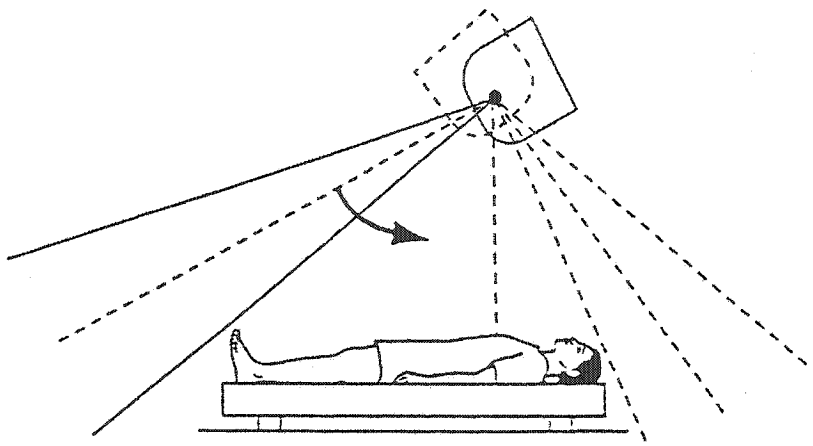

*Figure 1.3* The sweeping motion of the radiation beam produces a large field for total body irradiation. The arrow indicated the arc swept by the central axis so that the trailing and leading edges of the beam clear the patient. [Figure from "Special Techniques in Radiotherapy" in *The Modern Technology of Radiation Oncology: A compendium for Medical Physicists and Radiation Oncologists*, Medical Physics Publishing, Madison, WI, USA, p. 649, 1999.]

### 1.6.4 Linear accelerator at an extended SSD

Instead of relying on the complicated motion of the source or patient, the simplest method to produce a large field is to take advantage of beam divergence. When a large treatment room is available, the laterally oriented beam from a linear accelerator can be used to obtain a large field (see *Figure 1.4*). The dimensions of the room in which treatments are held become the limiting factor for field size. The MUHC in Montréal, QC, Canada, used this method to provide TBI for its paediatric patients between 1982 and 1994. Modern linear accelerators have the option of increasing the pulse repetition rate to increase the output of the machine, thereby compensating for the reduction in output due to the extended source to surface distance (SSD).

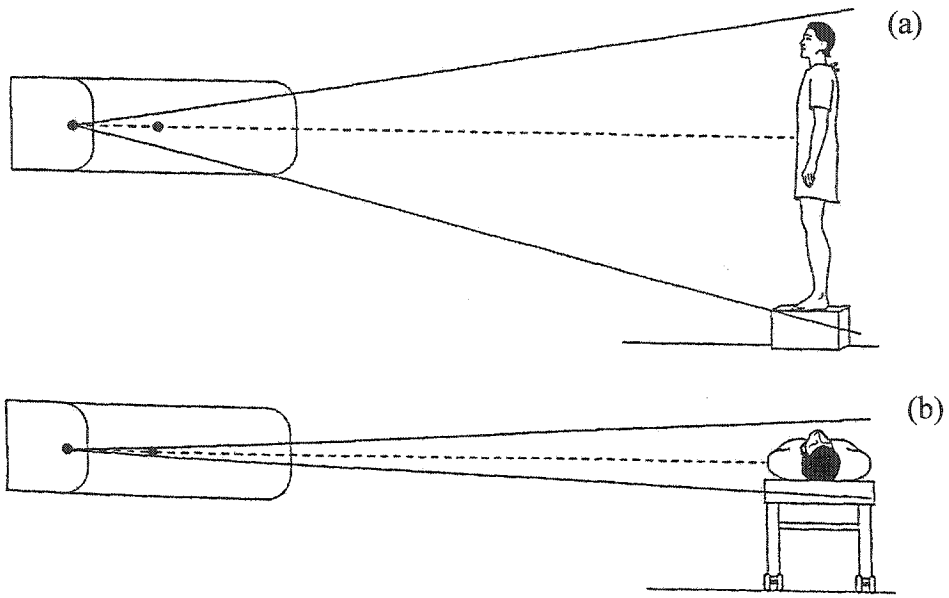


***Figure 1.4*** Patient in: (a) standing position to have AP-PA parallel-opposed beams and (b) lying down position to have laterally parallel-opposed beams. [Figure from "Special Techniques in Radiotherapy" in *The Modern Technology of Radiation Oncology: A compendium for Medical Physicists and Radiation Oncologists*, Medical Physics Publishing: Madison, WI, USA, p. 648, 1999.]

Many health care institutions have elected to use the extended SSD technique due to its ease of implementation when a large room is available. On the other hand, there are problems in dose uniformity if the patients receive the radiation lying on a bed. For laterally parallel-opposed fields (*Figure 1.4* (b)), the radiation must cross a larger patient thickness than in the case of an AP-PA irradiation (*Figure 1.4* (a)), leading to a reduction of dose uniformity throughout the patient. A method to improve the dose uniformity in the lateral aspect is to use a high-energy photon beam with bolus. Any material placed against the patient can be considered as bolus, but typical materials are rice or flour placed in bags. Radiation interacting with the bolus material scatters and thus increases the dose received by the patient when compared to the case when no bolus is present. Alternatively, some centres [20, 21] have corrected this problem by placing the patient in a standing position using a harness and a bicycle seat to support the patient during the treatment. For both approaches, it is necessary to compensate for the relatively large build-up region present with high-energy photon beams. Beam spoilers placed near the patient are used to add electron contamination to the radiation beam and

therefore increase the surface dose of the patient. The goal is to have dose uniformity throughout the patient, including the skin, within the ± 10% presently tolerated.

### 1.6.5 Modified cobalt-60 teletherapy unit

In a similar manner to the extended SSD technique using linear accelerators, one can obtain large radiation fields from a cobalt-60 unit. Taking advantage of the fact that a cobalt-60 teletherapy unit emits radiation isotropically (i.e. uniformly in all directions), these units can be used to produce large fields if the collimating and shielding materials are modified (see *Figure 1.5*) [22, 23]. This technique was first developed at the Princess Margaret Hospital, Toronto, ON, Canada, in 1977 by adapting a cobalt-60 unit to provide a TBI technique at a short SSD (90 cm). Problems with this technique arose due to electron contamination from the collimator. The electron contamination caused the skin dose to rise to unacceptable levels and was therefore corrected by using electron filters. In addition flattening filters must be used to obtain a homogeneous dose distribution and to correct for the strong reduction in dose off-axis following the inverse square law.

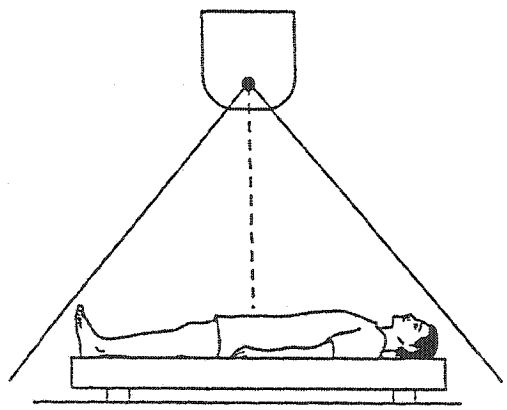

*Figure 1.5* A modified cobalt-60 unit produces a large field that encompasses the patient. [Figure from "Special Techniques in Radiotherapy" in *The Modern Technology of Radiation Oncology: A compendium for Medical Physicists and Radiation Oncologists*, Medical Physics Publishing: Madison, WI, USA, p. 648, 1999.]

## 1.7 SUMMARY

Techniques to perform total body photon irradiation are numerous, and each technique meets different constraints regarding space, cost, ease of use and availability of resources. TBI techniques strive to deliver a relatively uniform dose distribution in a timely and practical manner, and it is the hospital environment in which TBI will be administered that indicates which technique is most appropriate.

TBI is a treatment that is available in most major clinical radiotherapy centres. As discussed previously, there are many different techniques available to produce large fields for total body irradiation. The McGill University Health Centre (MUHC) radiotherapy clinic in Montreal, QC, Canada, recently developed a TBI technique by installing a modified cobalt-60 teletherapy unit. This technique was chosen due to its straightforward ease of use and resource availability in the clinic.

The cobalt-60 teletherapy unit was modified in-house to be able to produce large fields. The extensive modifications required the acquisition of a new set of data, including measurement of absolute dose output, surface dose, percent depth-dose and tissue-phantom ratios. In addition, extensive measurements of off-axis ratios and the construction of a flattening filter were required so as to ensure that the dose deposition throughout a patient was uniform. Special care was taken to explore dose deposition in the lung. This thesis discusses the use of cobalt-60 for conventional radiotherapy total body irradiation and presents the data associated with the development of a dedicated wall mounted cobalt-60 total body photon irradiation technique.

## 1.8 REFERENCES

[1] "Canadian Cancer Statistics 2001", National Cancer Institute of Canada, Toronto, ON, Canada, 2001.

[2] T.H. Kim, B.J. Gerbi and J.N. Lo, "Total body irradiation for bone marrow transplantation" in *Levitt and Tapley's Technological Basis of Radiation Therapy: Practical Clinical Applications*, Lea and Ferbiger, Philadelphia, PA, USA, 1992.

[3] E.J. Hall, *Radiobiology for the Radiologist*, Medical Department Harper and Row, New York, NY, USA, 1973.

[4] ICRU, "Measurement of absorbed dose in a phantom irradiated by a single beam of X or gamma rays", ICRU Report 23, International Commission on Radiation Units and Measurements, Bethesda, MD, USA, 1973.

[5] Task Group 29 of the Radiation Therapy Committee, American Association of Physicists in Medicine (AAPM), "The Physical Aspects of Total and Half Body Photon Irradiation", published for the American Association of Physicists in Medicine by the American Institute of Physics, New York, NY, USA, 1986.

[6] E.B. Podgorsak and M. Podgorsak, "Special Techniques in Radiotherapy" in *The Modern Technology of Radiation Oncology: A compendium for Medical Physicists and Radiation Oncologists*, edited by J. Van Dyk, Medical Physics Publishing, Madison, WI, USA, pp. 641-662, 1999.

[7] J.A. del Regato, "One hundred years of radiation oncology" in *Current Radiation Oncology*, Oxford University Press Inc., New York, NY, USA, 2000.

[8] A. Barrett, "Total Body Irradiation", Reports on practical Oncology and Radiotherapy, 4(3), 47-64, 1999.

[9] E.D. Thomas, "Bone Marrow Transplantation — Past, Present and Future" in *Les Prix Nobel 1990*, Almqvist & Wiksell International, Stockholm, Sweden, 1991.

[10] E.W. Webster, "Physical Considerations in the Design of Facilities for the Uniform Whole-Body Irradiation of Man", Radiology, 75, 19-33, 1960.

[11] A.C. Heublein, "A preliminary report on continuous irradiation of the entire body", Radiology, 18(6), 1051-1062, 1932.

[12] H. Smith, "Evolution of the ICRP System of Protection" in *Radioprotection et droit nucléaire: Entre les contraintes économiques et écologiques, politiques et éthiques*, Georg Editeur, Geneva, Switzerland, 1998.

[13] O.D. Sahler, "Development of a Room Specifically Designed for Total-Body Irradiation", Radiology, **72**, 266-267, 1959.

[14] L.J. Peters et al., "Radiobiological considerations in the use of total-body irradiation for bone-marrow transplantation", Radiology, **131**, 243-247, 1979.

[15] E.D. Thomas et al., "Marrow transplantation for patients with acute lymphoblastic leukemia in remission", Blood, **54**, 468-476, 1979.

[16] J.R. Cunningham and D.J. Wright, "A Simple Facility for Whole-Body Irradiation", Radiology, **78**, 941-949, 1962.

[17] M. Chrétien et al., "A variable speed translating couch technique for total body irradiation", Med. Phys., **27**(5), 1127-1130, 2000.

[18] M. Pla, S.G. Chenery, and E.B. Podgorsak, "Total body irradiation with a sweeping beam". Int. J. Radiat. Oncol. Biol. Phys., **9**(1), 83-89, 1983.

[19] S. Hussein and E. el-Khatib, "Total body irradiation with a sweeping $^{60}$Cobalt beam", Int. J. Radiat. Oncol. Biol. Phys., **33**(2), 493-497, 1995.

[20] R. Miralbell et al., "Can a total body irradiation technique be fast and reproducible?", Int. J. Radiat. Oncol. Biol. Phys., **29**(5), 1167-1173, 1994.

[21] A. Ho, S. Kishel, and G. Proulx, "Partial lung shield for TBI", Med. Dosim., **23**(4), 299-301, 1998.

[22] P.M. Leung et al., "Cobalt-60 therapy unit for large field irradiation". Int. J. Radiat. Oncol. Biol. Phys., **7**(6), 705-712, 1981.

[23] C. Dominique et al., "A modified $^{60}C$ teletherapy unit for total body irradiation", Int. J. Radiat. Oncol. Biol. Phys., 33 (4), 951-957, 1995.

# Chapter 2

# Fundamentals of radiation physics



## 2.1 PHOTON INTERACTIONS

The use of photons in medicine to treat disease is based on the physical processes associated with ionising radiation. For all atoms, the necessary energy to ionise outer orbital electrons is of the order of a few electron-volts (eV). The lowest ionisation potential is found in alkali atoms, at about 5 eV, while the highest ionisation potential is found in helium at 24.5 eV. More tightly bound inner electrons require a higher energy to be removed from the atom, with the highest energy being for the K-shell electrons in high atomic number atoms. As an example, the K-shell potential of Dubnium (Z=105) is about 150 keV. Photons with sufficient energy to ionise an atom do so indirectly, the first step being the transfer of all, or part of, the photon energy to a secondary electron. The second step is a transfer of energy through Coulomb collisions from the secondary electron to neighbouring bound electrons.

These electrons are either excited to higher energy levels in the atom or receive a sufficient amount of energy to break the bond with the nucleus of the atom and leave, thereby creating a positive ion. The free electron, when in contact with an electronegative atom such as oxygen forms a negative ion. In dry air, the energy necessary for the formation of an ion pair is 33.97±0.05 eV [1]. The possible photon interactions leading to the creation of the secondary electron include the photoelectric effect, Compton scattering and pair production.

### 2.1.1 Photoelectric effect

The photoelectric effect is the interaction between a photon and a tightly bound electron. The photon transfers all its energy to the bound electron and ceases to exist (see *Figure 2.1*). The electron leaves the atom with energy equal to that of the photon less its own binding energy. The photoelectric cross-section τ, a measure of the probability for the photoelectric interaction to occur, is highest when the impinging photons have an energy almost equal but higher to that of the bound electron. An electron is tightly bound when its binding energy is comparable to the photon energy. As the photon energy increases, the photoelectric cross-section decreases. Discontinuities appear when lower shell electrons are able to contribute to the photoelectric effect. Generally, as the photon energy rises, the mass attenuation coefficient $\tau/\rho$ decreases as:

$$\left(\frac{\tau}{\rho}\right) \propto \left(\frac{Z}{h\nu}\right)^3 . \tag{2.1}$$

In equation (2.1), Z is the atomic number, $h$ is Planck's constant and $\nu$ is the incoming photon frequency where $h\nu$ is the quantum energy of the photon. The photoelectric effect is the dominant photon interaction for low energy photons [2].

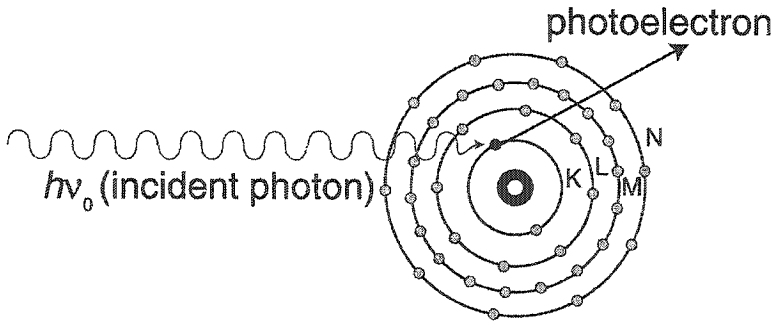


*Figure 2.1* Diagram illustrating the photoelectric effect.

### 2.1.2 Compton scattering

At higher photon energies, Compton scattering is the dominant photon interaction. This type of interaction is between a photon and a loosely bound electron. An electron is considered to be loosely bound when the photon energy is much higher than the electrons' binding energy. In a Compton interaction, the photon loses part of its energy, changes direction of motion by an angle $\phi$ and a secondary electron leaves the atom with an angle $\theta$ (see *Figure 2.2*).

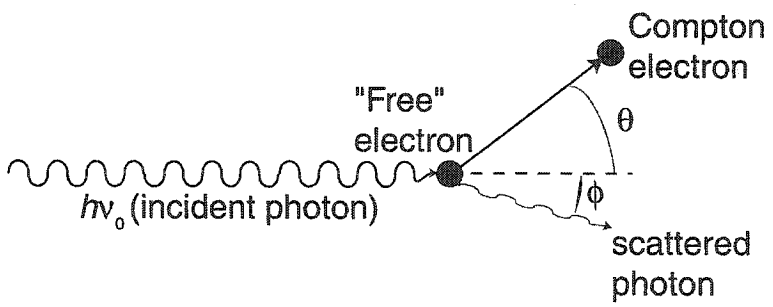


*Figure 2.2* Diagram illustrating Compton scattering.

The energy given to the electron is:

$$E = h\nu_0 \frac{\frac{h\nu_o}{m_e c^2}(1-\cos\phi)}{1+\frac{h\nu_0}{m_e c^2}(1-\cos\phi)}, \tag{2.2}$$

while the energy of the scattered photon is:

$$h\nu' = h\nu_0 \frac{1}{1+\frac{h\nu_0}{m_e c^2}(1-\cos\phi)}. \quad (2.3)$$

Where the incident photon energy is $h\nu_0$ and $m_e c^2$ is the rest mass energy of the electron (0.511 MeV). The Compton mass attenuation coefficient, $\sigma/\rho$, is independent of the atomic number Z of the medium. As shown in *Figure 2.4*, the mass attenuation coefficients for lead and water are the same at photon energies near 1 MeV where Compton scattering is the dominant effect.

Rayleigh scattering is an interaction between a tightly bound electron and a photon. This interaction leads to the scattering of the incident photon but not to the ejection of a secondary electron as in Compton scattering. No energy is therefore transferred to the medium or lost by the incident photon. The Rayleigh scattering mass attenuation coefficient $\sigma_R/\rho$, however, adds to the total mass attenuation coefficient at very low photon energies.

### 2.1.3 Pair production

Pair production occurs when a photon in the field of an atom transforms into a positron-electron pair (see *Figure 2.3*). Since energy is converted into matter, this photon interaction cannot occur below a certain threshold energy, $h\nu_{thr}$. Applying energy and momentum conservation rules, $h\nu_{thr}$ is found to be equal to:

$$h\nu_{thr} = 2m_e c^2\left(1+\frac{m_e c^2}{m_a c^2}\right), \quad (2.4)$$

where $m_e c^2$ and $m_a c^2$ are the rest mass energies of the electron and the atom respectively. In a first approximation, the threshold energy is defined as 1.022 MeV.

A special case is when a photon in the field of another electron transforms into an electron-positron pair (see *Figure 2.3*). This is called triplet production. The threshold energy for triplet production is $4m_e c^2$ =2.044 MeV.

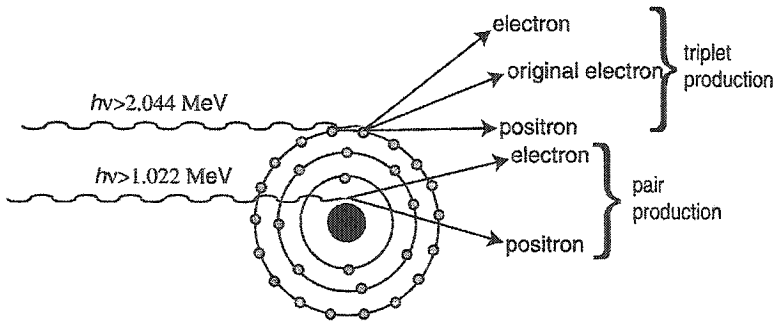


*Figure 2.3* Atom nucleus and surrounding electrons with the absorption of photons according to pair and triplet production.

Cobalt-60 gamma rays have a photon energy of 1.25 MeV, the contribution from the pair production mass attenuation coefficient $\kappa/\rho$ to the total mass attenuation coefficient is only for the photons with energy between 1.022 and 1.25 MeV. Triplet production does not contribute since the threshold is above the energy of the cobalt-60 gamma rays. The pair production mass attenuation coefficient increases above the threshold energy as the logarithm of the photon energy (ln E) [3].

### 2.1.4 Total mass attenuation coefficient

The total mass attenuation coefficient $\mu/\rho$ is given as:

$$\frac{\mu}{\rho} = \frac{\tau}{\rho} + \frac{\sigma}{\rho} + \frac{\sigma_R}{\rho} + \frac{\kappa}{\rho}, \tag{2.5}$$

where $\rho$ is the density of the medium and $\tau$, $\sigma$, $\sigma_R$, $\kappa$ are the photon interaction cross-sections for photoelectric, Compton scattering, Rayleigh scattering and pair production, respectively. In *Figure 2.4*, the total mass attenuation coefficient is plotted for lead and water as a function of the incident photon energy. At low energies, edges are present in the curve for lead that are attributable to the photoelectric effect. Water does not exhibit these edges since the photon energy range (1 keV to 1.25 MeV) is too high for the photoelectric effect too occur. Electrons in water molecules have a much lower ionisation potential than M, L or K-shell electrons in lead.

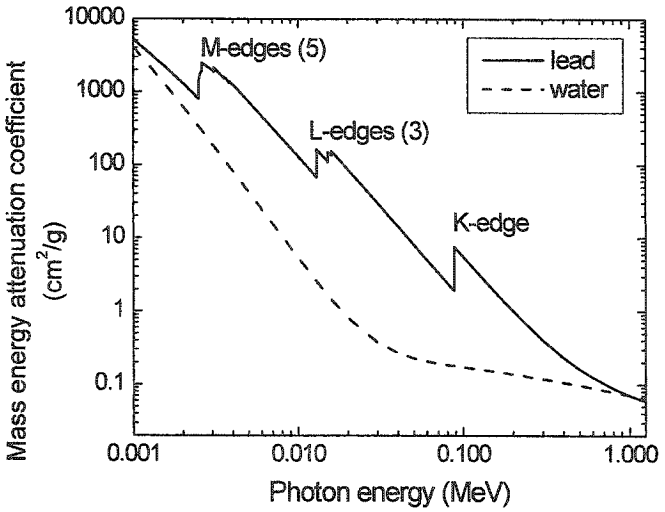


*Figure 2.4* Total lead and water mass attenuation coefficients ($\mu / \rho$) as a function of photon energy (from NIST database).

## 2.2 SECONDARY ELECTRON INTERACTIONS

### *2.2.1 Stopping power*

The secondary electrons created by the different photon interactions deposit dose through a succession of small energy transfer interactions in the medium. Energy loss of the secondary electrons is either through Coulomb collisions with neighbouring electrons (collisional loss) or through Coulomb interactions between the secondary electron and an atomic nucleus (radiative loss). Energy lost through collisions is absorbed in the medium near the electron track, while radiative losses lead to an escape of energy in the form of photons. The mass stopping power describes the energy loss of the secondary electron when moving through the medium due to collisional and radiative losses. In *Figure 2.5*, the collisional, radiative and total stopping powers of electrons are plotted as a function of their kinetic energy. The maximum energy available to the secondary electron is the original photon energy. Therefore, as indicated in *Figure 2.5*, for photons produced by a cobalt-60 source the collisional losses are dominant over radiative losses.

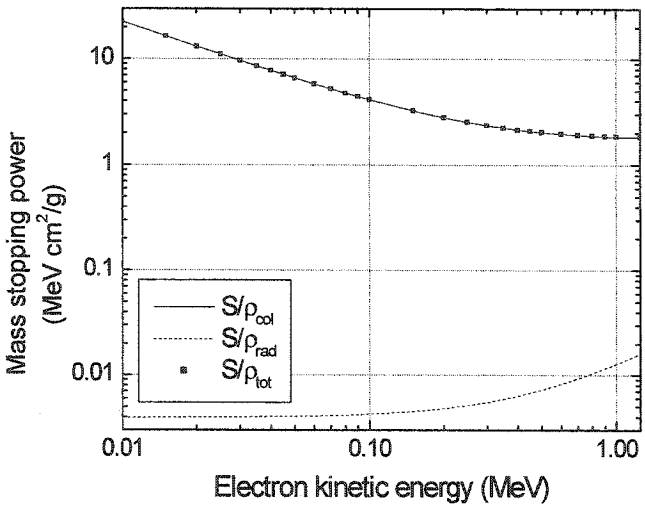


*Figure 2.5* Collisional, radiative and total stopping power as a function of the electron's kinetic energy (from NIST database).

Additionally, from the total mass stopping power, the range of the secondary electron can be determined under the continuous slowing down approximation (CSDA). Applying the CSDA, any hard collision between a secondary electron and a neighbouring electron leads to the deposition of energy locally, not to an energetic electron able to bring its energy away from the secondary electron track. The range is defined as:

$$R = \int \frac{dT}{\frac{S(T)}{\rho}}, \tag{2.6}$$

with $T$ the kinetic energy of the secondary electron in MeV and $S(T)/\rho$ the total mass stopping power in MeV cm$^2$/g [2].

### 2.2.2 Dose

The concept of dose is based on the energy from the secondary electrons absorbed by the medium. Dose $D$ is the energy absorbed ($E_{abs}$) in an incremental volume of medium of mass $dm$:

$$D = \frac{dE_{abs}}{dm_{med}}. \tag{2.7}$$

Dose is the quantity used to characterise the radiation beam when passing through a medium of interest, whereby dose is expressed in units of Gray [J/kg].

### 2.2.3 *Inverse square law*

The inverse square law describes the variation of the photon fluence produced from a point-like radiation source. The photon fluence varies inversely as the square of the distance from the source. Measurements can be corrected for the effects of the inverse square law by:

$$D'_P = \left(\frac{A}{A'}\right)^2 D'_Q, \tag{2.8}$$

where $D'_P$ is the dose measured in a small mass of medium in air at a distance $A'$ from the source and $D'_Q$ is the dose measured in a small mass of medium in air at a distance $A$ from the source.

## 2.3 CHARGED PARTICLE EQUILIBRIUM

The different possible interactions leading to the creation of a secondary electron have been covered in section 2.1. These secondary electrons are not still, but move in the medium and have a range, as defined in equation (2.6). Electrons therefore do not deposit their energy where they are created. In the patient or phantom, electrons set forth in a first layer of medium deposit dose throughout the distal or lower layers, but these layers also see the production of additional secondary electrons. A build-up effect is seen where more and more charged particles exit a layer then enter it. Photons are attenuated exponentially according to:

$$N(x) = N_0 e^{-\frac{\mu}{\rho}\rho x}, \tag{2.9}$$

where $N(x)$ is the number of photons leaving a layer of thickness $x$ with $N_0$ the number of photons entering the layer and $\mu/\rho$, the mass attenuation coefficient, as defined in equation (2.5). At a depth where as many charged particles enter as exit a layer, charged particle equilibrium is attained. Beyond this depth, due to the lower number of photons interacting in the layer, fewer electrons are set forth and fewer charged particles exit the layer than enter. Under these conditions, charged particle equilibrium is lost. If the distance between the point where the secondary electron is set in motion and the point where dose is measured from that electron is constant, then transient charged particle equilibrium is established.

### 2.3.1 Depth of dose maximum

The depth in a medium where the maximum dose is deposited corresponds to the layer where charged particle equilibrium is reached. This depth is known as depth of dose maximum, $d_{max}$, and will be used in defining different dosimetric quantities (see section 2.4). Following BJR 25 recommendations, the depth of dose maximum, $d_{max}$, is defined as a depth of 0.5 cm in water for photons produced from a cobalt-60 source, irrespective of any effects found to change the depth were $d_{max}$ physically occurs [4].

## 2.4 DOSIMETRIC QUANTITIES

The Percent Depth Dose (PDD) illustrates the build-up effects, the depth of dose maximum and the fall-off due to attenuation and inverse square law effects of the photon beam through a thickness of medium. For a given Source to Surface Distance ($SSD$), field size ($A$) and beam energy ($E$), the $PDD$ is defined as:

$$PDD(d, A, SSD, E) = 100\% \frac{D_Q(d, A)}{D_P(d_{max}, A)}, \qquad (2.10)$$

where d is the depth in the phantom where dose $D_Q$ is measured and $D_P$ is the dose measured at depth $d_{max}$, as illustrated in *Figure 2.6*.

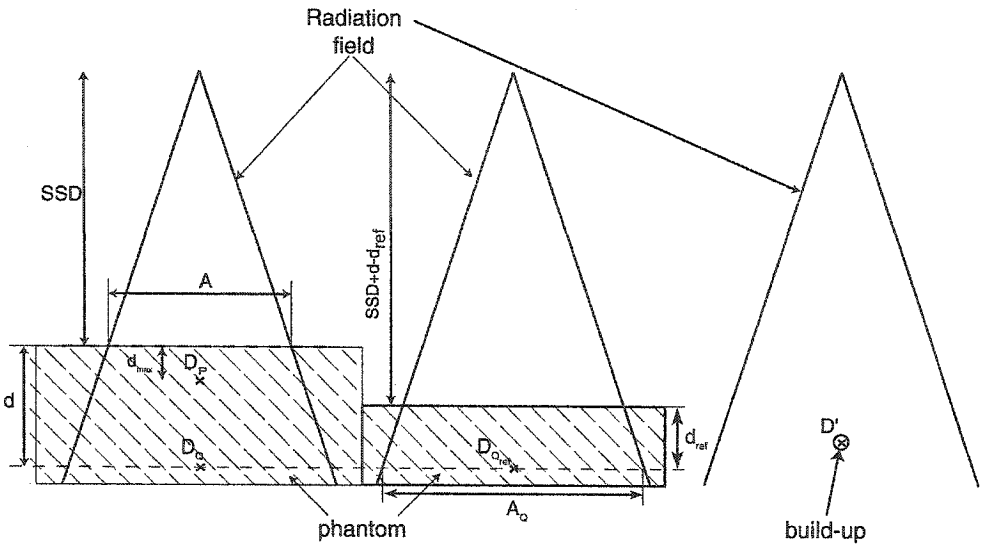


*Figure 2.6* Diagram indicating SSD, A, $A_Q$, $d_{max}$, $d_{ref}$, d, $D_P$, $D_Q$, $D_{Qref}$ and D′ used in calculating dosimetric parameters.

To measure the PDD, a dosimetric probe (see Chapter 4) is displaced throughout the medium at different distances from the radiation source while maintaining the *SSD* and field size *A* constant on the surface of the phantom. The graphical representation of PDD is as a function of the depth of $D_Q$ in the phantom. A sample PDD curve is presented in *Figure 2.7*.

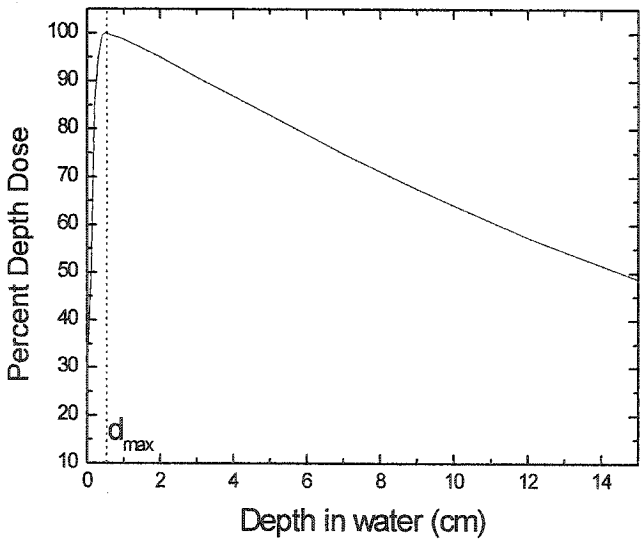


*Figure 2.7* Sample PDD curve for cobalt-60 gamma rays

Another dosimetric quantity, similar to PDD in the way that it is graphically presented as a function of depth of $D_Q$ in medium, is the Tissue-Phantom-Ratio (TPR). The TPR is

independent of the SAD since the dosimetric probe stays at a constant distance from the radiation source while the surrounding medium is modified to change the depth of the probe. The TPR is defined as:

$$TPR(d, A_Q, E) = \frac{D_Q}{D_{Q_{ref}}}, \tag{2.11}$$

with $d$ the thickness of phantom where $D_Q$ is measured, $A_Q$ the field size at depth $d$ and $E$ the photon energy. $D_{Qref}$ is the dose measured at the same position as $D_Q$, but with only a reference phantom thickness placed above. *Figure 2.6* geometrically describes the different parameters.

A relationship can be established between the two dosimetric quantities, PDD and TPR, by considering the Peak Scatter Factor (PSF) which is a function of the field size at the surface of the phantom, A. The PSF is defined as:

$$PSF(A) = \frac{D_P}{D'_P} \tag{2.12}$$

where $D_P$ is the dose measured in a phantom at depth $d_{max}$ and $D'_P$ is the dose measured at the same position, but in air with a small surrounding mass of medium. The small mass of medium acts as build-up material to achieve charged particle equilibrium.

With PSF defined, a relationship between PDD and TPR can be established giving the following result:

$$TPR(d, A_Q) = \frac{PSF(A)}{PSF(A_{ref})} \left( \frac{SSD_{ref} + d_{max}}{SSD + d_{max}} \right)^2 \frac{PDD(d, A, SSD)}{PDD(d_{ref}, A_{ref}, SSD_{ref})} \tag{2.13}$$

where

$$A_{ref} = A \left( \frac{SSD + d - d_{ref}}{SSD} \right) \tag{2.14}$$

and

$$SSD_{ref} = SSD + d - d_{ref} . \tag{2.15}$$

This result is similar to equation 3a given in appendix B of supplement 25 of the British Journal of Radiology [4].

### 2.4.1 Off-axis-ratio

Another useful dosimetric quantity when studying a radiation beam is the beam profile or off-axis ratio (OAR). A beam profile is measured with a dosimetric probe at a constant depth in the phantom which is scanned across the radiation beam. The distance between the source and the surface of the phantom is constant and the radiation beam is perpendicularly incident onto the phantom. Beam profiles are often normalised to the dose at the centre of the radiation field, so that:

$$OAR(d,x,y) = \frac{D_Q(x,y)}{D_Q(0,0)}, \tag{2.16}$$

where $D_Q(0,0)$ represents the dose at depth $d$ along the central axis of the radiation beam and $D_Q(x,y)$ represents the dose elsewhere in the field at the same source depth. The usefulness of the $OAR$ is to transform dosimetric quantities such as PDD or TPR measured along the central axis to their values elsewhere in the field. Also, the limit of the radiation beam is calculated from beam profiles at the point where the OAR is equal to 0.5. Beam flatness can also be verified, with a beam considered flat when the beam profile within the central 80% of the field size is within a tolerance of ±3% of the central axis value [5]. This requirement was also considered when designing the large radiation field used for TBI.

### 2.4.2 Output

All the dosimetric quantities presented considered ratios of doses (or in practice clinical measurements) giving information on dose distributions. Absolute dose at different positions within the phantom were not discussed. Absolute dosimetry source output expressed in cGy/minute requires the use of an ionisation chamber with a calibration factor traceable to a standards laboratory. The American Association of Physicists in Medicine TG-51 protocol [6] describes the corrections and calculations necessary to obtain the absolute output from a radiation beam and will be presented in more detail in chapter 4.

## 2.5 SUMMARY

Photon beams produced by a cobalt-60 source are able to ionise matter through the photoeletric effect, Compton scattering or pair production, whereby electrons are transferred varying amounts of energy. This energy is dissipated by two possible mechanisms: either through collisional losses with neighbouring electrons or through radiative photon emissions. Cobalt-60 photons are not able to produce electrons where radiative losses are very important as discussed in section 2.2.1 and therefore, most of the energy from the photons is absorbed by the medium through Coulomb collisions. Dose is a measure of the amount of energy absorbed in a given volume divided by its mass and dose deposition throughout a phantom occurs through the interaction of charged particles rather than by the impinging photons. This leads to build-up and attenuation effects within the phantom. From a known dose at a given point, quantities such as percent depth dose, tissue-phantom ratio and off-axis ratios are sufficient to describe the complete dose deposition in a patient or phantom.

## 2.6 REFERENCES

[1] M. Boutillon and A.M. Perroche-Roux, "Re-evaluation of the W value for electrons in dry air", Phys. Med. Biol., 32, 213-219, 1987.

[2] F. H. Attix, *Introduction to Radiological Physics and Radiation Dosimetry*, John Wiley and Sons, Madison, WI, USA, 1986.

[3] H.E. Johns and J. R. Cunningham, *The Physics of Radiology*, 4th ed., Charles C Thomas, Springfield, IL, USA, 1983.

[4] E.G.A. Aird et al., *British Journal of Radiology Supplement 25: Central Axis Depth Dose Data for Use in Radiotherapy*, British Institute of Radiology, Volume 25, London, England, 1996.

[5] F.M. Khan, *The Physics of Radiation Therapy*, 2nd ed., Lippincott Williams and Wilkins, New York, NY, USA, 1994.

[6] P.R. Almond et al., "AAPM's TG-51 protocol for clinical reference dosimetry of high-energy photon and electron beams", Med. Phys., 26 (9), 1847-1870, 1999.

# Chapter 3

# Cobalt teletherapy unit



## 3.1 INTRODUCTION

The transformation of an isocentrically mounted cobalt-60 teletherapy unit to a dedicated wall mounted cobalt-60 total body photon irradiation technique required an understanding of how the original unit functioned. Photon production from a cobalt-60 source comes from the beta decay of cobalt-60 to nickel-60 (see *Figure 3.1*). The nickel-60 atom, left in an excited state returns to its ground state by the successive emission of two gamma rays with an energy of 1.17 and 1.33 MeV [1]. Radiation from a cobalt-60 source is therefore continuous.

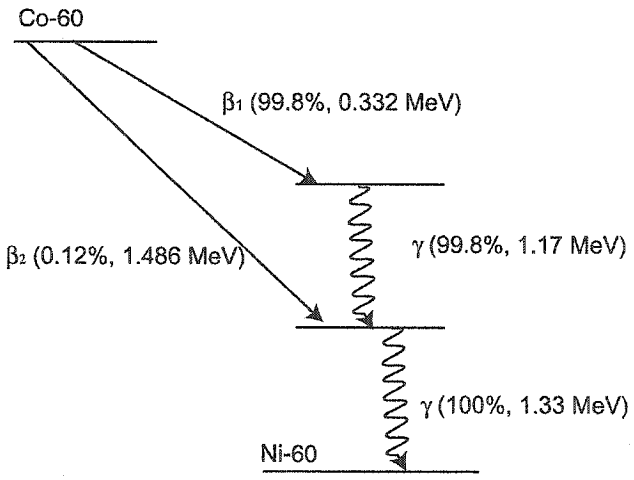


*Figure 3.1* Photon production by excited nickel-60 following beta decay of cobalt-60.

Cobalt-59, the naturally occurring isotope of cobalt, is bombarded with neutrons to artificially produce cobalt-60. Cobalt-59 is in the form of wafers or pellets and when activated to cobalt-60 has a half-life of 5.26 years as it decays to nickel-60. The high neutron flux required for activation of cobalt-59 is produced in a nuclear reactor. A typical rest time for cobalt-59 in the nuclear reactor is 3 years so as to attain a specific activity of 300 Ci/g [2]. A higher specific activity, on the order of 1100 Ci/g, could be reached if the cobalt-60 were carrier free, i.e. not contaminated with cobalt-59.

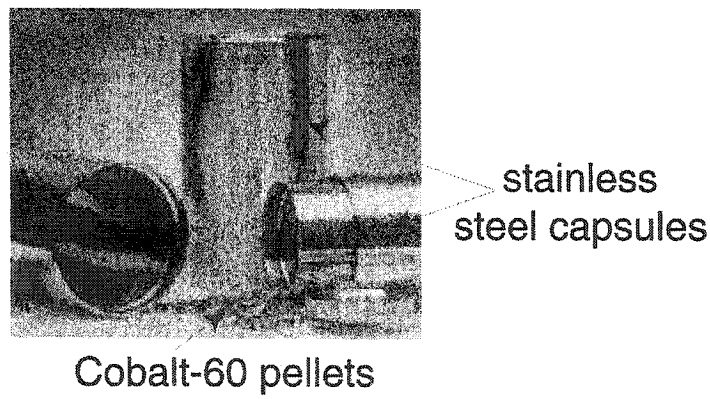


*Figure 3.2* Cobalt-60 pellets with accompanying stainless steel capsules.

As shown in *Figure 3.2*, cobalt-60 is in the form of nickel plated pellets. These pellets are tightly packed and doubly encapsulated in low carbon stainless steel capsules, with the capsules then welded shut using a tungsten inert gas method [3]. The beta particles produced during the decay from cobalt-60 to nickel-60 do not reach the patient since the casing that surrounds

the cobalt-60 pellets absorb them. Radiation emitted by a cobalt-60 source is isotropic (photons emitted in all directions equally) with a mono-energetic photons (photons of energy 1.17 or 1.33 MeV). The cobalt-60 source in the isocentric teletherapy unit was installed in 1996 and at the time of installation, had an activity of about 222 TBq (6 000 Ci).

## 3.2 ORIGINAL T-780 UNIT

An isocentric Theratron 780 (T-780) teletherapy unit was in clinical use at the McGill University Health Centre (MUHC, Montréal, Québec, Canada) until January 2000, when it was placed in storage and replaced with a linear accelerator. The main components of a Theratron-780 teletherapy unit are illustrated in *Figure 3.3*.

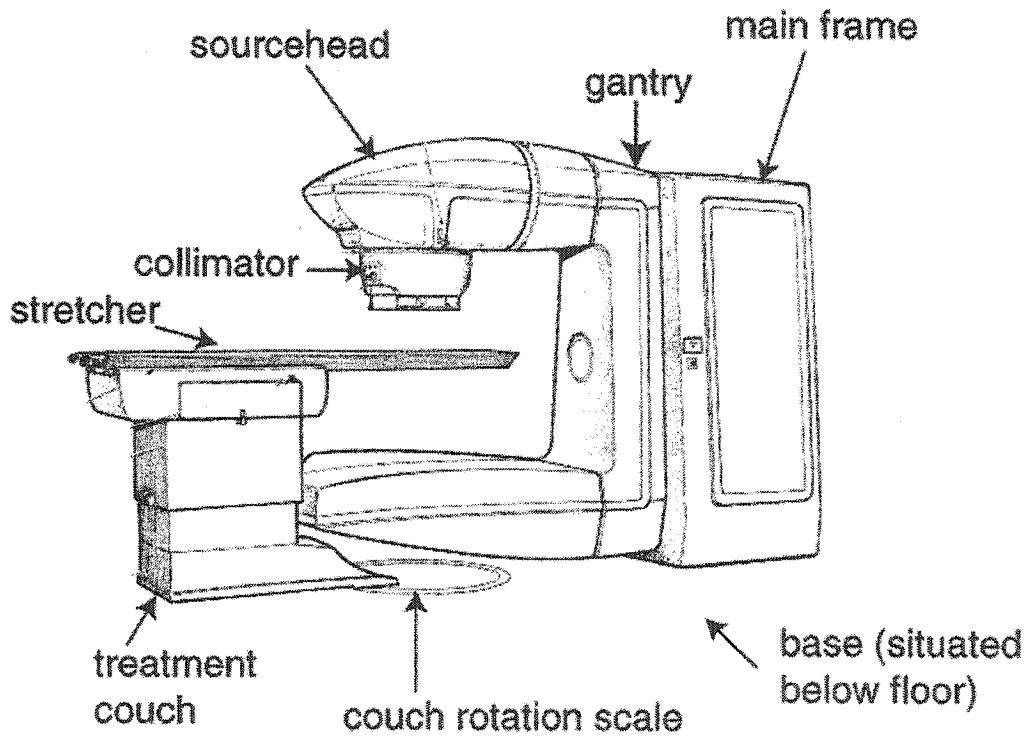


*Figure 3.3* Components of a Theratron 780 cobalt-60 teletherapy unit. [Drawing from "Operator's Manual for the Theratron 780-2 cobalt-60 teletherapy unit", Atomic Energy of Canada Limited: Commercial Products, Ottawa, ON, Canada, p 3.1, 1977.]

The treatment couch, the gantry and the collimator are able to rotate about an axis through the isocentre. The base is a steel frame mounted into the concrete floor that supports and aligns the main frame and the couch for isocentric set-up. The treatment couch rests on the base

which is about 100 cm below the isocentre and is aligned so that it can rotate about an axis intersecting the isocentre. The stretcher allows for motion in the vertical, lateral and longitudinal directions to position the patient for treatment as well as a rotation about it's own axis. The main frame supports the gantry rotation. By rotating the gantry, the angle of the radiation beam impinging on the patient is changed. The collimator is used to define the beam size, and the central axis of the beam intersects with the isocentre [4].

### 3.2.1 Sourcehead

The sourcehead is installed at the extremity of the gantry to project the radiation beam towards the isocentre. Shielding inherent to the sourcehead (see *Figure 3.4*) surrounding the cobalt-60 source is composed of lead and depleted uranium. These metals have a high density and atomic number giving them high attenuation characteristics. Depleted uranium is a waste product of the enrichment of uranium-235 and is composed of uranium-238 and its decay product uranium-234 as well as trace amounts of uranium-235. Depleted uranium has a density of 19.3 g/cm$^3$ and an atomic number of 92 as compared to 11.36 g/cm$^3$ and Z=82 for lead. Lead shielding surrounds the depleted uranium shield.

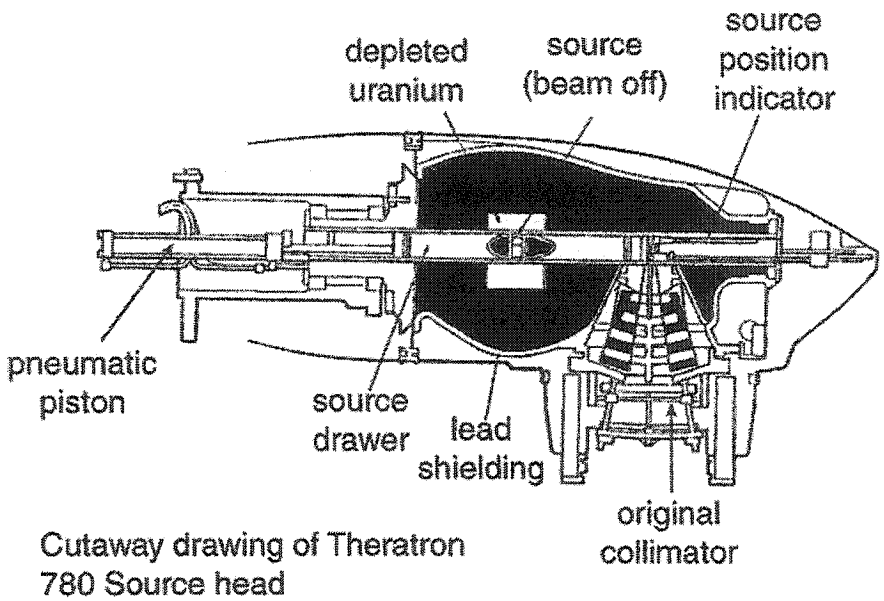


*Figure 3.4* Treatment head of the original cobalt-60 isocentric unit. [Drawing from Modern Technology of Radiation Oncology, "chapter 10: Cobalt-60 teletherapy", Medical Physics Publishing, Madison, WI, USA, p. 318, 1999.]

A pneumatic piston controls the position of the cobalt-60 source between the depleted uranium shielded position (beam-off) to above the collimator opening (beam-on). A schematic diagram of the pneumatic piston is presented in *Figure 3.5*. An air storage tank holds air to pressures between 241.3 and 344.75 kPa above the ambient air pressure. Effectively, for an air pressure of 101.3 kPa, the pressure in the tank may be between 342.6 kPa and 446.05 kPa. Through an air hose connection, air is either directed towards the back of the piston, effectively pushing the source out; or to the front, pushing the source back into the shielded position. An air regulator reduces the air pressure at the piston to 172.38 kPa above the ambient air pressure. A low-air pressure interlock is activated if the pressure goes below 137.9 kPa above the ambient air pressure in the air storage tank. If insufficient pressure is applied to the piston, it may not be able to move the 18-kg source drawer. Therefore, when the low-air pressure interlock is activated, the source drawer cannot slide to the beam-on position but it can return to the beam-off position as long as the air pressure stays above 103.43 kPa above ambient air pressure. Below this value, air pressure is insufficient and a rod must be used to manually return the source to its shielded beam-off position [5].

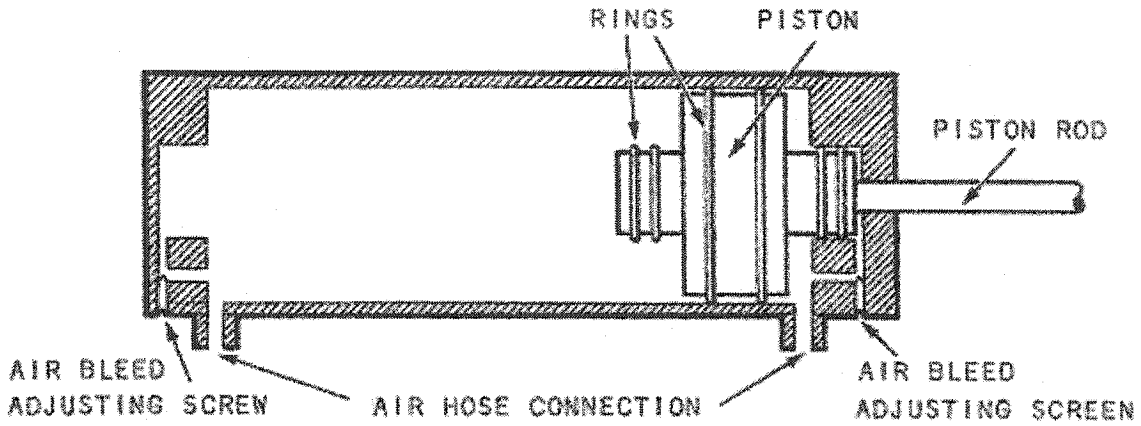


*Figure 3.5* Pneumatic piston used to move source drawer in the treatment head. [Drawing from Service Manual: Theratron-780 Cobalt 60 Teletherapy Unit, Atomic Energy Limited, Ottawa, ON, Canada, p. X-8, 1973]

The source capsule is a cylinder with a diameter of 1.5 cm and a length of 3 cm and is inserted in an opening of the source drawer. A hollow steel tube in the head allows the source drawer to slide from a beam-off position to a beam-on position when pushed by the pneumatic piston. A source position indicator rod is pushed outside the sourcehead to be visible when the source is in the beam-on position and also serves as part of the mechanism to manually return the source to the beam-off position in the event of an emergency. The source drawer, apart from the cobalt-60 source and surrounding lead shielding contains a beam defining lamp positioned above the collimator opening when the source is in the beam-off position.

When the cobalt-60 source is in the beam-on position, the field light is displaced out of view and the collimator defines the radiation beam size. The collimator device is composed of a depleted uranium fixed definer, two pairs of interlocking lead leaves and depleted uranium trimmer bars. The fixed definer acts as the initial collimator to produce a circular field while the leaves are movable shields that collimate the radiation beam to rectangular field sizes ranging from 5 cm to 35 cm on a side at 80 cm from the source. The bottom of the lowest leaf is 45 cm away from the source. Trimmer bars lowered near the patient limit and improve the geometrical penumbra. Depleted uranium is used for collimation due to its high attenuation characteristics. The 55 cm and 65 cm trimmers are attached to the collimator when needed. The collimator device can rotate about the central axis of the radiation beam with the central axis intersecting the isocentre. Cross-hair wires installed in the collimator

device help indicate the position of the beam's central axis when the light field is on. The distance from the isocentre to the source is nominally 80 cm.

### 3.2.2 Other components

The air compressor and air storage tank, necessary to operate the pneumatic piston, are located in the main frame of the teletherapy unit. The gantry rotation drive as well as the main electrical panel are stored in the same location. The gantry, supported by the main frame, allows for isocentric set-ups. The gantry can be in a fixed position or it can rotate when treatments are delivered. To produce a rotation treatment, the gantry rotates with the cobalt-60 source in the beam-on position. In the case of arc or skip therapy, the source is in the beam-on position for only a portion of the rotation.

The Theratron 780 teletherapy unit is controlled by a console situated outside the treatment room. The electronics to operate the unit are either in the main frame or in the console itself. It is at the console that the type of treatment (fixed, rotation, arc or skip) is determined and the irradiation time set. A hand-control installed in the room allows for control of mechanical components (gantry, collimator and couch) [4, 5].

With the Theratron-780 isocentric unit fully described, the task of presenting the modifications to the unit follows in the next section.

## 3.3 MODIFICATION OF THE T-780 ISOCENTRIC COBALT UNIT

The original Theratron-780 isocentric unit had a maximum field size of 35×35 $cm^2$ at 80 cm from the source. Even if the patient rested on the floor at an SSD of about 160 cm, the field size would be insufficiently large to cover the entire patient. To deliver a total body irradiation treatment, a method to deliver a large field was required. The production of a large radiation field with a cobalt-60 source could only be achieved by modifying the Theratron-780 isocentric unit. The first possible modification brought to the original unit that most increased the field size was the removal of the collimator device, which enabled the production of a 120 cm diameter radiation field at isocentre (80 cm from the source). This field size however was still insufficient to treat patients. Without the collimator, the Theratron-780 isocentric unit could

not be used for any treatment other than TBI. There was therefore no reason to keep the isocentric capabilities of the Theratron-780, since for TBI, a fixed source position is appropriate for treatment. The sourcehead was separated from the gantry and installation at an approximate height of 250 cm against the wall was planned. The increased height of the source enabled a greater distance between the source and the patient, therefore leading to the production of a sufficiently large radiation field without further modifying the shielding of the cobalt-60 source.

The first step in the development of the modified Theratron-780 TBI technique was the de-installation of the isocentric unit. The sourcehead was removed from the gantry and stored until its reinstallation as the newly modified cobalt-60 unit. A steel frame, shown in *Figure 3.6* was attached in the corner of a treatment vault which already contained a working linear accelerator.

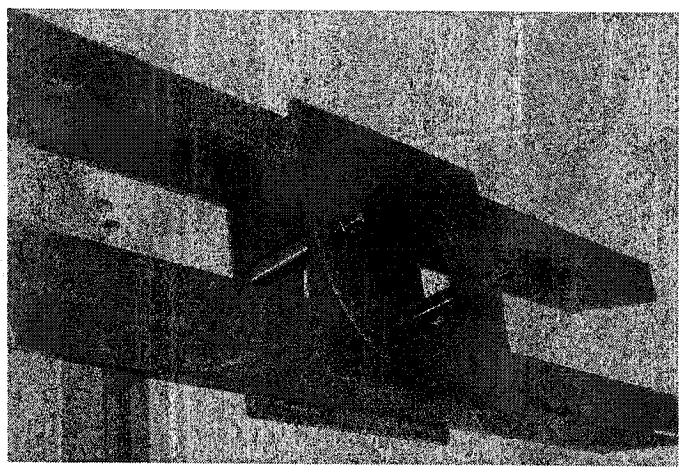

*Figure 3.6* Steel cross-members used to support the source head.

The installation of the sourcehead against the wall of the treatment room provided many challenges. The sourcehead contains all the shielding for the cobalt-60 source and weighs about 3000 kg. The weight exacts a strong torque on the steel cross-members used to fasten the sourcehead to the wall. The steel cross-members were welded to steel plates at both ends and attached to the cement wall with ten 2.5 cm diameter mounting bolts. When referring to the sourcehead, also considered was the neck used to join the sourcehead to either the gantry or the steel cross-members. The installation of the sourcehead and neck required the use of a special support to raise the assembly to the proper height before being fixed to the steel cross-

members. The neck allows for rotation of the sourcehead about its axis. This feature was kept to help in the installation and maintenance of the modified unit. The head lock interlock insures that when performing a treatment, the radiation beam is directed towards the floor. The sourcehead came to rest in a fixed position at a height of 251.2 cm above the floor.

With the sourcehead separated from the isocentric unit, the need for the base, main frame, gantry and treatment couch was eliminated. A stretcher raising the patient 12 cm above the floor replaced the treatment couch. The radiation field diameter at 250 cm below the source, without any added collimating device, was calculated to be 374 cm. This was more than sufficient to encompass any patient requiring TBI.

The modified treatment unit consists of the sourcehead and the original control mechanisms of which the hand and head panel controls were no longer necessary. The operating electronics originally housed in the main frame were re-installed in the console area next to the treatment room. The air compressor and the air storage tank (part of the pneumatic system previously also located in the main frame of the unit) were relocated to an electrical room adjoining the treatment room. Modifications brought to the operating electronics, before re-installation, eliminated the options previously available on the isocentric unit. Since the sourcehead shared a treatment room with a functioning linear accelerator, an additional interlock was necessary to avoid having both radiation sources on at the same time. This interlock was achieved by installing a switch directing power to the Theratron-780 and activating an interlock of the linear accelerator when in the on position or diverting power from the Theratron-780 when in the off position.

### *3.3.1 Collimator*

A custom built secondary collimator used to define the beam size was constructed of 5 cm thick lead sandwiched between two layers of mild steel to produce a fixed rectangular opening. The lead, cut in the shape of a semicircle, was made from two pieces with an overlap so as to minimise the transmission of radiation. Two photographs shown in *Figure 3.7* (a) and (b) illustrate the finished collimator and the pieces of lead used to build it, respectively.

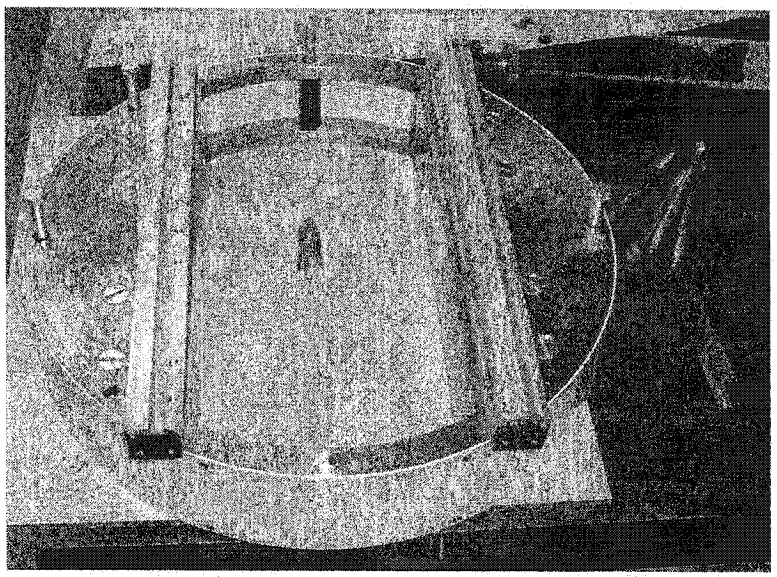

(a)

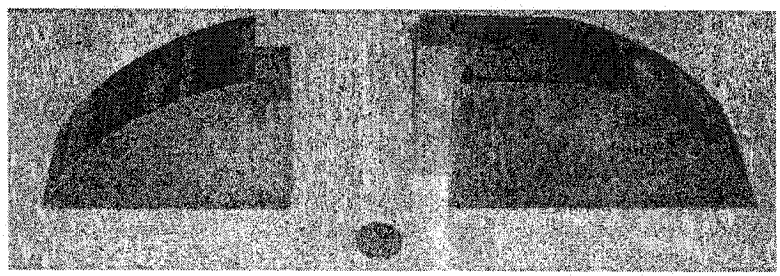

(b)

***Figure 3.7*** In photograph (a), a beam defining collimator is shown with an accessory rail and fastening bolts with the pen serving as a reference to scale. In photograph (b), the lead used to build the secondary collimator is shown with an overlap to minimise transmission of radiation, the penny serves as a reference to scale.

The new collimator was attached below the conical opening, as shown in *Figure 3.8*. The original collimator was held in place by 8 bolts and the same attachment method was used for the new collimator. Below the collimator, an accessory rail was added to slide a tray used to support a custom made flattening filter. The geometrically calculated field size with the collimator in place was $281 \times 130$ cm$^2$ at floor level.

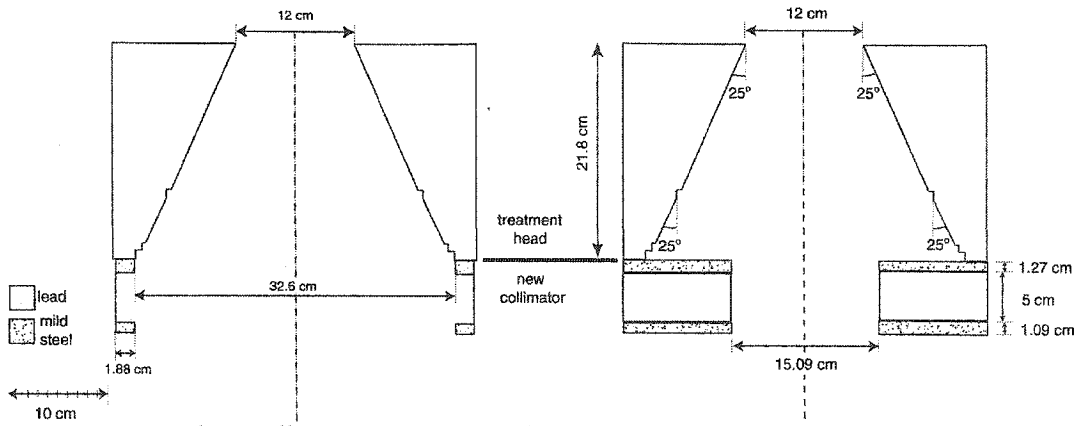


*Figure 3.8* Secondary collimator opening: a) length view (patient superior and inferior aspect) and b) width view (patient left-right aspect) below the treatment head with original collimator removed. [Lengths taken from technical drawings from Theratronics, Kanata, ON, Canada, drawing number A113208-030, sheets 2 and 4 of 5.]

### 3.3.2 Flattening filter

Even though cobalt-60 emitted radiation isotropically, the intensity of radiation at the patient level was not uniform. This was due to two factors: the first being the variation of radiation intensity with distance and the second being the scattering from the large field as defined by the lead conical opening and the new collimator. An empirically determined flattening filter therefore was used to correct variation in field intensity at a plane. The flattening filter was designed to produce a uniform radiation field within the central 180×80 $cm^2$ of the radiation field, 30 cm above the floor. The dimensions of the radiation field as defined by the beam defining light with the new collimator in place were 269×125 $cm^2$ at floor level. The difference between the light field and the flattening filter allow a shadow to reach the floor to help properly position the patient under the flattening filter.

### 3.3.3 Safety precautions

The installation of the sourcehead in a treatment room required the addition of radiation monitors and cameras to view the treatment area. They were installed before any operation of the source was attempted. Many additional precautions were taken to verify the proper operation of the mechanisms in the sourcehead before actually operating any source motion.

Since the electronics associated with the teletherapy unit were extensively modified, proper operation of the different switches was verified. Also, emergency off switches were installed and verified to be correctly operating. The piston used to move the source drawer was cleaned and tested separately to the source head so as to verify that the entire range of motion was available. The source drawer itself was moved a few cm in each direction to verify that it would not jammed. Source integrity was verified with a wipe test and a room survey was conducted. Once it was determined that the treatment head was operational, the covers were fitted and measurements of the radiation beam prior to clinical usage could begin.

## 3.4 SUMMARY

With a dedicated total body irradiation technique based on a modified cobalt-60 treatment head, equipment that would have otherwise been discarded, was continued to be used. The modifications brought to the Theratron-780 cobalt-60 teletherapy unit were extensive and the installation of the modified cobalt-60 unit required the collaboration between physicists, engineers and machinists. *Figure 3.9* summarises the steps the original Theratron 780 cobalt-60 teletherapy unit underwent before acquiring the capability to produce large fields.

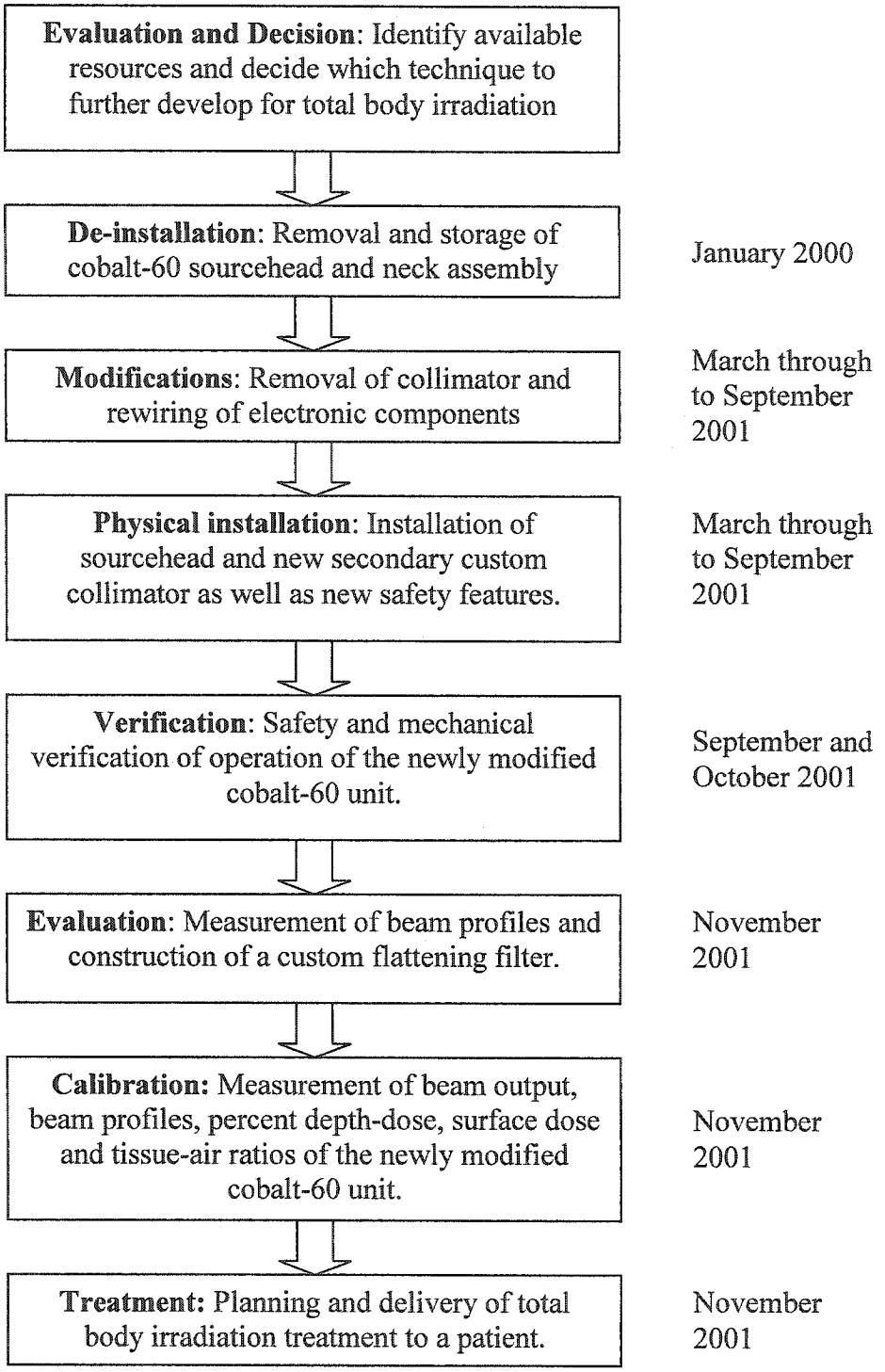


*Figure 3.9* Flow chart of steps taken to develop the modified cobalt-60 technique for TBI with approximative timeline to the right.

## 3.5 REFERENCES

[1] H.E. Johns and J. R. Cunningham, *The Physics of Radiology*, Charles C Thomas, Springfield, IL, USA, 1983.

[2] G.P. Glasgow, "Cobalt-60 teletherapy" in *The Modern Technology of Radiation Oncology: A compendium for Medical Physicists and Radiation Oncologists*, Medical Physics Publishing, Madison, WI, USA, 1999.

[3] MDS Nordion, "Sources: Integrity in the Product, the Process, the Company" MDS Nordion, Kanata, ON, Canada, 2001.

[4] M. Wise and D. Markwick, "Operator's Manual for the Theratron 780-2 cobalt-60 teletherapy unit", Atomic Energy of Canada Limited: Commercial Products, Ottawa, ON, Canada, 1977.

[5] AECL, "Service Manual Theratron-780 Cobalt-60 Teletherapy Unit", 1 ed., Atomic Energy Canada Limited, Ottawa, ON, Canada, 1973.

# Chapter 4

# Dosimeters and phantoms



## 4.1 DOSIMETERS

In general, methods for the detection of radiation can be classified into two groups: absolute and relative dosimetry. Examples of absolute dosimeters are calorimeters, Fricke dosimeters and free-air ionisation chambers; while some examples of relative dosimeters include calibrated ionisation chambers, film, thermoluminescent dosimeters, diodes, optically stimulated luminescent detectors and radioelectrets [1]. The dosimeters used in this work to study the TBI field produced with the modified cobalt-60 consisted of a variety of calibrated ionisation chambers, thermoluminescent dosimeters and film.

### *4.1.1 Ionisation chambers*

The ionisation chambers used consist of an air-filled cavity in the presence of an electric field. Under the action of the electric field, any positive or negative ions present in the air cavity contributes to an electric current. Cobalt-60 gamma rays interacting with the medium

surrounding the air cavity produce energetic electrons, either by photoelectric effect, Compton scattering or pair production as discussed in section 2.1. These electrons lose their energy mostly by Coulomb collision, exciting and ionising atoms along their path. These energetic electrons are able to enter the air cavity and form positively charged ions and free electrons. The positive ion and free electron consist of an ion pair. The average energy expended in dry air by the energetic electron in the production of an ion pair is $\overline{W}_{air} = 33.97 \pm 0.05\, eV$ [2]. Free electrons in air combine with oxygen, an electronegative gas, to form a negative ion. Positive and negative ions have a similar mobility and drift in opposite directions due to the electric field. Charge collection through an electrometer does not represent the absolute dose. Correction and calibration factors must be applied to the raw charge measurement according to the TG-51 protocol from the American Association of Physicist in Medicine (AAPM) [3].

The electric field in the cavity is due to two electrodes between which a voltage is applied. The effect of the electric field on the ions is to attract them towards the opposite electrode. One of the electrodes, the measuring electrode, is connected to ground through the electrometer that measures the accumulated charge. The other electrode defines the chamber polarity and is named the biasing electrode. The bias voltage applied to every ionisation chamber in this study was either +300 V or – 300 V.

The magnitude of the voltage has an effect on the collection efficiency of the ionisation chamber. A free electron and a positive ion or a negative and positive ion can recombine to form neutral atoms. Recombination occurring within electrons and ions produced along the path of an energetic electron is initial recombination. Initial recombination is independent of dose rate and dependent on the quality of the radiation (electrons, alpha particles, heavy ions...). Recombination occurring between electrons and ions produced by different energetic electrons is general recombination and increases with dose rate. Diffusion within the air cavity of ions moving against the electric field also limits the collection efficiency. Initial and general recombination, as well as diffusion reduce the available number of ions able to contribute to the electric current.

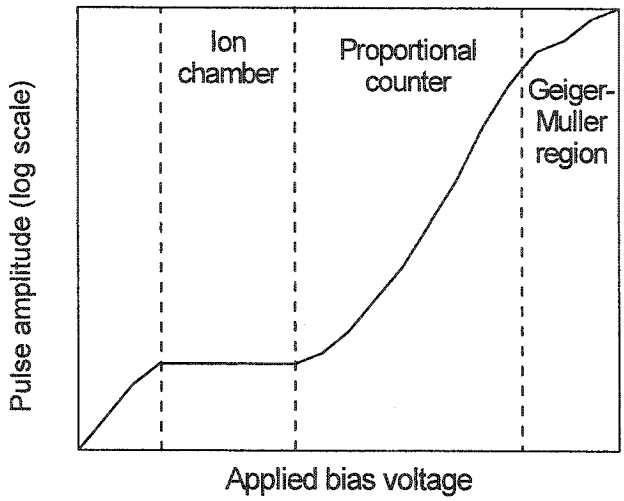


*Figure 4.1* Different charge collection behaviours according to applied bias voltage [From *Introductory Nuclear Physics*, John Wiley and Sons, Toronto, ON, Canada, p. 207, 1988].

Recombination effects are most important at low bias voltages. As the voltage is increased, a saturation region is reached where recombination is negligible. This saturation region is attained with bias voltages on the order of 300 V for the ionisation chambers used in this work. Beyond the saturation region, the bias voltage is sufficient to accelerate free electrons to have sufficient kinetic energy to ionise neutral atoms. This charge multiplication is known as a Townsend avalanche and is only stopped when all free electrons are collected at the anode. This is the principle behind the operation of proportional counters. At even higher bias voltages, charge collection enters the Geiger-Mueller region where secondary avalanches are produced. The avalanches are stopped when space charge effects around the anode effectively reduce the electric field and a quenching gas stops any positive ion from releasing an electron at the cathode [1, 4]. In *Figure 4.1*, the different regions are shown. The plateau region where ion chambers are operated is not perfectly flat and the collection efficiency correction, $P_{ion}$, takes this into consideration. The $P_{ion}$ correction for continuous radiation is measured with the half voltage technique and is given as:

$$P_{ion} = \frac{1.00 - (V_H/V_L)^2}{M^H_{raw}/M^L_{raw} - (V_H/V_L)^2}. \tag{4.1}$$

In equation (4.1) $V_H$ is the normal bias voltage, $V_L$ is a lower bias voltage, usually by half, than the normal bias voltage, $M_{raw}^{H}$ is the raw charge measurement at the normal bias voltage and $M_{raw}^{L}$ is the raw charge measurement at the lower bias voltage.

With the magnitude of the bias voltage set at 300 V to minimise recombination, other effects such as the bias voltage polarity must be taken into consideration. The polarity correction, $P_{pol}$, corrects electrometer measurements for any asymmetry in the measurement when the applied bias voltage is reversed. This difference is due to the measurement of charge not created in the sensitive volume of the chamber, but created at the electrodes or in the cable. The correction is defined as:

$$P_{pol} = \left| \frac{\left( M_{raw}^{+} - M_{raw}^{-} \right)}{2M_{raw}} \right| \tag{4.2}$$

where $M_{raw}^{+}$ is the charge (in nC) measured when the applied bias voltage at the biasing electrode is positive and $M_{raw}^{-}$ is the charge (in nC) measured when the applied bias voltage at the biasing electrode is negative. $M_{raw}$ is the charge (in nC) measurement taken at the normal bias voltage polarity for the chamber.

A source of the polarity effect is Compton current; that is, a photon interaction occurring directly on the collecting electrode that leads to the ejection of an electron that was not subsequently replaced by a landing electron. This effect is most notable in conditions where electron equilibrium has not yet been attained (see section 2.3). The ejected electron leads to a measurement not truly representative of the charge produced in the air cavity. When the biasing electrode is positive, the ionisation current (flow of electrons) moves from the power source to the collecting plate. An electron ejected from the collecting electrode forces the power source to compensate by increasing the ionisation current ($M_{raw}^{+} = \left| i_{+} + i_{Compton} \right|$). If the biasing electrode is negative, then the ionisation current moves from the collecting plate to the power source. The Compton current in this case is opposite to the ionisation current but of the same magnitude as when the collecting electrode was negative ($M_{raw}^{-} = \left| -i_{-} + i_{Compton} \right|$).

The polarity correction given in equation (4.2) cancels the Compton current from the measurement so as to have the true ionisation measurement.

An analogous situation to the polarity effect for photons exists for electron beams. When electrons stop on the collecting plate, the measurement at the electrometer is perturbed. Since the polarity effect for electron beams is opposite to the effect from photons (photons eject an electron while electron beams add an electron), a negative polarity at the biasing electrode of a parallel-plate chamber would lead to a higher measurement than the true ionisation ($M^{photons}_{raw} < M < M^{electrons}_{raw}$).

The last correction applied to measurements of charge from an ionisation chamber account for the ambient environment conditions in which the measurement was made. Temperature and pressure corrections are applied to return the measurement conditions to a set of reference environment conditions. These conditions are defined as a temperature of 295.15 K in North America or 293.15 K in Europe and a standard pressure of 101.325 kPa. Since the number of molecules in a given volume varies according to temperature and pressure, the collected charge depends on the number of molecules in the sensitive volume. A relationship between charge, pressure and temperature is derived based on the ideal gas law:

$$n = \frac{pV}{RT} \tag{4.3}$$

with $n$ representing the number of moles of air in the air cavity and proportional to the charge measurement M, $p$ is pressure, $V$ is volume, $R$ is the ideal gas constant and $T$ is the temperature. With equation (4.3), the temperature and pressure correction becomes:

$$P_{p,T} = \frac{M_{ref}}{M_{meas}} \propto \frac{n_{ref}}{n_{meas}} = \frac{\frac{p_{ref}V}{RT_{ref}}}{\frac{p_{meas}V}{RT_{meas}}} = \frac{p_{ref}}{p_{meas}} \times \frac{T_{meas}}{T_{ref}}. \tag{4.4}$$

Substituting the values of the reference conditions set above, the final relationship for the temperature and pressure correction is presented:

$$P_{p,T} = \frac{101.325}{p_{meas}} \times \frac{T_{meas}}{295.15\,K}. \tag{4.5}$$

The raw measurement initially obtained by the electrometer must therefore be corrected by the different correction factors:

$$M_{corr} = M_{raw} P_{p,T} P_{pol} P_{ion}. \tag{4.6}$$

This corrected measurement by itself does not give the dose deposited in water. To do this, we need an absorbed-dose to water calibration factor for a cobalt-60 photon beam, $N_{D,w}^{^{60}Co}$, traceable to a standards lab for the ionisation chamber used. The $N_{D,w}^{^{60}Co}$ calibration factor is defined as:

$$N_{D,w}^{^{60}Co} = \frac{D_w^{^{60}Co}}{M_{corr}} \tag{4.7}$$

where $D_w^{^{60}Co}$ is the dose to water from a cobalt-60 beam, usually determined with calorimetry methods, and $M_{corr}$ as previously defined.

Dose to water for any quality photon beam according to the AAPM's TG-51 protocol [3], $D_w$, is given by:

$$D_w = M_{corr} N_{D,w}^{^{60}Co} k_Q \tag{4.8}$$

with $k_Q$ a beam quality correction factor that is equal to 1.00 for a cobalt-60 radiation beam.

The sensitive volume of an ionisation chamber, as defined by the electric field, is the volume surrounding the collecting electrode where ions are collected. Ions produced inside the air cavity but not collected by the collecting electrode are considered to be outside the sensitive volume of the chamber and do not contribute to the measurement. To help define the sensitive volume, and to minimise leakage current between the two electrodes, guard electrodes surround the collecting electrode, as shown in *Figure 4.2*. There are two possible

arrangements for the two electrodes: the cylindrical ionisation chamber and the parallel-plate ionisation chamber. Both types have guard electrodes, although differently positioned, and were used to take measurements in the total body radiation field.

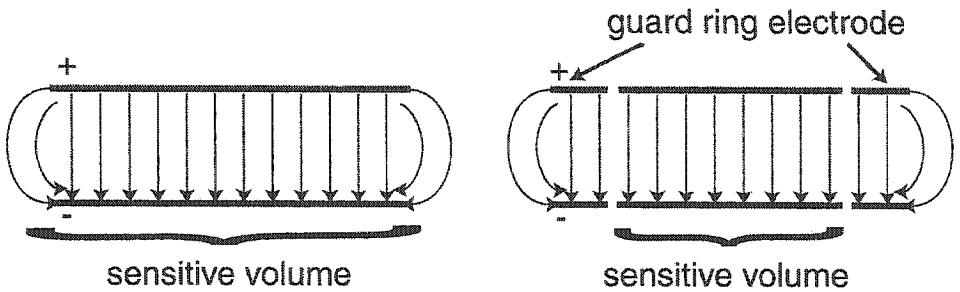


***Figure 4.2*** Electric field between two electrodes in a parallel-plate type chamber: in (a) edge effects are present in the definition of the sensitive volume, in (b) the guard ring electrode eliminate edge effect contamination of the sensitive volume.

Farmer-type ionisation chambers are recognisable by their cylindrical shape; they have an outer electrode wall shaped like a thimble while the central electrode is a conductive rod (see *Figure 4.3*). The small size of the rod limits the occurrence of Compton current and therefore, the polarity effects with this type of chamber. Neglecting edge effects, inside the outer electrode, the electric field, $\vec{E}$, is radially symmetric and has a magnitude of:

$$\left|\vec{E}\right| = \frac{\lambda}{2\pi\varepsilon_0}\frac{1}{r} \tag{4.9}$$

with $\lambda$ as the charge density along the central rod, $\varepsilon_0$ the free-space permittivity and $r$ the distance from the central rod. The ions produced in the sensitive volume between the two electrodes interact with the applied potential and a current is measured through the central electrode. The dose *point of measurement* is situated along the central electrode and in the centre of the sensitive volume defined by the electric field.

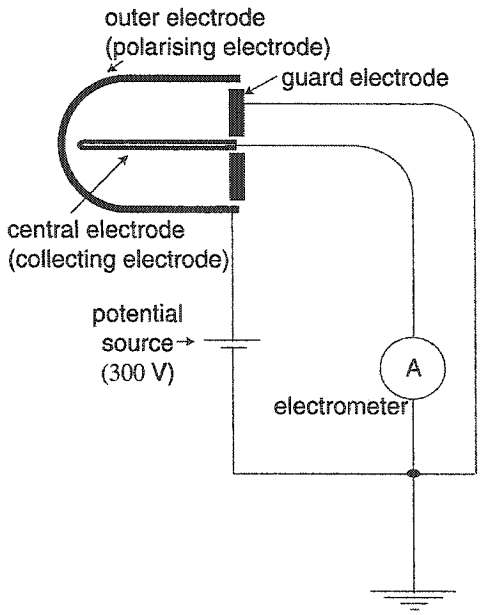


*Figure 4.3* Schematic diagram of a cylindrical ionisation chamber.

The first chamber used was manufactured by PTW-Freiburg (Freiburg, Germany), a 0.6 $cm^3$ Farmer-type ionisation chamber (type 30004) with an outer electrode wall composed of 0.425 mm thick graphite with a density of 1.85 $g/cm^3$ and with the inner electrode composed of 99.98% aluminium. The inner electrode is a rod 21.2 mm long with a 1 mm diameter. The chamber's effective *point of measurement* is 13 mm from its outer tip along the central electrode and a technical drawing is presented in *Figure 4.4* [5]. The chamber is vented and is not waterproof. Measurements with this chamber could only be conducted in solid phantoms, to be presented in section 4.2.

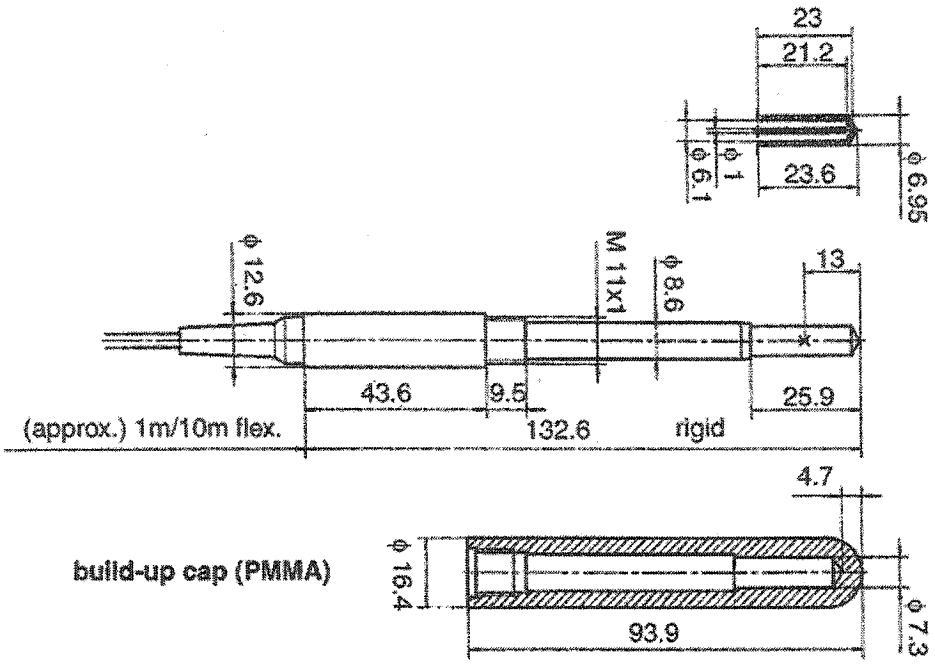


*Figure 4.4* Technical drawing of a 0.6 $cm^3$ Farmer-type ionisation chamber from PTW Freiburg. Measurements are in mm. [Figure taken from 0.6 $cm^3$ Farmer-Type Ionization Chambers Type 30001, Type 30002, Type 30004, Type 30006, Freiburg, Germany, 2000].

An IC 10 chamber was used with the "Wellhofer Dosimetrie" (Schwarzenbruck, Germany) watertank (to be presented in section 4.2). It is a compact cylindrical ionisation chamber. The IC 10 chamber wall, central electrode and cylindrical guard ring are made from plastic material, Shonka C 552, composed (by mass) of 2.473% hydrogen, 50.161% carbon, 0.453% oxygen, 46.529% fluorine and 0.384 % silicon and with a density of 1.76 $g/cm^3$ [6]. The wall thickness is 0.4 mm, the central electrode has a 1 mm diameter and is 3.8 mm long, and the chamber volume is 0.14 $cm^3$. The IC 10 chamber is waterproof and was only used in water.

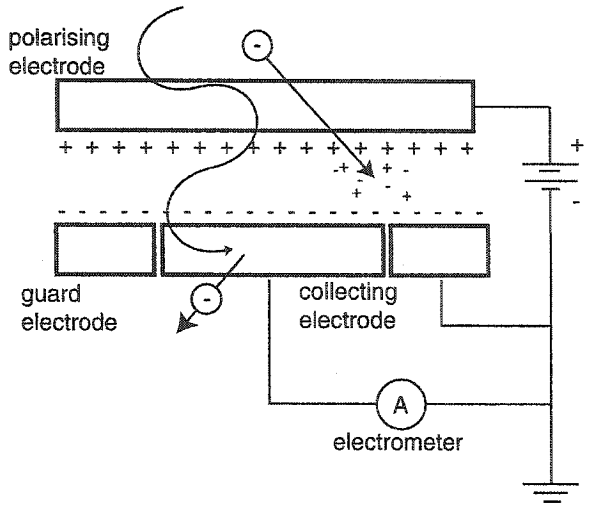


*Figure 4.5* Model of a parallel-plate ionisation chamber.

A parallel-plate ionisation chamber consists of two electrodes arranged to form a flat chamber as shown in *Figure 4.5*. A voltage is applied between the electrodes and the ions that are attracted to the collecting electrode produce a current from which an integrated charge is obtained by the electrometer. For a parallel plate ionisation chamber, the effective *point of measurement* is defined as being at "the front (upstream side) of the air cavity at the centre of the collecting region"[3].

The Roos End Window Chamber manufactured by PTW-Freiburg (Freiburg, Germany), model N34001, is a parallel-plate chamber with a front window and collecting electrode made of 1 mm thick acrylic. The gap between the front window and the collecting electrode is 2 mm and the chamber has a sensitive volume of 0.35 $cm^3$. Due to its thick front window, surface dose measurements (in the first mm depth) cannot be done. A wide guard ring surrounds the collecting electrode, minimising leakage of radiation across the insulator separating the front window with the collecting electrode. This chamber is waterproof, but it also has a customised solid water phantom within which it can be placed allowing for measurements in solid phantoms.

The Attix Plane-Parallel ionisation chamber (model 449) manufactured by Gammex/RMI (Middleton, WI, USA) has a thin Kapton front window, 0.025 mm thick and a collecting electrode consisting of a layer of 0.13 mm polyethylene (see *Figure 4.6*). The sensitive volume

for charge collection between the two electrodes is 0.127 $cm^3$. This chamber's thin front window made it possible to do surface dose measurements. The polarity effect was prominent for this chamber and a polarity correction was always applied to the raw measurements. The chamber is not waterproof and could only be used with solid phantoms. The Attix Plane-Parallel ionisation chamber has been assembled within a solid water phantom to form a single piece. Its final dimension was 30×30×2.5 $cm^3$[7].

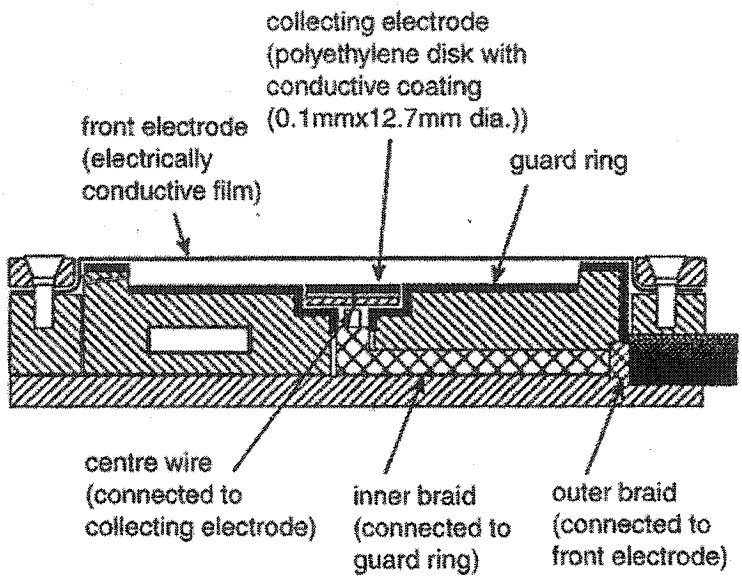


*Figure 4.6* Cross section of the Model 449 Attix plane-parallel ionisation chamber showing major components. [Figure from Attix Plane-Parallel ionisation chamber, Middleton, WI, USA, 1993]

### 4.1.2 Thermoluminescent dosimeters

Another relative dosimeter available when performing measurements on the radiation field for TBI are thermoluminescent crystals. This type of crystal accumulates radiation damage with time until stimulated by heat, when they emit an amount of light proportional to the accrued radiation damage. As such, thermoluminescent crystals are an example of a solid state integrating type dosimeter. The most common examples of crystals exhibiting thermoluminescent behaviour are lithium fluoride (LiF), calcium fluoride ($CaF_2$), calcium sulphate ($CaSO_4$) and aluminophosphate glass, when activated by magnesium and titanium [8].

Common uses for these crystals are for environmental and personnel dosimetry, and verification dosimetry inside small cavities.

A common thermoluminescent crystal is lithium fluoride. It is almost energy independent above 10 keV [8] with an effective atomic number of 8.2, near that of soft tissue at 7.4 [9]. The commercial thermoluminescent dosimeters (TLD) used were the Harshaw TLD-100 and TLD-700 crystals (Thermo Electron Corporation, Waltham, MA, USA).

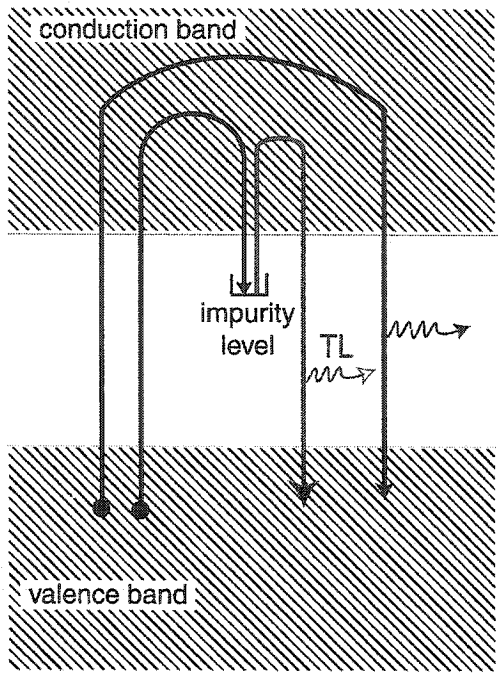


*Figure 4.7* Band structure of a thermoluminescent crystal.

Radiation damage is stored in TLD crystals in the form of trapped electrons as shown in *Figure 4.7*. These electrons, originally in the valence band, are excited to the conduction band following an interaction with an energetic electron. These energetic electrons are set forth after a photon interaction with the medium (either by the photoelectric effect, Compton scatter or pair production). Electrons in the conduction band lose their energy and return to a lower energy state. Some of these electrons do not return to the valence band, but are deposited in impurity energy levels present between the valence and conduction band. Most electrons remain in these impurity energy levels until they are re-excited to the conduction

band by heat. As they returned from the conduction to the valence band, photons in the visible range are emitted and read by a photomultiplier tube (PMT) present in a TLD reader.

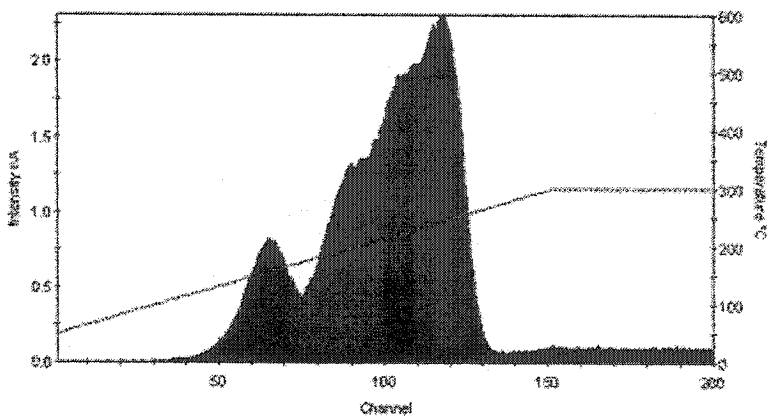


*Figure 4.8* Glow curve produced with HARSHAW QS 3500 system. Shaded area represents TLD response while line represents temperature of planchet.

The reading of the TLD crystals requires a heat source coupled to a PMT and a recording device. The system used was a HARSHAW QS 3500 (Thermo Electron Corporation, Waltham, MA, USA) and a micro-processor. The TLD crystal was placed on the planchet and the temperature of the planchet was raised up to 300°C while a PMT measured the amount of light emitted as a function of time to produce a glow curve as shown in *Figure 4.8*. If the abscissa were substituted for temperature instead of time, then the result would be a thermogram. The dose absorbed by the crystal is proportional to the area under the curve.

The calibration of TLD crystals required delivery of a known dose to the TLD crystals. A calibration factor was therefore obtained as the ratio of dose to that from the TLD reader measurement. Part of the calibration also entailed the verification of reproducibility of measurement for each TLD crystal, since a lack in reproducibility would indicate a defective crystal. Since the calibration factor was based on a known given dose, TLD crystals are relative dosimeters.

Before irradiation of the TLD crystals, it was important to eliminate any residual trapped electrons in the crystal lattice. The same preparation technique was used before irradiation of both the TLD-100 and TLD-700 crystals prior to calibration and measurement. This

annealing process began by heating the TLD crystals for one-hour at a temperature of 400°C, immediately followed by a two-hour annealing period at 100°C. The TLD crystals were then cooled down to room temperature before being irradiated.

TLD crystals come in a variety of forms (chips, wafers and powder). The particular TLD-100 crystals used to acquire measurements were 1mm×1mm×6mm rods and the TLD-700 crystals were 3.2mm×3.2mm×0.15mm chips. The chemical composition of the TLD crystals used was LiF: Mg,Ti with 7.5% $^{6}$Li and 92.5% $^{7}$Li for the TLD-100 crystals [9] and 100% $^{7}$Li for the TLD-700 crystals. The different chemical composition of the TLD crystals had an incidence on the ability of the crystal to detect dose from neutrons. Since these crystals were used in a cobalt-60 photon beam, sensitivity to neutron dose was not an issue. The particular clinical situation in which TLD crystals were used in conjunction with the modified cobalt-60 dedicated TBI technique will be presented in chapter 5.

### 4.1.3 Film dosimeters

The last of the dosimeter's used with the dedicated cobalt-60 photon beam for TBI was film. Film is an example of a chemical dosimeter consisting of silver halide grains suspended in a gelatine emulsion that is deposited on both sides of a polymer base. Photons interact with the silver halide grains in the emulsion and electrons are set in motion. Through collisions, the initial electron ionises its surroundings and frees many low-energy electrons. Electrons in the conduction band of the silver halide then combine with a positive hole in the silver halide lattice to form a silver atom. As such, this silver atom is unstable alone, but when two or more silver atoms are created in a given silver halide grain, it is stable and the grain is known as sensitised. Through this process of sensitisation, more and more sensitised silver halide grains are accumulated and a latent image is formed. The latent image is transformed into a fixed image through chemical reactions during processing.

The initial step in processing is placing the film in a bath of reducing agent. The reducing agent swells the gelatine without displacing the silver halide grains and converts sensitised silver halide grains to metallic silver. Following this bath, the film is placed in a "stopping" bath that stops the conversion of silver halide grains to metallic silver. Next, the film is placed

in a fixing bath. The purpose of this bath is to dissolve all the silver halide grains in the film that have not been converted to metallic silver. The last step for the development of the film is the washing of the film with water to eliminate any residual chemicals. Time spent in each bath affects the final image, and careful manipulation is therefore necessary. An RP X-OMAT Processor (Model M6B) from Kodak (Eastman Kodak Company, Rochester, NY, USA) was used to develop each film.

The metallic silver on the film post-development represents a visual indication for dose deposition. The greater the number of sensitised silver halide grains, the greater the amount of metallic silver and therefore the darker the film at that position. The optical density (OD) across a film is a measure of the darkening of the film and it is defined as:

$$OD = \log_{10}\left(\frac{I_0}{I}\right), \tag{4.10}$$

where $I_0$ was the intensity of the unattenuated light source and $I$, the light intensity with the film in place. The characteristic curve, also known as the Hurter and Driffield curve, is a graphical representation of the optical density with the logarithm of the relative exposure on the x-axis as shown in *Figure 4.9* [10].

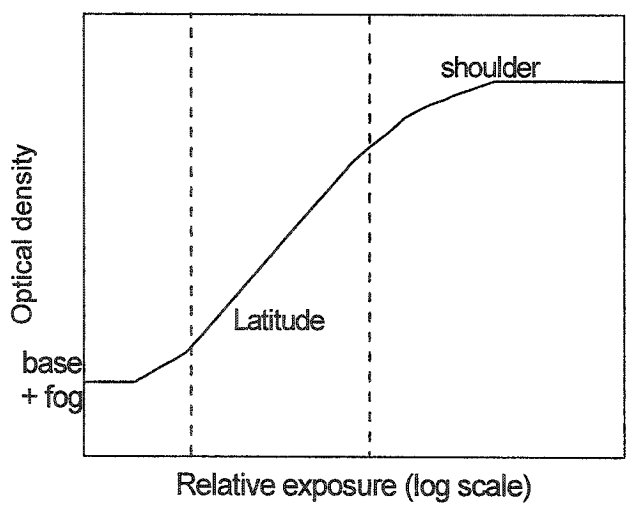


*Figure 4.9* Sample characteristic curve for film.

As shown in *Figure 4.9*, the characteristic curve does not go down to an optical density of 0 when the film is not exposed, but to a level indicated as base + fog. The polymer base is not transparent and attenuates the light source by a small amount. Fog is due to a small number of silver halide grains spontaneously sensitising and to the reducing bath converting un-sensitised silver halide grains into metallic silver. At the opposite end of the curve on *Figure 4.9*, the shoulder indicates that the film is nearing saturation levels due to the sensitisation of every silver halide grain available in the gelatine. Between those two extremes, a slope like relationship exists between dose and optical density and describes the latitude of the film.

Film is commonly used in clinical situations for localisation or verification purposes. Localisation films such as the Kodak Portal Pack PP-L film (Eastman Kodak Company, Rochester, NY, USA) were irradiated with low doses of the order of 2 cGy. Verification films such the X-Omatic V film (Eastman Kodak Company, Rochester, NY, USA) were irradiated with doses of the order of 100 cGy. The verification film was placed in an X-Omatic V radiation therapy cassette (Eastman Kodak Company, Rochester, NY, USA) that had a copper front screen and a black plastic back screen. The purpose of the copper front screen was to reduce film optical density, absorb scattered radiation and increase contrast [11]. The methods used to employ film will be described in chapter 5.

## 4.2 PHANTOMS

Discussion on dosimeters is incomplete without reference to the materials in which these measurements were conducted. Radiation dosimetry is conducted in phantom materials so as to mimic patient's composition and geometry. Protocols used in calibrating photon beams such as the American Association of Physicist in Medicine's (AAPM) TG-51 report recommend the use of water as a phantom [3]. Special equipment such as water tanks and waterproof chambers are to be used if water is the phantom. Solid alternatives such as Solid Water® are manufactured by Gammex-RMI (Middleton, WI, USA) to have a mass density and a number of electrons per gram close to that of liquid water have been developed [9]. Alternative solid phantoms were also available to mimic lung tissue and bone.

When using liquid water as a phantom, a "Wellhofer Dosimetrie" waterphantom (model WP 700) (Wellhofer, Schwarzenbruck, Germany) water tank was used. This system has the advantage that the ionisation chamber motion is computer controlled so that a variety of measurements can be done automatically. The inner dimension of the waterphantom, essentially the volume occupied by water, is an area of 48×48 $cm^2$ with a height that can reach 48 cm, determined when filling the Perspex container with water. Only the waterproof ionisation chambers can be used. Those chambers are the IC-10 cylindrical chamber and the Roos parallel-plate chamber described in section 4.1.1.

Solid Water® is a homogeneous phantom that has an average density of 1.035 $g/cm^3$ and an electron density relative to water of 1.015. This phantom is a water-equivalent plastic made of hydrogen, carbon, nitrogen, oxygen, chlorine and calcium and has an effective atomic number (Z) of 8.111, near that of water at 7.4. The phantom presents itself as sheets of a rigid red-brown plastic that is easily machined to allow openings for ionisation chambers or thermoluminescent dosimeters. The thickness of the 30×30 $cm^2$ sheets varied between 0.2 and 6 cm. Smaller sheets with the dimensions of 20×20×3 $cm^3$ were also available, either commercially or custom made. Every dosimeter, except the IC 10 ionisation chamber, presented in this chapter can be used with a Solid Water® phantom.

Another solid phantom produced to mimic lung tissue and named Solid Lung®, is also manufactured by Gammex/RMI (Middleton, WI, USA). It is made of an epoxy resin and has the same constituents as Solid Water®, but with different concentrations. It is a friable low-density phantom with an average density of 0.3 $g/cm^3$ [12]. Due to its friable nature, holes to accommodate ionisation chambers cannot be easily drilled and only TLD crystals and film can serve as dosimeters with this type of solid phantom.

## 4.3 SUMMARY

With the dosimeters and phantoms detailed in this present chapter and, with the radiation field produced with a modified cobalt-60 unit for TBI presented in Chapter 3, the tools necessary for the evaluation of the dedicated TBI field are given. The following chapter presents the

methods by which the large radiation field was studied and modified to be able to perform clinical TBI treatments.

## 4.4 REFERENCES

[1] G.F. Knoll, *Radiation Detection and Measurement*, 3rd ed., John Wiley and Sons, Inc., Toronto, ON, Canada, 2000.

[2] M. Boutillon and A.M. Perroche-Roux, "Re-evaluation of the W value for electrons in dry air", Phys. Med. Biol., **32**, 213-219, 1987.

[3] P.R. Almond et al., "AAPM's TG-51 protocol for clinical reference dosimetry of high-energy photon and electron beams", Med. Phys., **26** (9), 1847-1870, 1999.

[4] K.S. Krane, *Introductory Nuclear Physics*, John Wiley and Sons, Toronto, ON, Canada, 1988.

[5] "0.6 $cm^3$ Farmer-Type Ionization Chambers", PTW-Freiburg, Freiburg, Germany, 2000.

[6] "WP 700 and WP 700s: Operating Instruction for IBM-AT compatible computers", Wellhofer Dosimetrie, Schwarzenbruck, Germany, 1994.

[7] "Attix Plane-Parallel Ionization Chamber: Model 449 – User's Guide", Gammex/RMI, Middleton, WI, USA, 1993.

[8] W.H. Tait, *Radiation Detection*, Butterworths, Toronto, ON, Canada, pp. 224-226, 1980.

[9] F.M. Khan, *The Physics of Radiation Therapy*, 2nd ed., Lippincott Williams and Wilkins, New York, New York, U.S.A., 1994.

[10] D.R. Dance, "Diagnostic Radiology with X-rays" in *The Physics of Medical Imaging*, Institute of Physics Publishing, Philadelphia, PA, USA, 1988.

[11] "Kodak X-Omat V Film", Eastman Kodak Company, Rochester, NY, USA, 1994.

[12] ICRU, "Tissue Substitutes in Radiation Dosimetry and Measurements", ICRU Report 44, International Commission on Radiation Units and Measurements, Bethesda, MD, USA, 1989.

# Chapter 5

# Methods



The implementation of a new technique to deliver a total body irradiation treatment required a complete study of the radiation beam produced by the modified cobalt-60 unit. A first series of measurements were made in order to verify that the new unit met safety regulations. A second set of measurements was then made to acquire data to construct a flattening filter. With this flattening filter in place, a last series of measurements was taken to study the dosimetric properties and absolute output of the radiation field.

## 5.1 SAFETY CONSIDERATIONS

### 5.1.1 Wipe test

According to the Nuclear Substances and Radiation Devices Regulations from the Canadian Nuclear Safety and Control Act, the integrity of a sealed radioactive source must be verified every 12 months when a source is in clinical use and every 24 months when in storage. A leak test was therefore conducted on the cobalt-60 source when it was taken out of storage after 18 months. An alcohol-moistened filter paper was wiped in the vicinity of the source. The wipe medium was analysed so as to detect leakage contamination. The expected measurement was negative indicating no radioactive substance leak due to the source.

### 5.1.2 Room survey

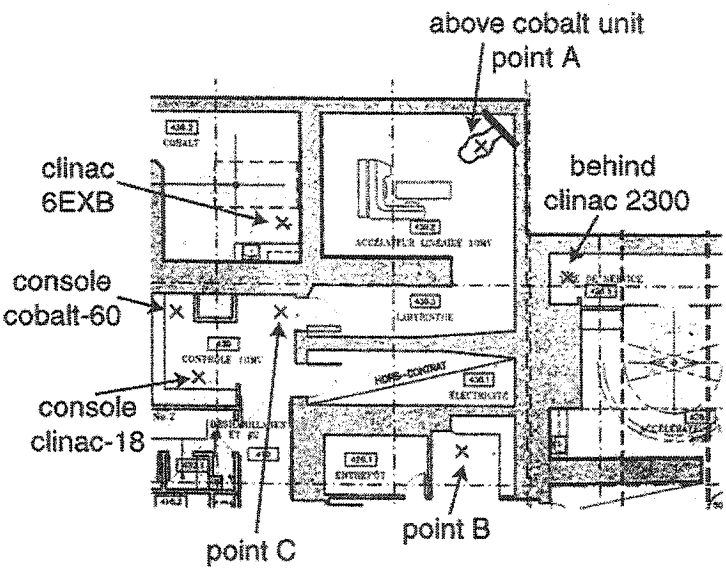


*Figure 5.1* Room layout of vault with the modified cobalt-60 unit as well as surrounding rooms. Crosses indicate sites for room survey measurements.

Once the source integrity was established, the operation of the newly installed modified cobalt-60 unit proceeded. Source integrity was not the only safety concern to be verified: room shielding to minimise any leakage of radiation outside the treatment vault was also analysed. To verify adequate shielding, a room survey with a calibrated survey meter (model Victoreen 450P) was conducted in the vicinity of the vault with the radiation beam on. The different

sites for measurements are indicated in *Figure 5.1*. Following verification and fulfilment of all the safety requirements, measurements continued with the modified cobalt-60 unit to construct the flattening filter.

## 5.2 CHAMBER AND PHANTOM POSITIONING

A cylindrical Farmer-type ionisation chamber and solid water combination were used to take many of the measurements of the cobalt-60 radiation beam. A solid water phantom, 12×30×30 $cm^3$, served as the basis of the set-up. A hole was bored in the phantom with its centre 15 cm from either side and at a depth of 9 cm from the phantom surface, and the ionisation chamber with a solid water build-up cap fit in this hole. Solid water was then added below the block until the total solid water phantom had dimensions of 30×30×32.2 $cm^3$. The entire solid water phantom then rested upon a 7.7 cm thick slab of Styrofoam, as indicated in *Figure 5.2*. This set-up was used to measure attenuation coefficients and beam profiles through the radiation field.

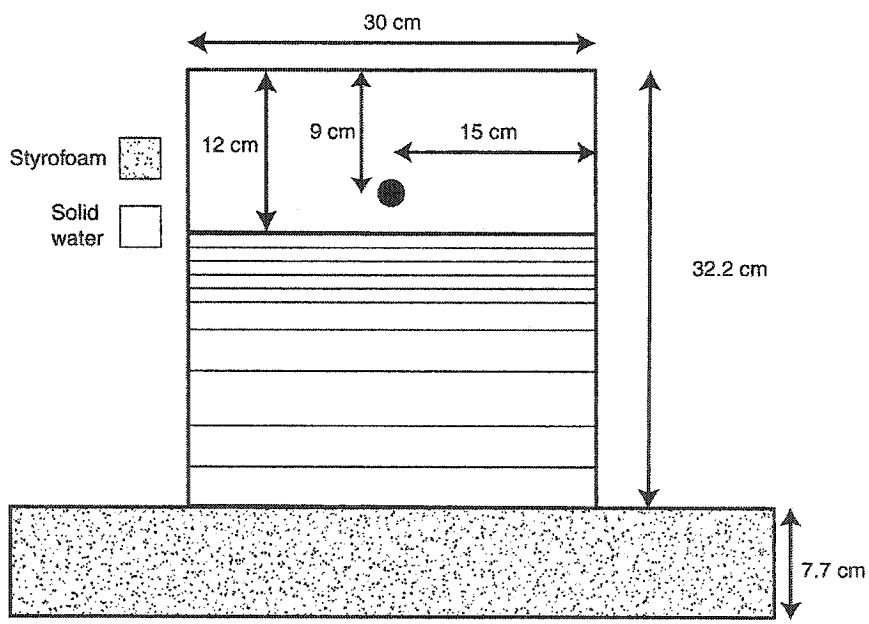


*Figure 5.2* Set-up of solid water above Styrofoam with hole for Farmer-type ionisation chamber.

## 5.3 LEAD AND CERROBEND ATTENUATION

Lead and CerroBend were used for the construction of attenuators and shielding used for this work. The advantages of using lead were its high density (11.36 g/cm$^3$) and atomic number (82) giving it high attenuation characteristics. If an attenuator was needed for complicated organ shapes (lungs, liver, kidney, etc.) [1], then CerroBend could be used instead. CerroBend, an alloy with 50% bismuth, 26.7% lead, 13.3% tin and 10% cadmium, can be poured into any desired shape due to its low melting point (70°C). CerroBend also has a relatively high density (9.76 g/cm$^3$) and effective atomic number (76.9) giving it high attenuation characteristics. Measurements to determine the thickness of lead and CerroBend required to attenuate the radiation dose by a given amount were conducted two different ways. The first was to determine the broad-beam attenuation coefficient with the attenuator material placed near the source while the second was with the attenuator material placed above the patient.

When the attenuator material was placed near the source, most photons reaching the dosimeter probe had passed through the attenuator while, when the attenuator material was placed above the patient, a large proportion of photons reaching the dosimeter probe would be scattered photons (see *Figure 5.3*). It is due to this difference that two attenuation coefficients were measured, since attenuator material would be placed near the source to construct a flattening filter and near the patient when organ dose attenuation was necessary.

An attenuation curve was measured by placing an ionisation chamber in solid water as in section 5.2 at the centre of the radiation field. The first measurement was performed without any attenuating material placed in the radiation beam and then successive measurements were taken with varying thickness of material placed at one of two positions (below the radiation source or above the patient) at the centre of the radiation field. The measurements were normalised to the first measurement and plotted against the thickness of attenuating material present in the field.

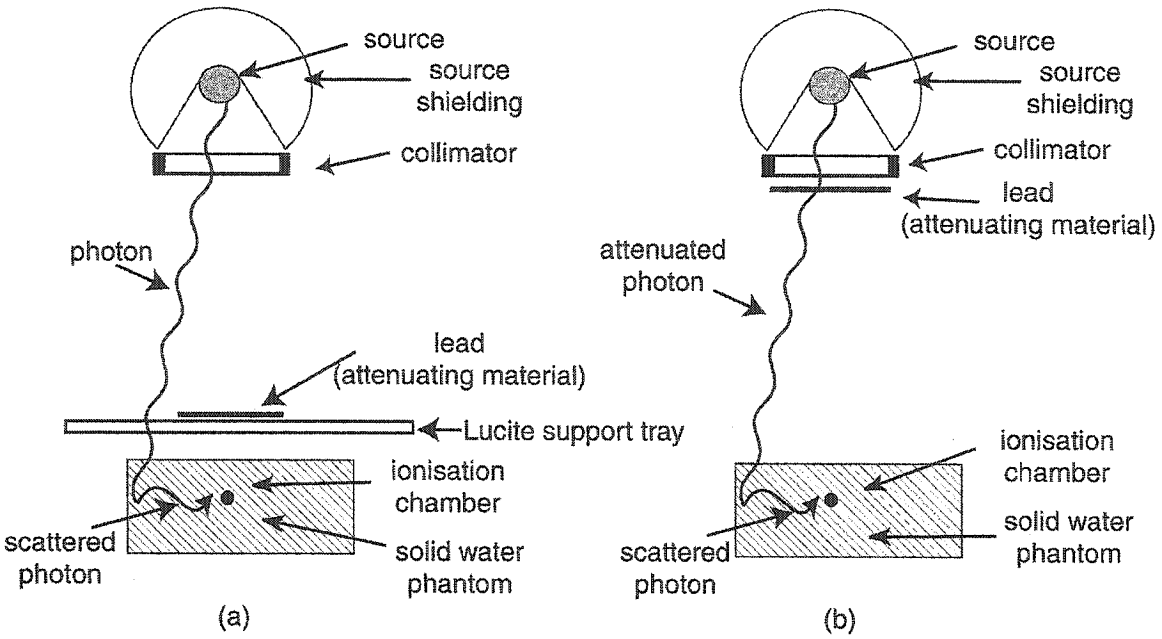


*Figure 5.3* Photon attenuation measurements depend on the position of the attenuating material. In a) the attenuating material was near the chamber and scattered photons not initially attenuated could reach the chamber. In b) the attenuating material was near the source and all photons were attenuated before reaching the chamber.

Alternative methods to measure an attenuation curve were conducted with thermoluminescent crystals and with the Attix and Roos ionisation chambers in a solid water phantom. Each measurement consisted of an irradiation time of one minute for all ionisation chambers and of four minutes for the thermoluminescent crystals. Measurements made with all ionisation chambers were repeated twice while measurements made with TLD-700 crystals used three thermoluminescent crystals at a time.

Lead sheets with thicknesses of 0.4 mm, 0.75 mm and 1.75 mm were used to create a wide range of lead attenuators. CerroBend sheets varied in thickness between 2.5 and 5.2 mm. The lead attenuation curve was determined in the two possible positions (below source and above patient) while for CerroBend, the attenuation curve was measured directly above the phantom, on a Lucite support tray located 42 cm above the floor

From the attenuation curve, the half-value layer (HVL) could be determined. The HVL is defined as the thickness of material necessary to attenuate the beam of radiation to half its

original intensity. For a mono-energetic radiation beam, such as from a cobalt-60 source, every successive half-value layer is equal and the attenuation coefficient (μ) is given by:

$$\mu\left(cm^{-1}\right) = \frac{\ln 2}{HVL(cm)}. \tag{5.1}$$

Equation (5.1) is based on the exponential attenuation of the photon fluence in the attenuating material as $I = I_0 e^{-\mu x}$ where $I$ is the intensity of the beam past a thickness $x$ of attenuating material, $I_0$ is the original intensity and $\mu$ is the attenuation coefficient of the attenuating material [2]. As mentioned previously, the geometry of the set-up affects the final result. Furthermore, attenuation coefficients found in the literature are for narrow-beam, not broad-beam geometry. Scattered radiation reaching the dosimeter may change the attenuation coefficient and values obtained from equation (5.1) may differ from values in the literature.

## 5.4 BEAM PROFILES

With the attenuation from the lead known, the next step in the construction of a flattening filter is to determine the shape and thickness of lead required. This is done by first measuring the beam profile (i.e. the relative dose at numerous locations across the radiation field at a fixed depth in the phantom) from which isocontour lines are then extracted. Beam profiles were measured both in solid water and in a three-dimensional waterphantom (described in section 4.2) for comparison purposes.

The same solid water and ionisation chamber combination was used to take measurements throughout the radiation field as presented in section 5.2. Measurements were taken across a grid formation throughout the radiation field. The radial symmetry of the source emission was observed and taken advantage of to reduce the number of measurements to a quadrant. The measurement grid along the patient inferior to superior aspect, as well as the lateral aspect is indicated in *Figure 5.4*. The shape and thickness of the flattening filter was then determined from the isocontours. Once the flattening filter was installed, a second set of profiles was obtained to confirm beam flatness.

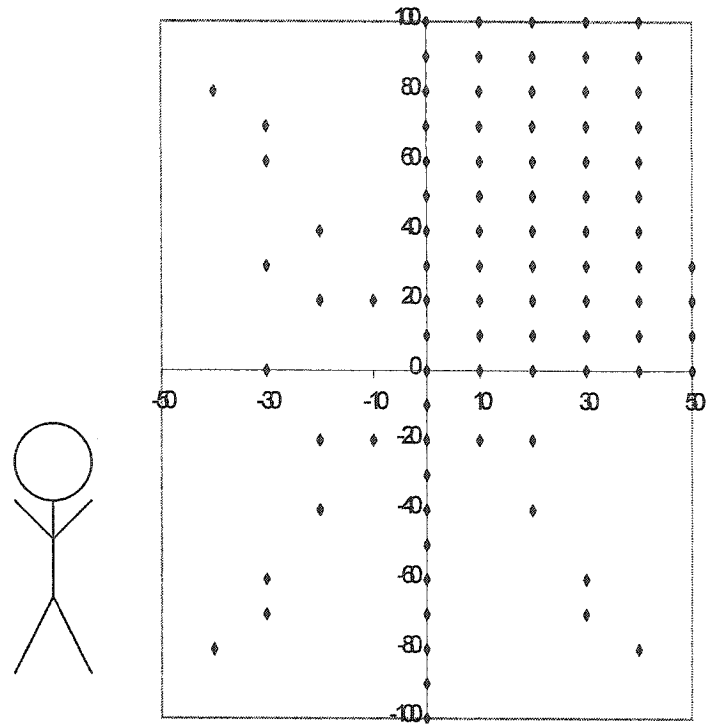


*Figure 5.4* Measurements in grid formation taken in a solid water phantom of the radiation field. The distance in cm from the central axis is indicated as well as the patient orientation.

Following the production of the lead custom flattening filter from data acquired with a solid water phantom, beam profiles were acquired with the three-dimensional waterphantom to confirm solid water measurements. The surface of the water was set at 211.2 cm from the source (corresponding to a water height of 40 cm). Profiles were measured with the waterproof IC 10 chamber at different depths. Unlike the point measurements taken in solid water, the waterphantom allowed a scan motion of the chamber in all three cardinal as well as diagonal directions. This meant that the chamber approached the edges of the three-dimensional waterphantom. The dimensions of the waterphantom were 50×50×50 $cm^3$, much less than the total body radiation field, set by the light field at 269×125 $cm^2$. The waterphantom was therefore moved to several locations in the large beam so as to produce composite measurements.

## 5.5 SHUTTER ERROR

When the cobalt-60 source is in transit in the head of the unit (for example, from the beam-off to the beam-on position), radiation is not instantaneously turned on and there is a period during which the dose rate increases to its full value as the source moves into the "ON" position. The same is true during the beam-off procedure. The time spent by the source in transit has an impact on the final dose and must be taken into consideration by measuring the shutter error. To determine the shutter error of the newly installed modified cobalt-60 unit, an ionisation chamber was placed in the radiation field and irradiated for 10 minutes. The following step was to irradiate the same ionisation chamber for the same total time, but by increments of 1 minute. The electrometer was only reset after the total ten-minute irradiation. The value of the shutter error, $\tau$, was obtained by comparing the dose rate of the two sets of measurements:

$$\frac{M_{10}}{t+\tau} = \frac{M_{10\times1}}{t+10\tau}. \tag{5.2}$$

In equation (5.2), $M_{10}$ is the charge obtained from a 10 minute irradiation, $M_{10\times1}$ is the charge obtained from a succession of 10 one minute irradiations and $t$ is the total set irradiation time at 10 minutes. Solving equation 5.2 for $\tau$ yields:

$$\tau = \frac{t\left(M_{10} - M_{10\times1}\right)}{M_{10\times1} - 10\cdot M_{10}}. \tag{5.3}$$

All measurements in the radiation field were constantly made without any correction for the shutter error, only using the set time as a reference. However, when irradiating patients or determining the absolute output, the time was corrected by the shutter error.

In the case where $M_{10\times1}$ was greater than $M_{10}$, the shutter error must be subtracted from the total irradiation time. In the opposite case, then the shutter error must be added. An alternative method by which the shutter error can be determined is graphically, by plotting the measurement on the electrometer as a function of the set irradiation time. By varying the set

irradiation time, a plot is built where the abscissa represents the shutter error. If the value at the abscissa is positive, then the shutter error must be added to the calculated time.

## 5.6 VERIFICATION OF THE INVERSE SQUARE LAW

The photon fluence produced by the cobalt-60 source, when sufficiently far to consider the source as a point-like object, varies inversely as the square of the distance from the source. This characteristic is often named "inverse square law". With the many modifications brought to the cobalt-60 unit, scattered radiation from the collimator and from the floor may invalidate the use of the inverse square law. Applicability of the inverse square law cannot be taken for granted and must be verified. To do this, a PTW-Freiburg Farmer chamber in a solid water build-up cap was used to measure points between the source and the floor, as presented in *Figure 5.5*.

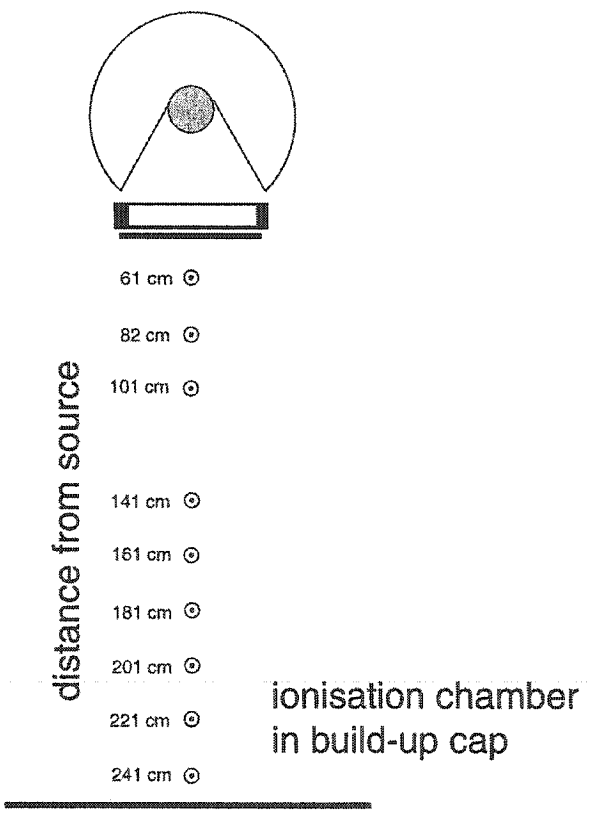


*Figure 5.5* Different positions of the cylindrical ionisation chamber in a build-up cap between the source and the floor.

The ionisation chamber's point of measurement varied with distance $A$ from the source and the measurements were corrected by the inverse square law $(A(cm)/A_{ref}(cm))^2$, with $A_{ref}$ referring to a standard patient source to surface distance taken to be 220 cm. Only if the corrected intensities were constant throughout the different source distances could the inverse square law apply.

## 5.7 PERCENT DEPTH DOSE

Percent Depth Dose (PDD) measurements were taken with the "Wellhofer Dosimetrie" water tank with the water level set at 221.2, 211.2 and 201.2 cm from the source. The Roos parallel plate chamber was placed in the centre of the radiation field with its front surface level with the surface of the water to determine the origin. During the data acquisition, the chamber was continuously moved up from the floor towards the water surface with the radiation beam on. The chamber measurements were subsequently normalised to form a PDD curve. A PDD curve was measured for each water level. A similar method was also used to measure a PDD curve with an IC 10 chamber with the water level set at 211.2 cm from the source.

A second method was used to measure PDD curves with a solid water phantom with which many different ionisation chambers were used. A similar set-up to that in section 5.2 was used for the PTW-Freiburg Farmer ionisation chamber but it was also modified to permit use of parallel-plate ionisation chambers. The depth of the ionisation chamber was varied within the solid water phantom by adding or subtracting solid water slabs. The measurements from the different ionisation chambers were then normalised by the measurement taken at a depth of 0.5 cm being $d_{max}$ for a classical cobalt-60 source [3].

## 5.8 SURFACE DOSE

Special attention was paid to the surface region and up to the classical depth of dose maximum at 0.5 cm for cobalt-60. Sheets of unexposed and developed Kodak Portal Pack Localization Imaging PP-L Film (Eastman Kodak, Inc., Rochester, NY, USA) were used as a thin layered substitute for water. Each sheet used had a thickness of about 200 μm. An Attix parallel plate ionisation chamber was used in the same set-up as used to determine PDD in solid water

(chamber, solid water and Styrofoam phantom with the upper surface height of 40 cm above the floor). Sheets of developed film were laid one by one above the chamber. The maximum thickness of the twenty sheets was 4 mm. Since the thinnest solid water sheet available was 0.2 mm, it was not possible to do a "true" PDD curve because the source-surface distance varied by increments of 0.2 mm. After ten sheets of film, a 2 mm thick sheet of solid water was removed below the Attix parallel plate chamber. It was assumed that the effect of a 2 mm error on the surface position would be negligible due to the large source to surface distance of approximately 211 cm. Knowledge of dose deposition within the build-up region of the phantom is important to determine how much bolus should be added onto the patient so as to bring the surface dose to maximum. Therefore, additional surface dose and build-up region measurements were conducted with different bolus combinations. These included a single bed sheet, a double-ply blanket and a sheet and blanket combination used in the past in the clinical situation to increase patient comfort.

## 5.9 MEASUREMENTS AT A SSD OF 80 CM

Most available data for radiation from a cobalt-60 source is given for source to surface (SSD) distances between 60 and 140 cm [3]. With an SSD of greater than 200 cm, and greatly modified collimating device, we could not compare the radiation beam from the modified cobalt-60 unit to tabulated data. In order to do this, Percent Depth Dose data was also acquired at an SSD of 80 cm with the Roos ionisation chamber in solid water phantom. Normally, cobalt-60 units did not have a flattening filter and the custom-made one for the modified unit was removed and substituted with a Lucite tray. Since the source head is fixed to the wall, the solid water was elevated to have an SSD of 80 cm. The depth of the Roos ionisation chamber in the solid water phantom was manually varied and the measurements normalised with the measurement at a depth of 0.5 cm, so as to construct a classical Percent Depth Dose curve.

## 5.10 TISSUE PHANTOM RATIO

Tissue Phantom Ratio (TPR) was measured with the chamber at two different source to chamber distances. For the first set-up, the chamber was 205 cm from the cobalt-60 source;

using the stretcher, Styrofoam slabs and solid water to raise the chamber surface to the proper height. In the second case, the chamber was positioned at 235 cm from the source; using only Styrofoam and solid water to raise the chamber to the proper height (see Figure 5.6). The Roos parallel plate ionisation chamber resting in its solid water phantom was used for both measurements and sheets of solid water were manually added above the chamber to change the depth of the ionisation chamber in the phantom. Measurements were normalised to a reference depth of 10 cm. TPR is an example of a dosimetric quantity used for source to axis distance (SAD) setups, with the source to surface distance varying. Since the source head is fixed at a certain height and patients vary in thickness, TPR data is typically used for clinical set-ups and calculations.

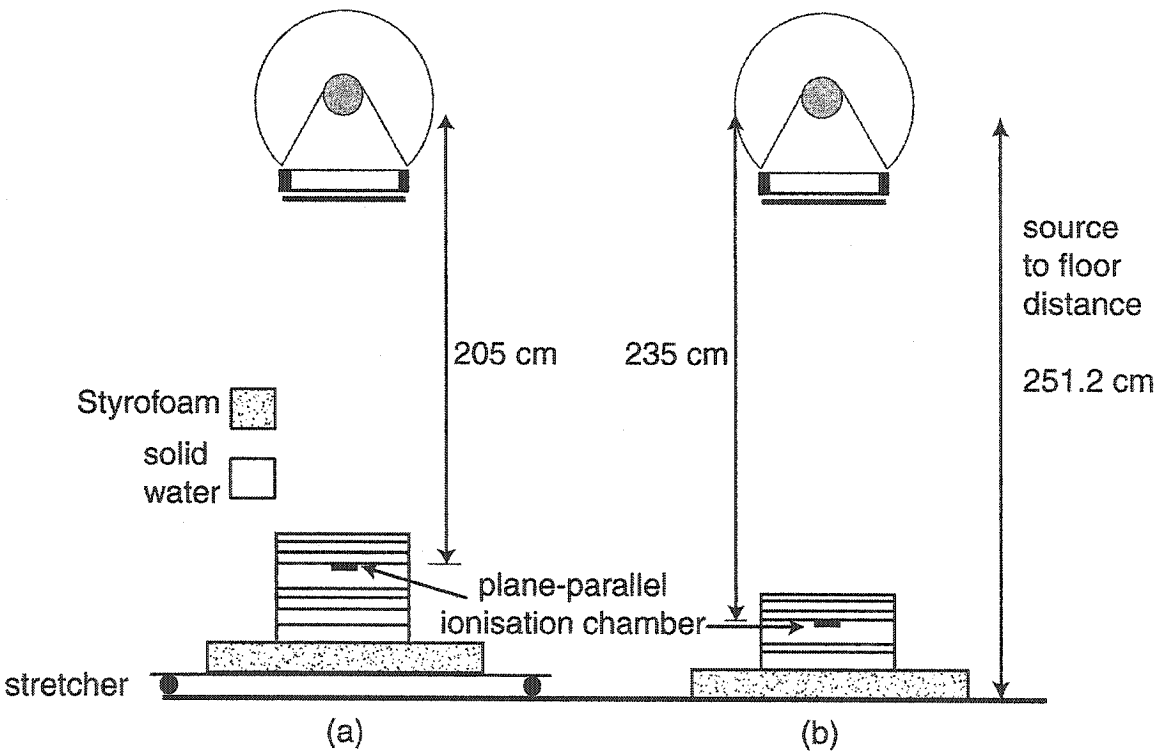


*Figure 5.6* (a) Set-up to measure TPR with the ionisation chamber at 205 cm from the source and (b) the set-up to measure TPR with the ionisation chamber at 235 cm from the source.

## 5.11 PHANTOM SIZE EFFECTS

Another possible source of dose variation is field area and phantom thickness. Since with the modified cobalt-60 unit, the field area is fixed, we varied the area of the phantom within the

field. TPR measurements with the Roos parallel-plate ionisation chamber at 235 cm from the source were repeated with solid water and bolus surrounding a 30×30 $cm^2$ wide phantom. Three different set-ups were used to reproduce different clinical situations. The first of these set-ups was the same as that used to determine TPR for clinical use. It consisted of Styrofoam and a solid water phantom, and represented the set-up with minimal backscatter since Styrofoam can be considered as air equivalent. The second set-up consisted entirely of solid water and represented the set-up with maximum backscatter. The last set-up consisted of three different sections of solid water atop a stretcher and mattress with a combination of bolus bags made to reproduce the patient scattering conditions. The different solid water blocks consisted of a 19.7×19.8×16 $cm^3$ phantom (head block), a 30×30×10 $cm^3$ phantom (chest block) and of an umbilical block where TPR measurements were conducted. A Roos ionisation chamber was used to carry out the measurements and was placed in the specially designed solid water phantom with dimensions of 30×30×4 $cm^3$. Two bolus bags on either side reproduced the arms and ten bolus bags represented both legs. They are all presented in *Figure 5.7.*

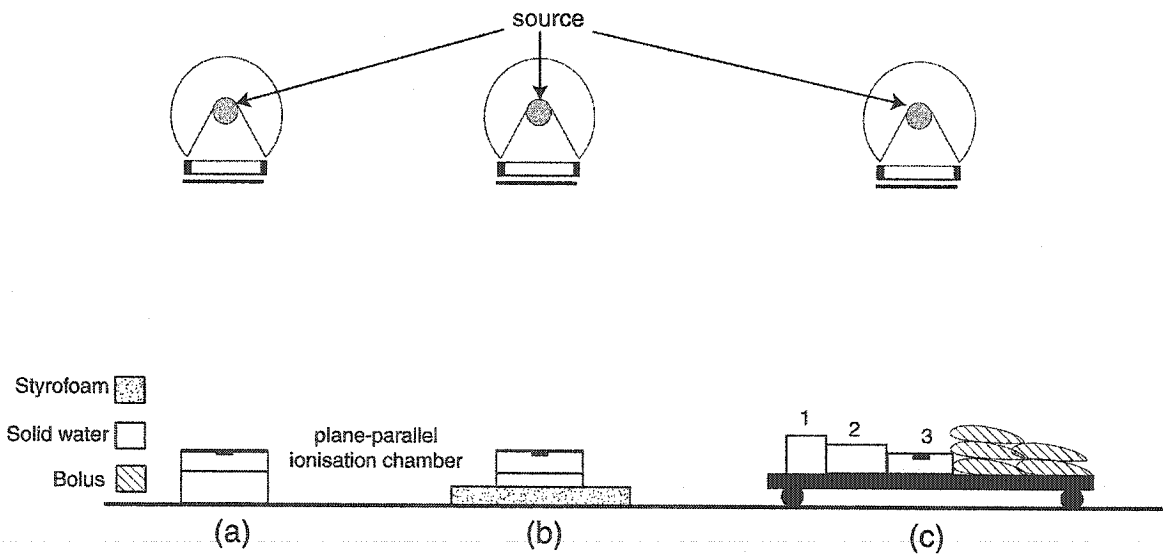


*Figure 5.7* Different phantom set-ups to measure TPR at 235 cm from the source. In (a), with maximum back-scatter conditions, in (b) with minimum back-scatter conditions and in (c), a simulated patient with: 1 the head block, 2 the chest block and 3 the umbilical block and bolus bag legs (shown) and arms (not shown).

Other verifications on the effects of phantom thickness on the final dose deposition were conducted. The first verification was based on measurements with the Attix ionisation

chamber at a depth of 0.5 cm in solid water to determine if the output was independent of the back-scattering thickness, whereby successive layers of solid water were removed from the phantom set-up. The inverse square law correction was applied to correct for the varying SSD. Another method substituted solid water with Styrofoam. The same 12 cm thick solid water and PTW-Freiburg Farmer ionisation chamber combination was used as described in section 5.2, but with the block upside-down so that the ionisation chamber was at a depth of 3 cm. Styrofoam was used as a solid water substitute because it is a low-density material that contributes very little scattered dose. The available Styrofoam slabs were 7.5 cm, 12.5 and 17.5 cm thick.

## 5.12 DOSE TO SOLID LUNG

Another source of dose variation is the presence of tissue inhomogeneities throughout the patient. The inhomogeneity causing the greatest dose variation is lung tissue. Solid lung has a density close to that of human lung at 0.3 g/cm$^3$, however ionisation chambers could not be easily used with solid lung due to the composition of the chamber and the complicated nature of the phantom. Thermoluminescent dosimetry (TLD) was therefore used to measure dose in the lung. A TLD phantom was assembled to model the patient's thorax with solid water and solid lung (see *Figure 5.8*).

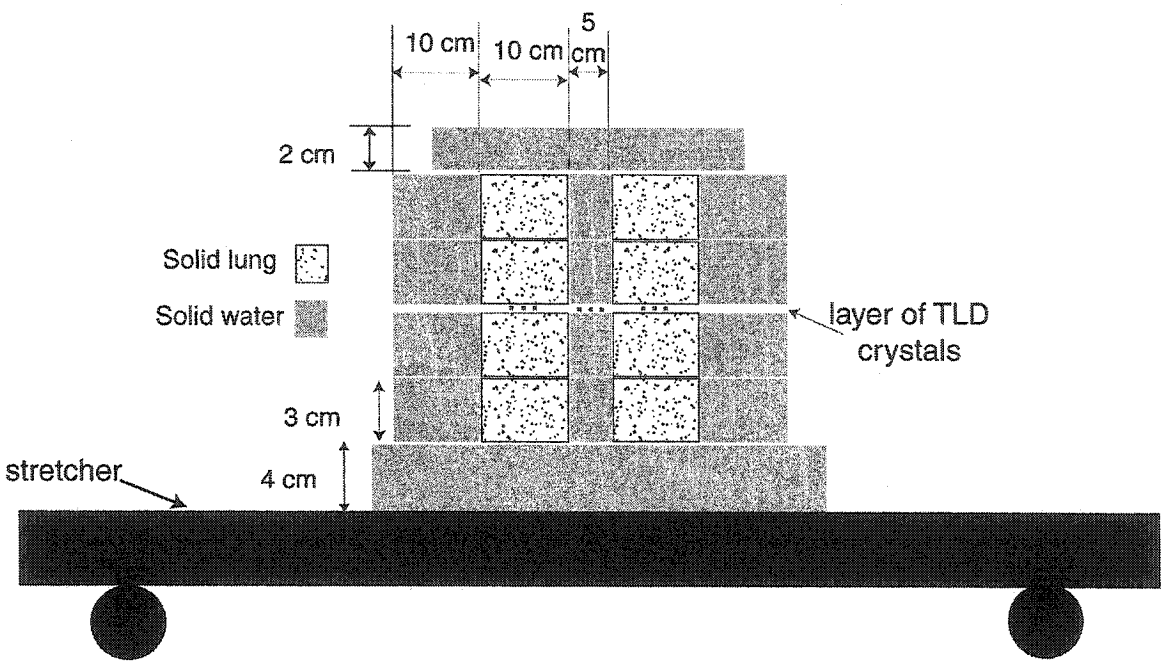


*Figure 5.8* Model of patient thoracic area with solid water and solid lung material to simulate tissue and lung. A total of 6 TLD's are shown in the solid lung phantom, and 3 TLD's are shown in the central solid water region.

The TLD-700 crystals were positioned in small slots located midway through the lung in the solid lung phantom and in the solid water phantom. Lead sheets (0.4 mm each) were added above the solid lung phantom on the Lucite support tray. The goal for this measurement was to determine the thickness of lead that would attenuate the beam so as to equalise the dose in the solid lung as compared to that in the solid water in the patients midline region.

## 5.13 ABSOLUTE OUTPUT

Measurements were carried out to determine the absolute output of the modified cobalt-60 unit. When acquiring absolute output information, the shutter error was accounted for. Measurements were made in water at a depth of 10 cm with a cylindrical waterproof ionisation chamber (Exradin, Middleton, WI, USA) having a calibration factor $N_{D,w}^{^{60}Co}$ traceable to the National Research Council Canada (NRCC, Ottawa, Canada) standard. Additional correction factors presented in section 4.1.1 were also applied. The height of the water was set at the same height as a patient would be at on the treatment stretcher so as to have similar source to

surface distances. Since it was dose to muscle and not dose to water that was desired, the dose measured by the ionisation chamber was multiplied by 0.99, the ratio of $f_{muscle}$ to $f_{water}$, where $f_{medium} = 0.876(\mu_{ab}/\rho)_{medium}$ with values for $(\mu_{ab}/\rho)_{medium}$ available in the literature for cobalt-60 photon energies.

## 5.14 SUMMARY

Beam data was acquired from the modified cobalt-60 unit used for total body irradiation. Most information was acquired with a variety of ionisation chambers and phantoms, but TLD-700 thermoluminescent crystals were also used. The priorities when evaluating the modified cobalt-60 beam were verification of safety issues, building of any additional beam modifiers and acquisition of data to plan clinical treatments.

The evaluation of the radiation field flatness and therefore of the flattening filter was accomplished by measuring beam profiles. Data necessary to plan clinical treatments included the Percent Depth Dose and the Tissue Phantom Ratio. Special attention was also given to possible effects near the surface of the patient's skin as well as the effects of bolus on the dose to skin. Since patients varied in thickness and in width, measurements were also conducted to verify any dependence of dose on patient size and changing source to surface distances. Finally, dose to patient inhomogeneities such as the lung was also measured with the necessary lead compensation needed to obtain uniform dose deposition throughout the patient. Results from the measurements done employing the methods described in this chapter are presented in chapter 6.

## 5.15 REFERENCES

[1] R. Corns et al., "Designing attenuators for total-body irradiation using virtual simulation", Med. Dosim., **25** (1), 27-31, 2000.

[2] H.E. Johns and J. R. Cunningham, *The Physics of Radiology*, 4th ed., Charles C Thomas, Springfield, IL, USA., 1983.

[3] E.G.A. Aird et al., *British Journal of Radiology Supplement 25: Central Axis Depth Dose Data for Use in Radiotherapy*, British Institute of Radiology, Volume 25, London, England, 1996.

# Chapter 6

# Results and discussion



## 6.1 SAFETY CONSIDERATIONS

Following the removal of the cobalt-60 unit from storage, a wipe test was performed to confirm the integrity of the source capsule. The reading was negative, meaning the source capsule was not leaking. Also, a complete room survey was conducted with the source in the on position with a calibrated survey meter and the results are shown in *Table 6.1* for positions previously shown in *Figure 5.1.* Limits are set by the Radiation Protection Regulations of the Canadian Nuclear Safety and Control Act and are shown in *Table 6.2* which also show the limits when the As Low As Reasonably Practicable (ALARP) principle is applied. The ALARP principle lowered by a factor of 10 the Canadian limits to radiation workers since they may be

exposed to sources of radiation exposure other than radiation leakage during their day to day activities.

*Table 6.1* Room survey for bunker with modified cobalt-60 unit for TBI

| Position | Measurement |
|---|---|
| Background measurement | Less than 0.77 mSv/y |
| Point A (above source head in parking area) | Less than 0.77 mSv/y |
| Point B (at console Clinac- 2300) | Less than 0.77 mSv/y |
| Point C (at vault door) | Maximum value of 17.65 mSv/y |
| Console cobalt-60 | 1.15 mSv/y |
| Console Clinac-18 | 1.53 mSv/y |
| Behind Clinac-2300 | 2.30 mSv/y |
| Clinac- 6EX B | Less than 0.77 mSv/y |

*Table 6.2* Radiation limits for nuclear energy workers and general public

| | **Canadian Radiation Limit** | **Canadian Radiation Limit ALARP applied** |
|---|---|---|
| **Nuclear Energy Worker** | 50 mSv/y | 5 mSv/y |
| **Nuclear Energy Worker (over 5 years)** | 100 mSv/5y average becomes 20 mSv/y | 2 mSv/y |
| **General public** | 1 mSv/y | |

The door was the area where the highest signal was measured with 17.65 mSv/y, followed by the Clinac 2300 vault with 2.30 mSv/y. Both are higher than the limit stated in *Table 6.2* when considering the ALARP principle, but they are still below the Canadian limit set for nuclear energy workers. As well, both areas are generally unoccupied during the delivery of total body irradiation.

## 6.2 LEAD AND CERROBEND ATTENUATION

The attenuation curves as measured with the methods described in chapter 5 are presented in this section. In *Figure 6.1*, attenuation data measured with lead placed near the source is presented, and these results were used to build the flattening filter for the new modified cobalt-60 unit used for total body irradiation.

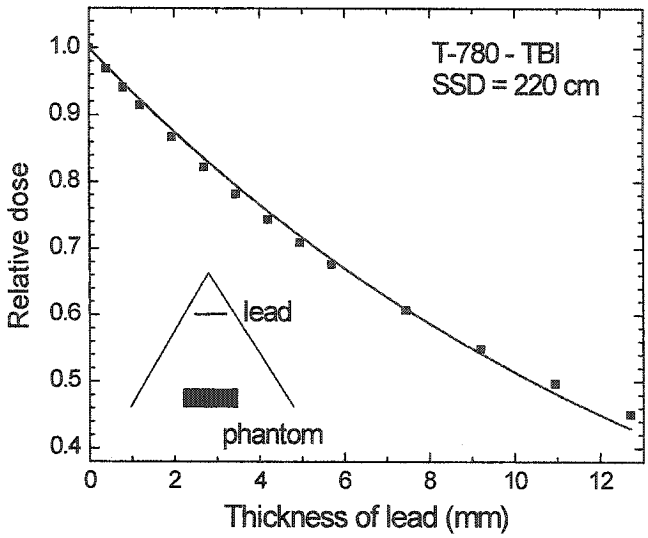


*Figure 6.1* Plot of the attenuation from lead placed near the source.

The lead sheets available for the construction of the flattening filter all have a thickness of about 0.4 mm. The available data was therefore fitted to an exponential decay and the following expression was obtained:

$$y = e^{-(0.0666 \pm 0.0009)x}. \tag{6.1}$$

The $R^2$ value is 0.996 and the $\chi^2$ value is 0.00013, indicating a good fit between data and the expression in equation (6.1). To build the flattening filter, another fit was used:

$$y = (0.205 \pm 0.008) + (0.792 \pm 0.008)e^{-x/(10.9 \pm 0.2)}. \tag{6.2}$$

The $R^2$ value for this fit was 0.99993 and the $\chi^2$ was 0.0000028. With this second fit, resulting beam intensities were calculated from a succession of 0.4 mm lead sheets later used to build a flattening filter.

Using equation (6.1) we have an attenuation coefficient equal to 0.0666± 0.0009 $mm^{-1}$ and a corresponding HVL = 10.4±0.1 mm Pb. Since equation (6.2) is not a straight exponential decay, we cannot determine an attenuation coefficient from it. Using the principle that a cobalt-60 source emits mono-energetic radiation and the attenuation coefficient found in the literature of 0.0660 $mm^{-1}$, the half value layer of lead in narrow-beam cobalt-60 radiation is

calculated to be 10.50 mm [1] which is in close agreement with the value determined experimentally. As mentioned in chapter 5, a difference is expected between the attenuation coefficients measured in narrow-beam and in broad beam geometry. Additional attenuation coefficient measurements were carried out using lead and CerroBend placed near the patient.

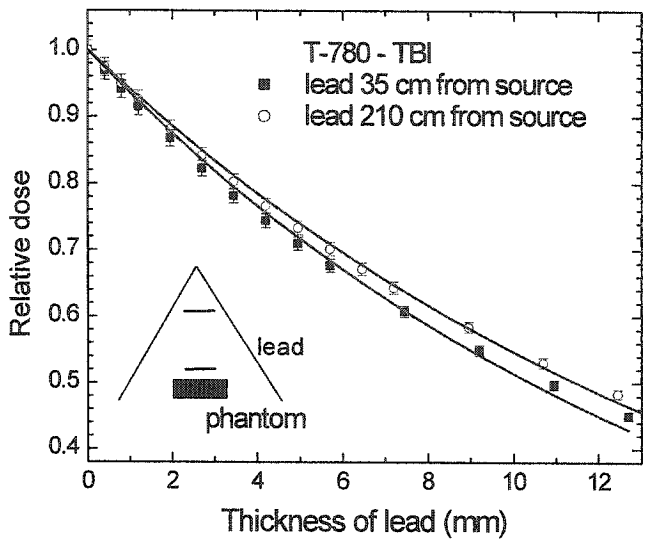


*Figure 6.2* Attenuation from lead placed near the cobalt-60 source and near the patient.

In *Figure 6.2*, the attenuation of lead placed near the source or near the patient is compared. The maximum difference in attenuation between the two is of the order of 3%, being greatest at maximum depth. An exponential decay fit of the attenuation of lead placed near the patient gives:

$$y = e^{-(0.0604 \pm 0.0006)x} \tag{6.3}$$

The $R^2$ value is 0.9978 and the $\chi^2$ is 0.00007, again showing a good quality of fit. The attenuation coefficient for lead placed near the patient is 0.0604±0.0006 $mm^{-1}$ and the HVL is 11.5±0.1 mm Pb. The difference between the value given in the literature (10.50 mm Pb) and the value obtained experimentally may be due to scattered unattenuated photons reaching the dosimeter.

Attenuation resulting from layers of CerroBend placed above the phantom in the radiation beam is presented in *Figure 6.3*. Measurements were conducted with an Attix ionisation chamber and with TLD-700 thermoluminescent crystals.

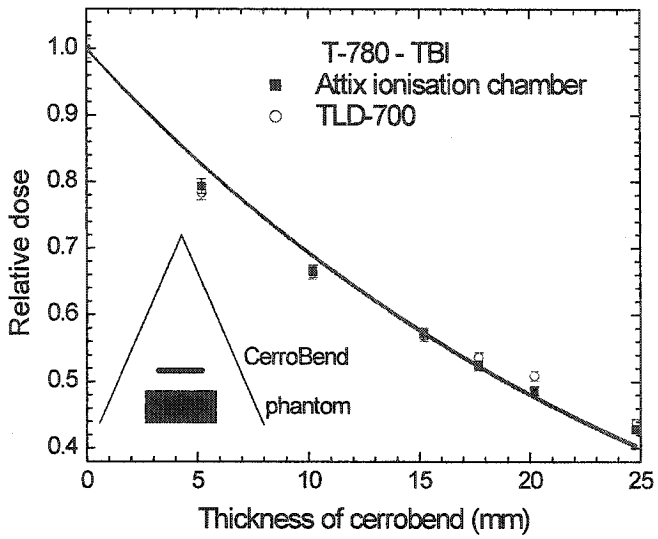


***Figure 6.3*** Plot of the attenuation from CerroBend placed near the patient as measured with an Attix ionisation chamber and with TLD-700 thermoluminescent crystals.

The correspondence between data collected with an ionisation chamber and with TLD-700 crystals is good except for that at 20.2 mm CerroBend. An exponential decay is fitted to the data collected with the ionisation chamber gives:

$$y = e^{-(0.037\pm0.001)x}. \tag{6.4}$$

The $R^2$ value is 0.989 and the $\chi^2$ is 0.00046. The attenuation coefficient of CerroBend is 0.037±0.001 $mm^{-1}$ and the HVL is 18.7±0.5 mm of CerroBend. The result from the exponential decay fit of the data collected with TLD-700 crystals is

$$y = e^{-(0.036\pm.002)x} \tag{6.5}$$

The $R^2$ value is 0.981 and the $\chi^2$ is 0.00077. In this case the attenuation coefficient is 0.036±0.002 $mm^{-1}$ and the calculated HVL 19±1 mm CerroBend. The attenuation coefficients

measured with the Attix parallel plate ionisation chamber and with TLD-700 crystals are essentially equal. A summary of the results is presented in *Table 6.3*.

*Table 6.3* Attenuation coefficients for lead and CerroBend

| Material | Positioning | Method | $\mu$ | $R^2$ | $\chi^2$ |
|---|---|---|---|---|---|
| Lead | Near source | IC* | 0.0666±0.0009 | 0.996 | 0.00013 |
| Lead | Near patient | IC | 0.0604±0.0006 | 0.9978 | 0.00007 |
| CerroBend | Near patient | IC | 0.037±0.001 | 0.989 | 0.00046 |
| CerroBend | Near patient | TLD** | 0.036±0.002 | 0.981 | 0.00077 |

* IC = ionisation chamber
** TLD = thermoluminescent dosimeter

## 6.3 SYMMETRY STUDY

The initial measurements across the field were acquired in solid water to establish the radial symmetry of the field. *Figure 6.4* through *Figure 6.6* show the measurements taken along two different diagonals crossing the patient at their umbilicus. Both diagonals were at an angle of ±26.6° to the longitudinal axis of the patient to accommodate the rectangular nature of the field size. The different quadrants are identified in relationship to a patient lying supine in the radiation field.

The agreement between all diagonals indicates radial symmetry throughout the field. The greatest discrepancy was observed with the lower left quadrant, and it is on the order of 1% at the field's extremity, as shown by the percent difference curve on *Figure 6.4* through *Figure 6.6*. As a consequence, measurements taken in a quadrant are mirrored to the other three quadrants of the field to simplify the production of the flattening filter.

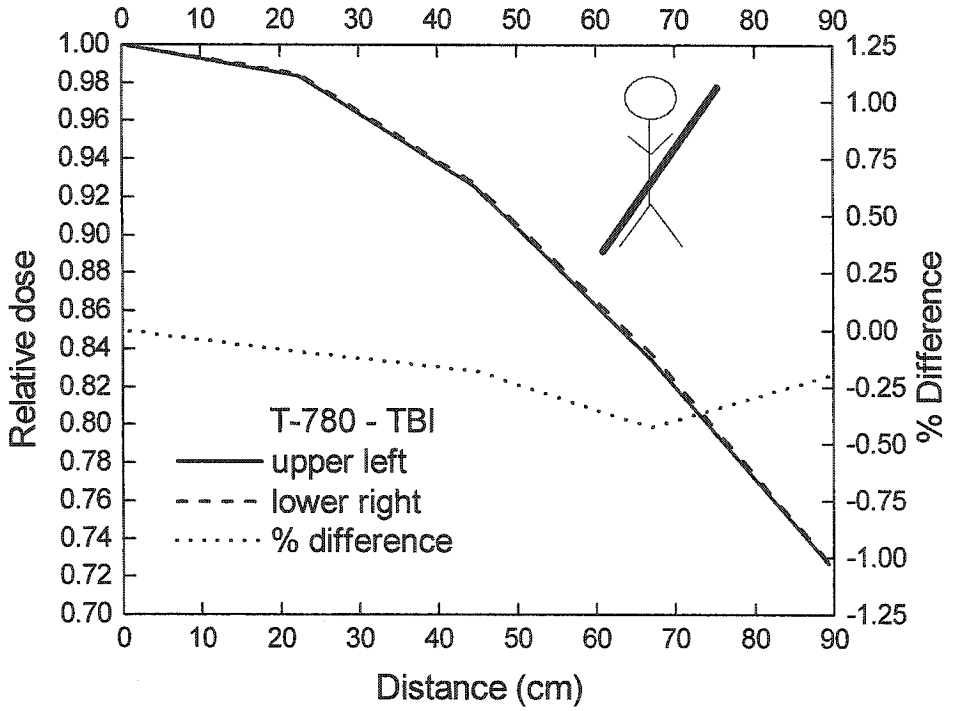


(a)

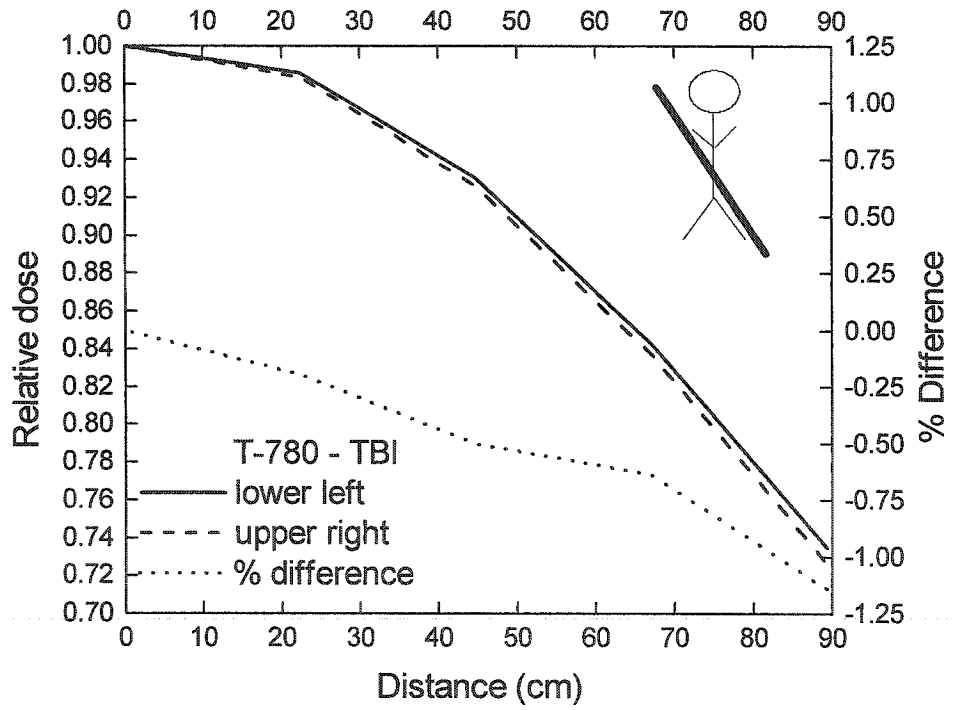


(b)

*Figure 6.4* Left hand axis represents off-axis ratios while the right hand axis represents difference in percentage between the two curves. In (a) the radial symmetry is compared between the upper left and lower right quadrants while in (b) it is for the lower left and upper right quadrants.

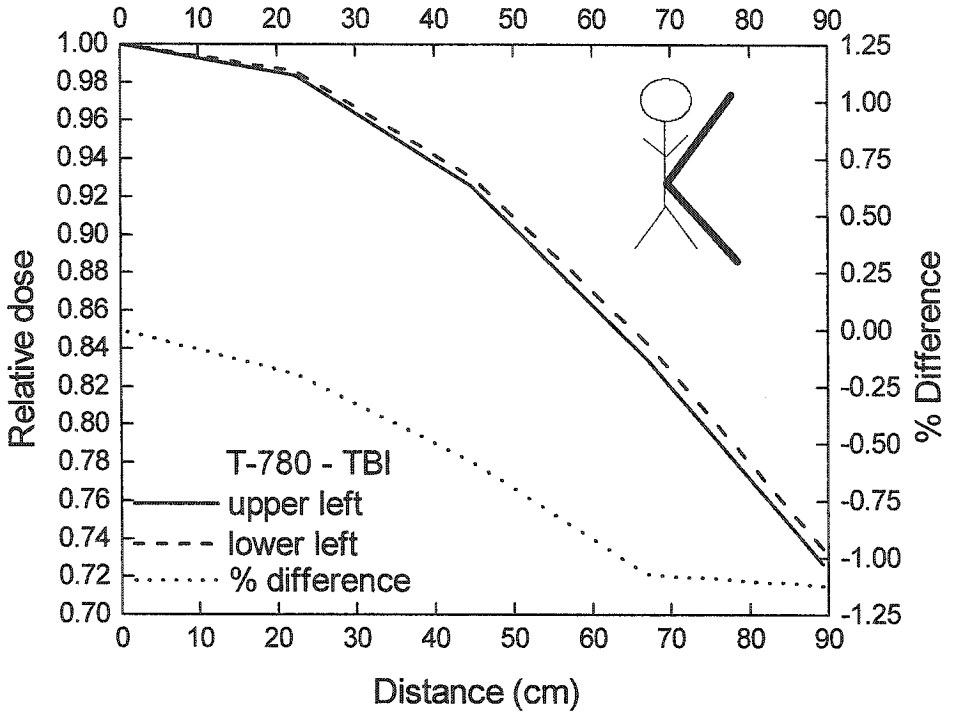


(a)

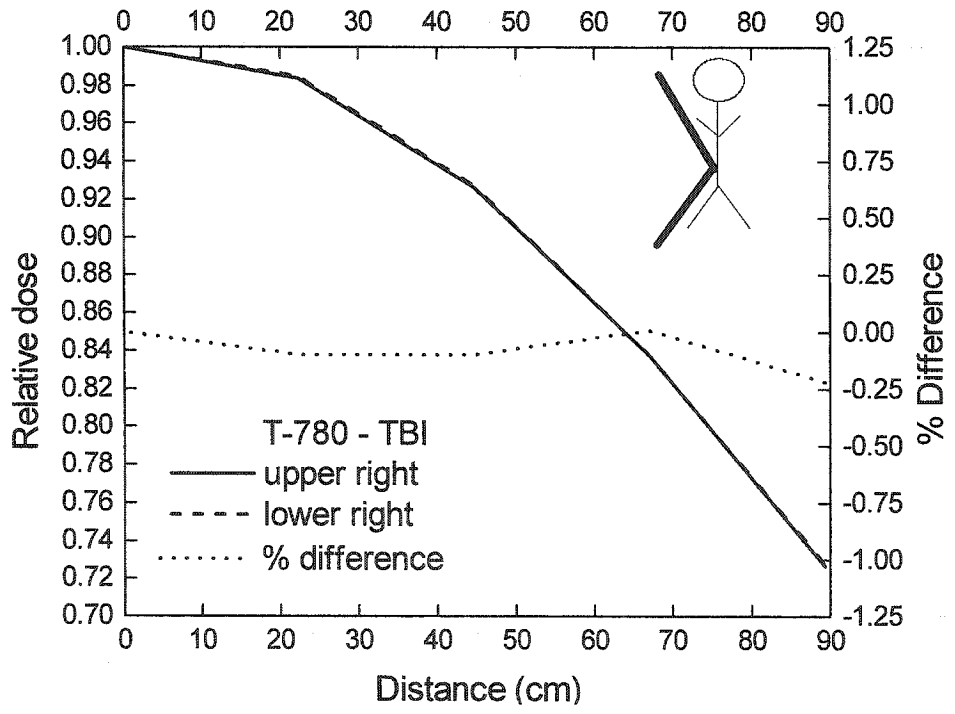


(b)

*Figure 6.5* Left hand axis represents off-axis ratios while the right hand axis represents difference in percentage between the two curves. In (a) the radial symmetry is compared between the upper and lower left quadrants while in (b) it is for the upper and lower right quadrants.

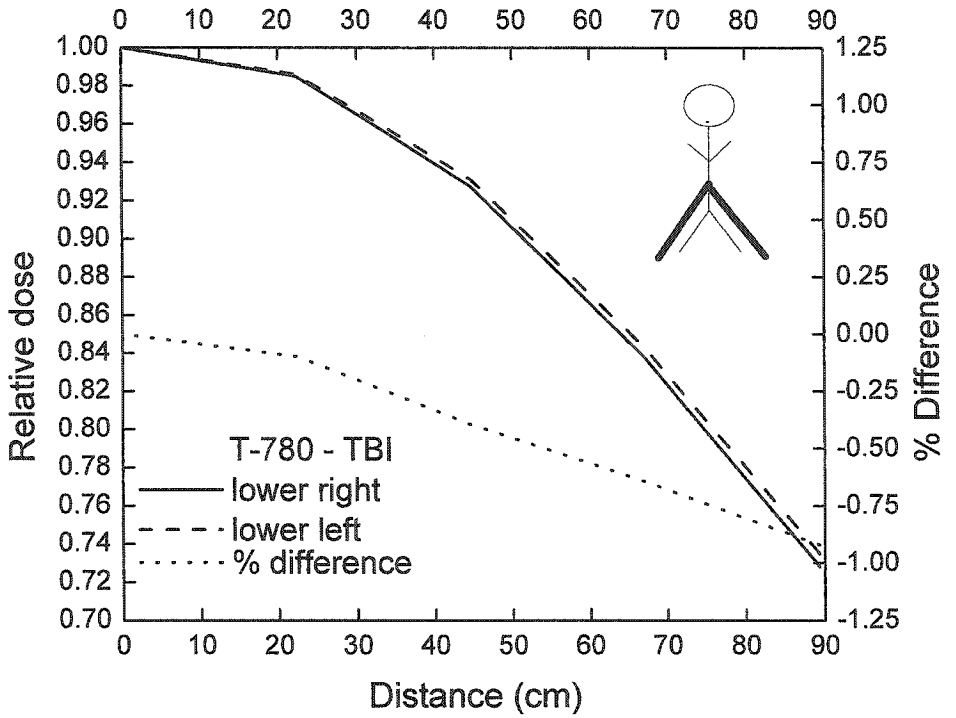


(a)

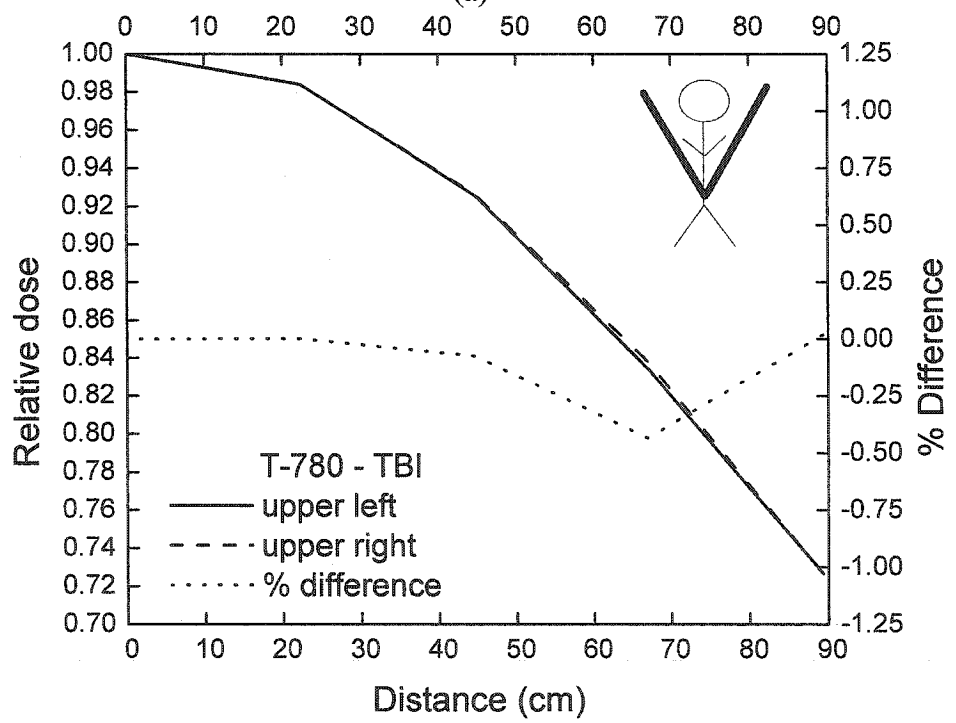


(b)

*Figure 6.6* Left hand axis represents off-axis ratios while the right hand axis represents difference in percentage between the two curves. In (a) the radial symmetry is compared between the lower right and left quadrants while in (b) it is for the upper right and left quadrants.

## 6.4 FLATTENING FILTER

Measurements to determine the dimensions of the flattening filter were taken in a grid formation in the upper left quadrant (as shown in *Figure 5.4*). The grid measurements were mirrored to the other three quadrants and used to form isodose contour lines (*Figure 6.7*).

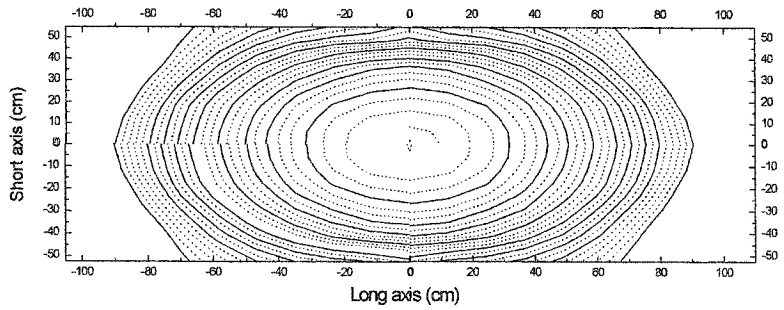


*Figure 6.7* Succession of isodose contour lines, only the full lines selected were used to build the custom flattening filter.

The flattening filter was constructed from a succession of lead sheets with a thickness of 0.4 mm. The resulting relative dose for different number of layers, as calculated with equation (6.2), is presented in *Table 6.4*. The isodoses corresponding to an available lead thickness are marked in *Figure 6.7* as full lines.

*Table 6.4* Beam intensity attenuation from 0.4 mm layers of lead.

| Number of layers | Total thickness of lead (mm) | Relative dose |
|---|---|---|
| 0 | 0 | 1.00 |
| 1 | 0.4 | 0.97 |
| 2 | 0.8 | 0.94 |
| 3 | 1.2 | 0.92 |
| 4 | 1.6 | 0.89 |
| 5 | 2.0 | 0.86 |
| 6 | 2.4 | 0.84 |
| 7 | 2.8 | 0.82 |
| 8 | 3.2 | 0.80 |
| 9 | 3.6 | 0.78 |
| 10 | 4.0 | 0.75 |

A scaling of *Figure 6.7* was required to have the proper dimensions at the accessory tray below the collimator and the scaled contour lines were used as a template to cut the lead sheets into the required shape. Mirror images of the contour lines were used for the three other quadrants. Two additional sheets of lead were placed in the centre of the field on an empirical basis, with the goal of improving the overall flatness of the radiation field. *Figure 6.8* shows the final flattening filter designed to flatten a beam area 180 cm long and 80 cm wide.

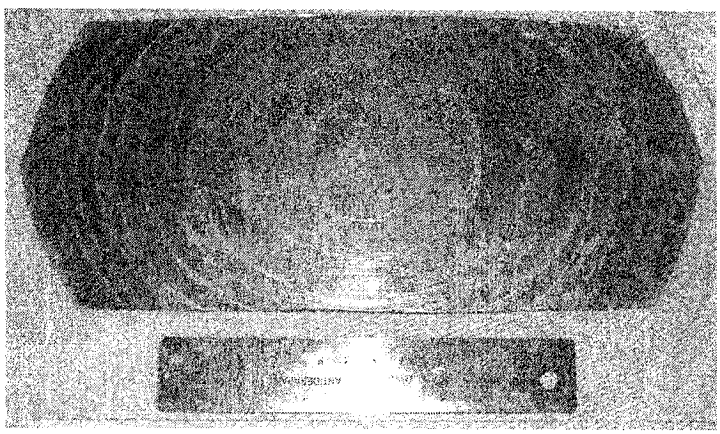

*Figure 6.8* Custom flattening filter made of 0.4 mm sheets of lead used to flatten the radiation field of the modified cobalt-60 unit. A 15 cm long ruler serves as a reference to scale.

Verification of beam flatness with the custom flattening filter was conducted with the 3D waterphantom at different depths in water and in a solid water phantom at a depth of 9 cm. The data acquired with the IC 10 ionisation chamber in the Wellhofer water tank suffered from a high level of noise due to the low signal at the extended SSD and was subsequently smoothed as shown in *Figure 6.9*.

The beam profiles are relatively flat under the flattening filter. Beyond the flattening filter, the beam profiles behave as they would if there were no flattening filter. Flatness specification was defined in chapter 2 as a variation to within ±3% of the central axis measurement within 80% of the field size. This specification was met at a depth of 10 cm, as expected since the flattening filter had been designed to flatten the radiation beam at a depth of 9 cm in solid water.

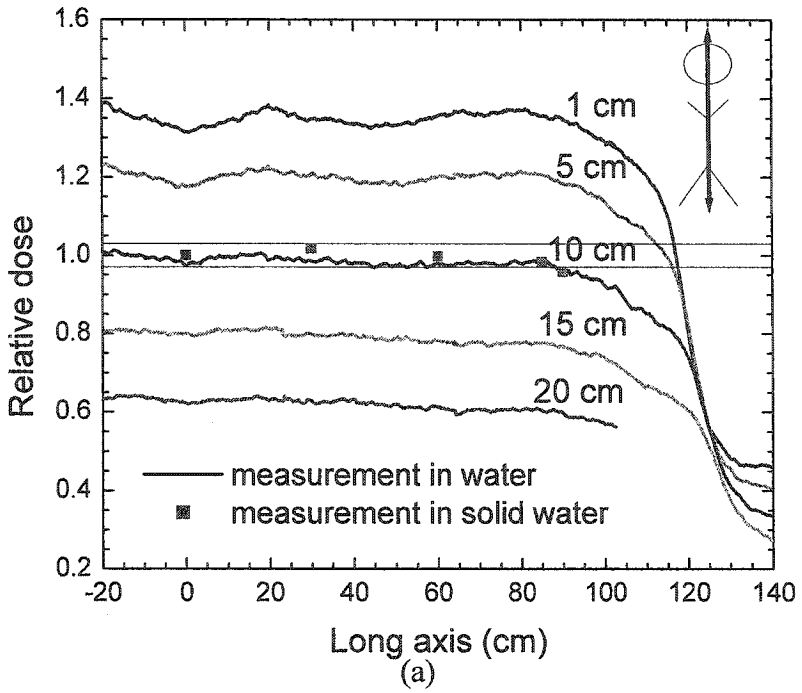


(a)

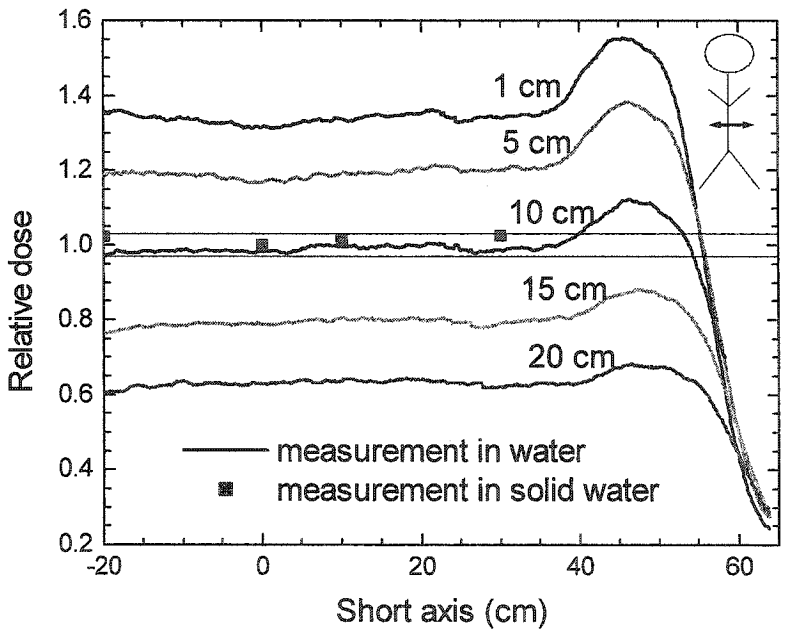


(b)

*Figure 6.9* Beam profiles acquired in the Wellhofer 3D waterphantom with the IC 10 ionisation chamber at various depths in water and with a Farmer-type ionisation chamber at a depth of 9 cm in solid water (SW). The different profiles are normalised with respect to the profile at a depth of 10 cm. Graph (a) shows the beam profiles along the long axis of the radiation field while (b) shows the beam profiles along the short axis of the radiation field.

The beam profiles in *Figure 6.9* did not cover the whole range along their respective axes since it was determined from measurements in solid water that the field was symmetric within ± 0.5%. The water tank was displaced four times along the long axis and twice along the short axis to be able to cover the area from the central axis towards one of the limits of the field. All the curves were normalised with respect to the beam profile measured at a depth of 10 cm. From the beam profile we can determine the length of the field along both axes. The beam profile at the 50% level was 122 cm on the long axis and 58.4 cm on the transverse axis from the central axis point at a source to surface distance of 221.2 cm. The radiation field dimension was therefore 244×116.8 $cm^2$ 30 cm above the floor, or 277×132.6 $cm^2$ at floor level versus the dimensions of the light field measured at 269×125 $cm^2$.

## 6.5 SHUTTER ERROR

The shutter error was calculated according to the method described in chapter 5. Data collected 235 cm from the source with a Roos ionisation chamber is presented in *Table 6.5*. The standard deviation was taken as the error of the average measurement.

*Table 6.5* Measurements used to calculate the shutter error of the modified cobalt-60 unit

| Irradiation | Measurement I | Measurement II | Average |
|---|---|---|---|
| One irradiation of 10 minutes | 7.8761 nC | 7.8711 nC | 7.874 ± 0.002 nC |
| Ten irradiations of 1 minute | 8.0208 nC | 8.0222 nC | 8.0215 ± 0.0007 nC |

With these measurements, the shutter error was calculated to be 0.0208±0.0003 minutes. At the console of the modified cobalt-60 unit, the time can only be entered with a precision of up to two digits beyond the decimal. The times entered at the console are therefore corrected by a shutter error of 0.02 minutes. In this case, the shutter error must be subtracted from the calculated beam time.

Additional series of measurements were carried out to determine the shutter error at different distances from the source. The results are shown in *Table 6.6*.

*Table 6.6* Shutter error for modified cobalt-60 unit.

| Distance from source | Shutter error (minute) |
|---|---|
| 235 cm | 0.021 |
| 221 cm | 0.021 |
| 141 cm | 0.022 |
| 80 cm | 0.023 |

As the dosimeter nears the source, the shutter error increases since the solid angle of the dosimeter to the source drawer beyond the shielding is greater, as shown in *Figure 6.10* and as indicated in *Table 6.6*.

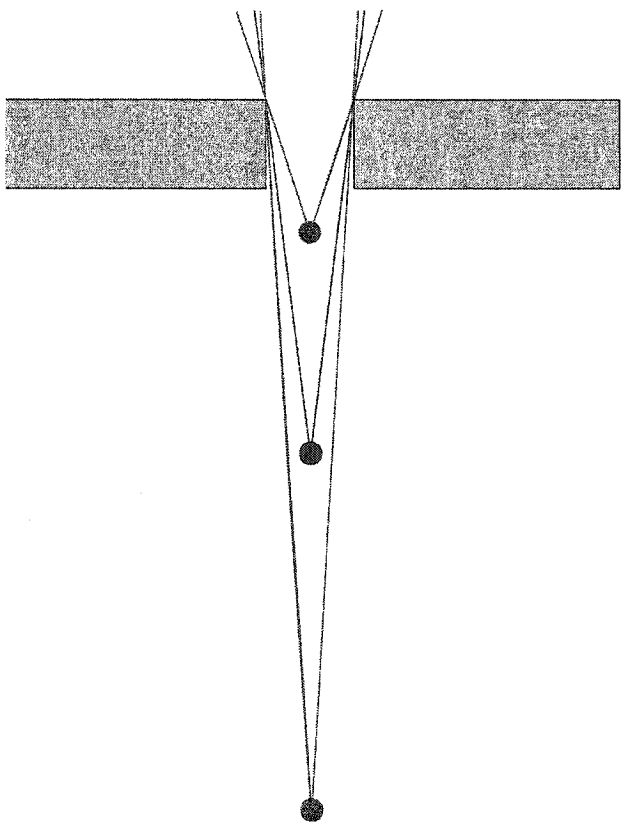

*Figure 6.10* Variation in solid angle view from the source drawer to the ionisation chamber.

## 6.6 INVERSE SQUARE LAW VERIFICATION

Verification of the applicability of the inverse square law for the large radiation field was measured with a Farmer-type ionisation chamber in a build-up phantom.

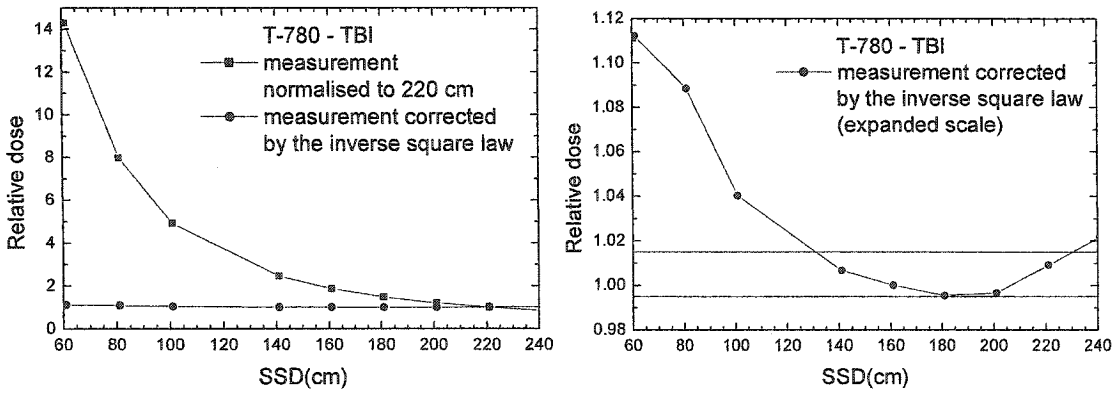


***Figure 6.11*** Measurements taken with a Farmer type ionisation chamber at SSD's from 60 to 240 cm. *Figure 6.11* (a) shows the measurements normalised at 220 cm and the measurements corrected by the inverse square law. *Figure 6.11* (b) presents the measurements corrected for the inverse square law on an expanded scale.

In *Figure 6.11*, the inverse square law correction applied to the normalised measurement was:

$$\left(\frac{(SSD(cm)+0.5\,cm)}{(SSD_{ref}(cm)+0.5\,cm)}\right)^2. \qquad (6.6)$$

The *SSD(cm)* was the source to surface distance in centimetres and the $SSD_{ref}(cm)$ was a reference distance set at 220 cm from the source. From *Figure 6.11* (a), we see that the inverse square law correction brings the normalised data to a nearly straight line, producing a deviation from unity up to 10%. *Figure 6.11*(b) indicates the range with which the inverse square law deviates by less than ±1%. Van Dyk conducted a similar verification of the inverse square law on a modified cobalt-60 unit and similar results were reported [2]. Since the bottom of the modified collimator is situated 29 cm below the source, scattered radiation from the collimator reaching the ionisation chamber will increase the measurement near the collimator. A similar effect is seen near the floor where floor scatter will increase the measurement. In-air measurements are thus too greatly affected by scattered radiation in the large field to be used for clinical dosimetry.

## 6.7 MEASUREMENT OF PERCENT DEPTH DOSE CURVES

In *Figure 6.12* (a), the percent depth dose curves measured at different SSD's are compared. The three PDD curves are similar to one another. From this observation, the percent depth dose curve can be considered as SSD independent in the region were the patient rests (200 to 220 cm away from the source). In *Figure 6.12* (b), the percent depth dose curves measured in different phantom and with different chambers are compared. The IC 10 ionisation chamber measurements do not agree with the parallel plate ionisation chambers (Attix and Roos) past a depth of 10 cm. The IC 10 ionisation chamber was not used to determine the PDD for dosimetric considerations.

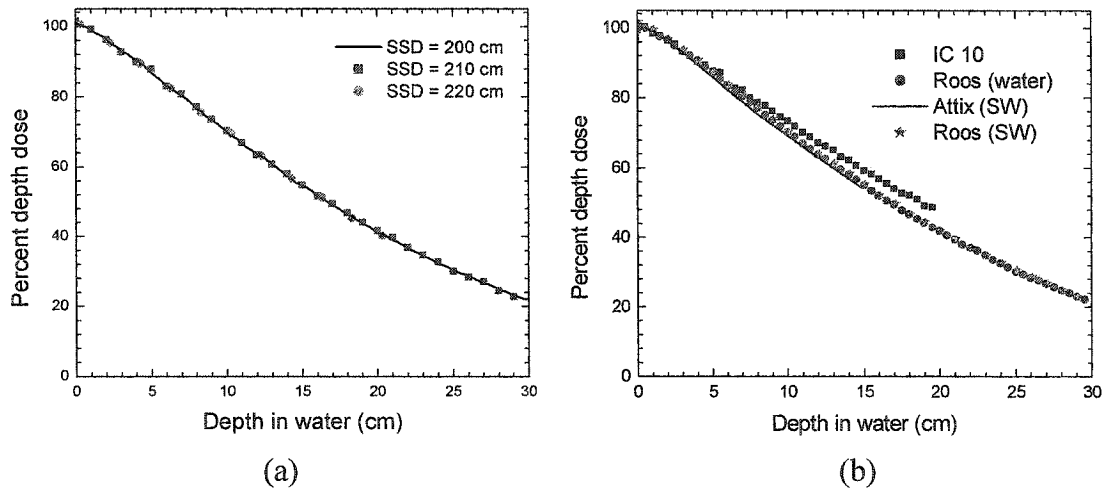


***Figure 6.12*** (a) Percent depth dose curves measured in various depths of water with the Roos ionisation chamber. (b) Percent depth dose curves measured at an SSD of 210 cm with the IC 10, the Roos and the Attix ionisation chambers in water or solid water.

## 6.8 SURFACE DOSE

The surface dose was measured with the Attix parallel plate ionisation chamber in solid water (*Figure 6.13*). Special attention was paid to the first centimetre of the phantom. Dose deposition in the layers near the surface did not follow classical data for cobalt-60 due to the large radiation field and the extended SSD. The peak in the first 2 mm of depth is thought to be due to electron contamination present in the beam and the depth of dose maximum ($d_{max}$) was therefore closer to the surface than the classical 5 mm. The normalisation of the percent depth dose was kept at a depth of 5 mm, following the recommendations in BJR 25 [3] for large fields contaminated with electrons.

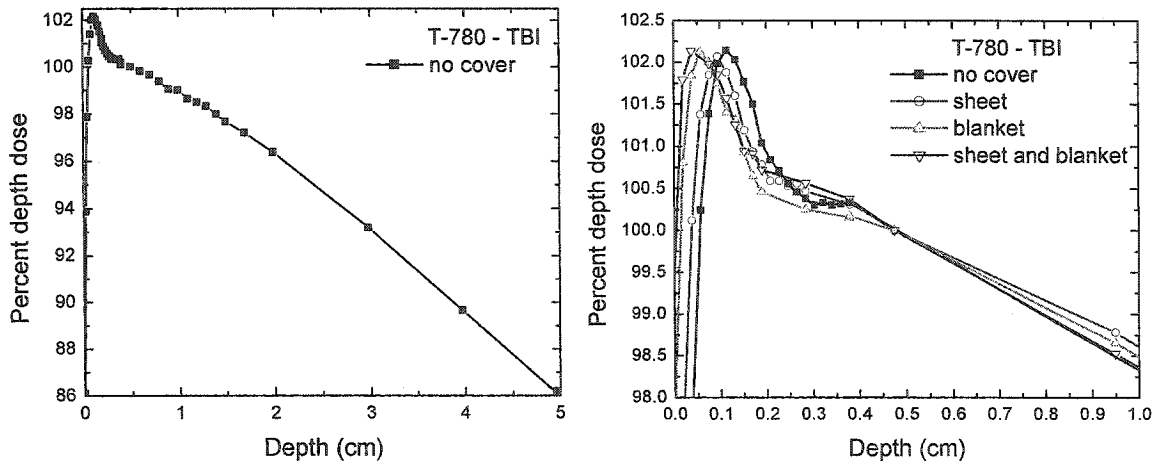


*Figure 6.13* Percent depth dose curve measured close to the phantom surface with various covering materials above phantom: (a) no additional covering material, (b) comparison between no additional covering material, sheet, blanket and sheet and blanket combination.

Patients are routinely covered with a sheet and a blanket for comfort. When no covering material was used, the surface dose was measured to be 85% of the normalised dose at 5 mm and when covering material was used, the surface dose increased and the electron contamination peak moved towards the surface (see *Table 6.7*). The covering material thus acts as a bolus against the skin, and the "skin sparing" effect of the high-energy gamma rays produced by cobalt-60 is further reduced. This effect was clinically acceptable since the goal of total body irradiation is to deposit a uniform dose throughout the body, including the skin of the patient. The choice of covering material used was representative of those available in the clinic.

*Table 6.7* Measurements at the surface normalised to 100 cGy at a depth of 0.5 cm

| Measurement condition | Surface dose | Maximum dose | $d_{max}$ |
|---|---|---|---|
| Open beam | 85.8 % | 102.1 % | 0.11 cm |
| Covering sheet | 93.4 % | 102.1 % | 0.09 cm |
| Covering blanket | 98.0 % | 102.1 % | 0.06 cm |
| Covering blanket and sheet | 99.5 % | 102.1 % | 0.04 cm |

## 6.9 DOSE UNIFORMITY

Using the PDD measured with the Roos ionisation chamber in water, the dose uniformity was studied as the thickness of the patient varied between 10 and 30 cm. The first step in defining the dose uniformity was to calculate the average PDD for the parallel-opposed beam set-up (see *Figure 6.15*). A summary of various depths normalised to the mid-line dose is shown in *Figure 6.14*.

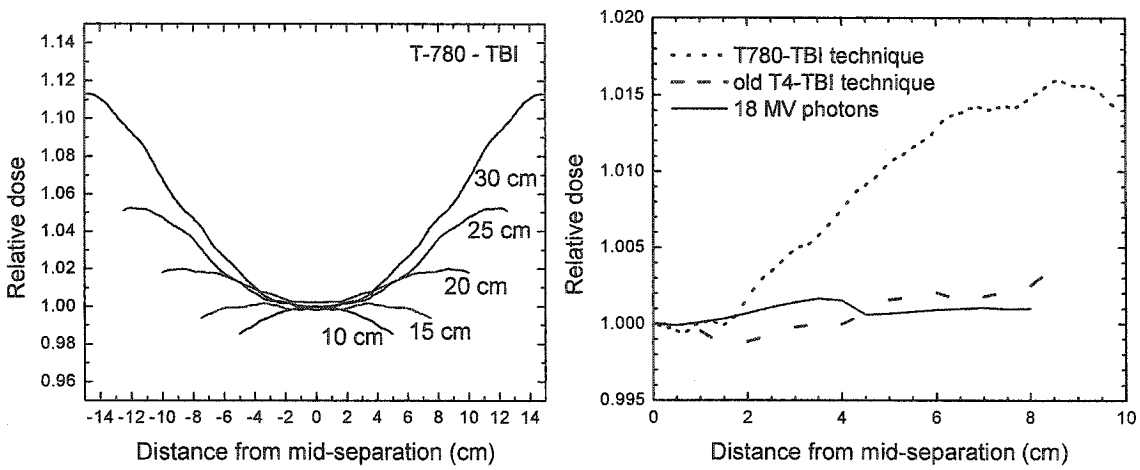


***Figure 6.14*** Dose variation within the phantom from two parallel opposed beams varies according to: (a) phantom thickness, (b) technique used.

In *Figure 6.14*(a), the maximum variation shown is ±6%. In chapter 1, it was stated that dose uniformity within the patient was acceptable if the dose varied by less than ±10%. The inherent dose variation due to the patient thickness in the modified cobalt-60 radiation beam does not reach ±10%, however, it is clear that the larger the patient separation, the larger the loss in dose uniformity. For patient separations above 20 cm, the dose at the mid-line was the lowest dose received by the patient. It was the opposite for curves representing patient separations of 10 or 15 cm due to an inflection point along the PDD curve. The highest dose in these cases was deposited at the mid-line.

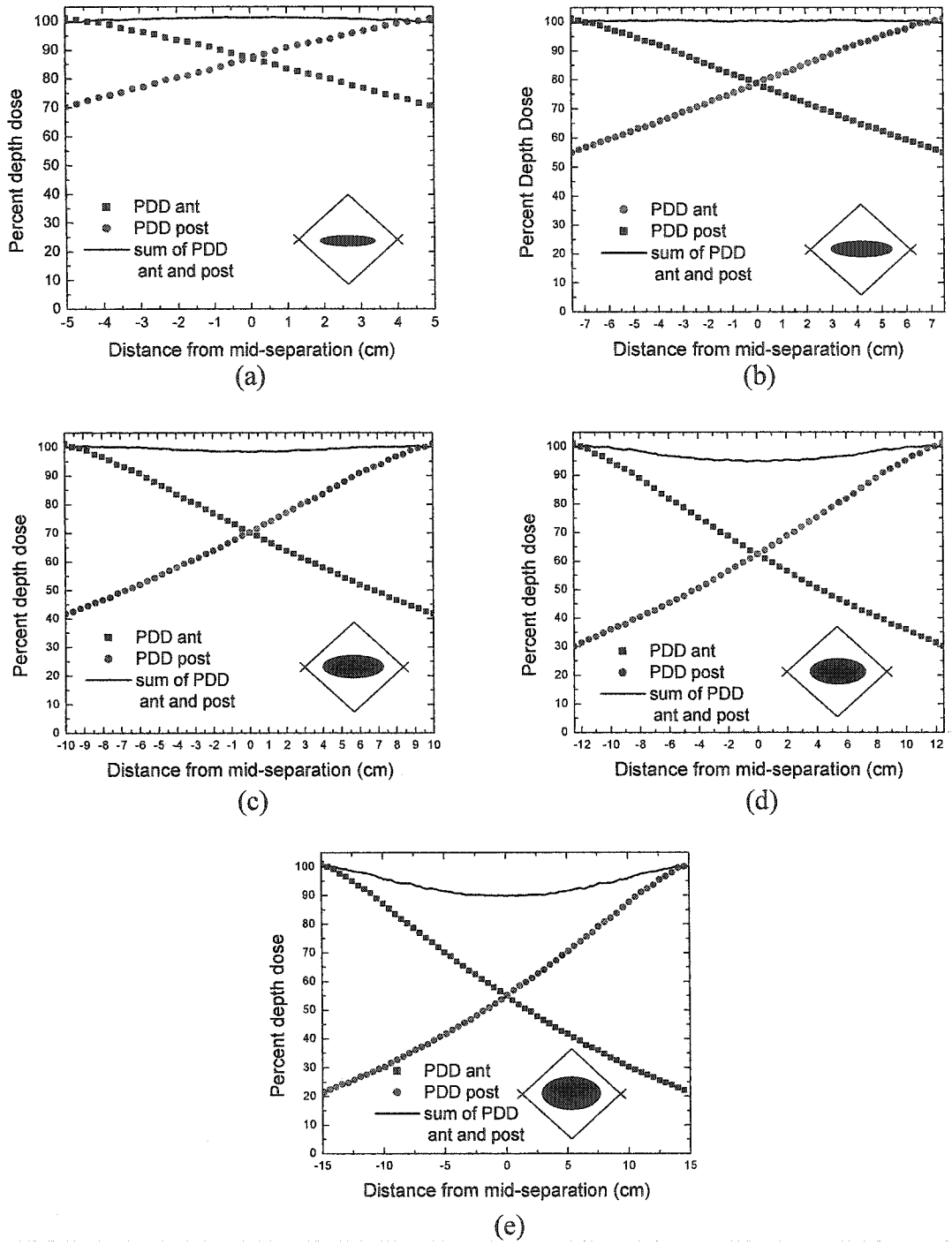


*Figure 6.15* Percent depth dose calculated for parallel-opposed beam from single beam measurements in phantom for various phantom thickness: (a) 10 cm, (b) 15 cm, (c) 20 cm, (d) 25 cm and (e) 30 cm. The icon in the lower right corner represents the two parallel-opposed beams incident on the patient in transverse cross-section.

In *Figure 6.14*(b), the dose uniformity for a phantom thickness of 20 cm is compared for different techniques. When comparing the modified cobalt-60 (T-780 – TBI) technique to the technique previously used at the McGill University Health Centre (MUHC) based on a sweeping beam from a column mounted 4 MV linear accelerator (T4-TBI) [4], a difference up to 2% can be seen, with the T4-TBI technique giving a better dose uniformity. An 18 MV photon beam was also used to compare the T-780 – TBI technique with a high-energy beam. Again, the dose uniformity of the high-energy beam is better by 2%. Dose uniformity within the thickness of the phantom with the modified cobalt-60 technique is still within the uniformity limits previously discussed, considering that the typical patient thickness is approximately 20 cm.

## 6.10 MEASUREMENTS AT AN SSD OF 80 CM

A percent depth dose (PDD) curve was measured in solid water at an SSD of 80 cm and compared to the data collected at an SSD of 210 cm. In *Figure 6.16* (a), the PDD measured at two different SSD's (80 and 210 cm) is presented. At an SSD of 80 cm, the phantom is no longer in the range where a patient would be treated, and the independence of the PDD with the SSD previously observed no longer applies. As expected, the PDD is highest for the SSD of 210 cm as compared to that at 80 cm. The Mayneord correction factor is used to convert a PDD acquired at a given SSD to another SSD. The Mayneord factor is a ratio of the inverse square law corrections and is given as:

$$\frac{PDD(d,r,f_2)}{PDD(d,r,f_1)} = \left(\frac{f_2+0.5}{f_1+0.5}\right)^2 \times \left(\frac{f_1+d}{f_2+d}\right)^2, \qquad (6.7)$$

where $d$ is the depth in the phantom, $r$ the field size at the surface of the phantom and $f$ the distance between the source and the phantom surface.

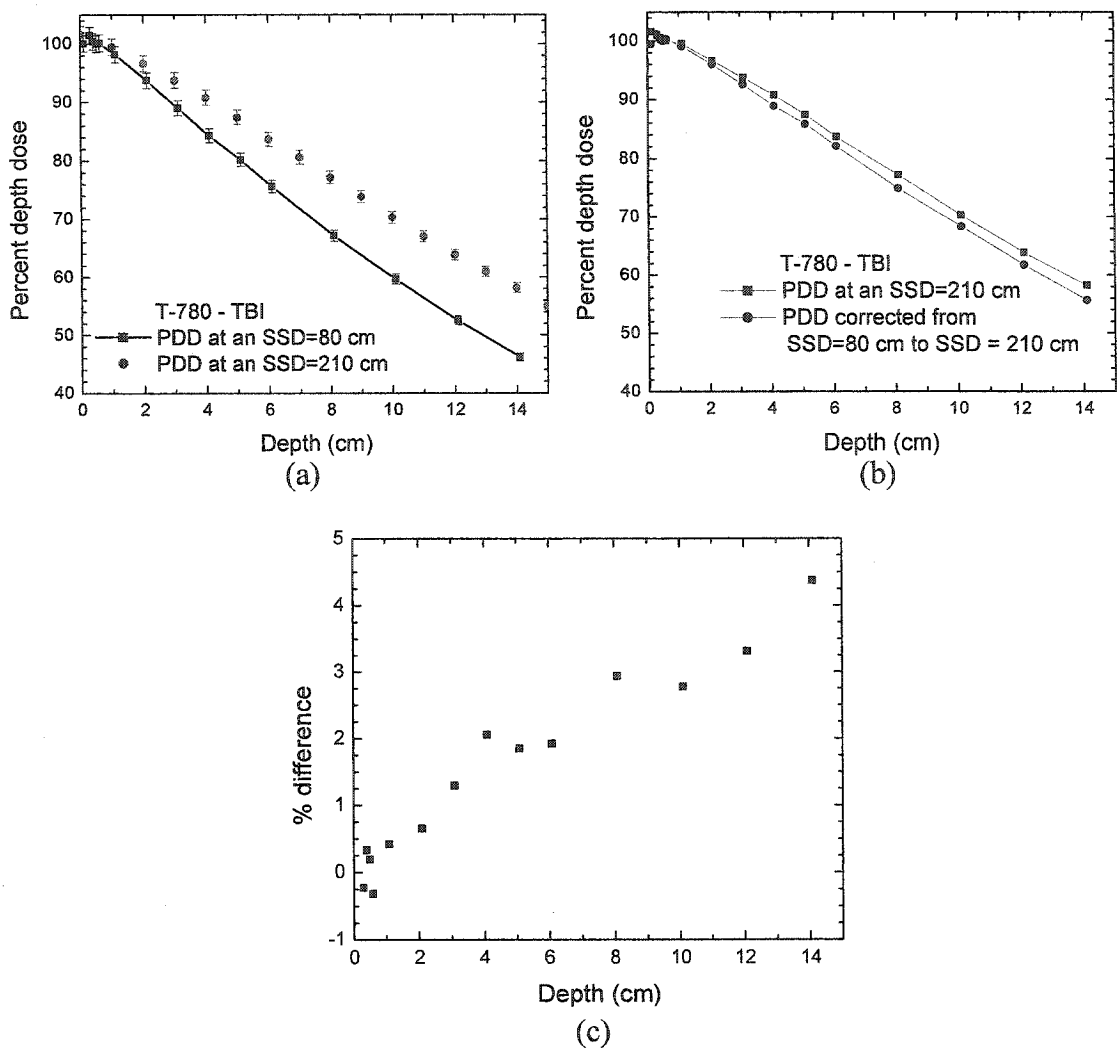


***Figure 6.16*** Percent depth dose curves: (a) measured at an SSD of 80 and 210 cm, (b) with Mayneord correction applied to PDD at SSD 80 cm and (c) % difference between PDD corrected to 210 cm and PDD measured at 210 cm.

In *Figure 6.16* (b), the Mayneord correction was applied to the PDD measured at an SSD of 80 cm. The Mayneord correction is based on the inverse square law that was investigated in section 6.6. The results showed that the inverse square law correction was in error up to 10% near the collimator, but that between 125 and 240 cm from the source, the error was less than 2%. A difference is seen between the PDD corrected to SSD of 210 cm with the PDD measured at an SSD of 210 cm. The difference, shown in *Figure 6.16* (c), increases with depth in the phantom to 5 %. The upwardly trend may be due to limitations in the Mayneord factor correction that do not adequately take into consideration scatter and field size.

## 6.11 TISSUE-PHANTOM RATIO

The tissue phantom ratio (see section 5.10) was measured in solid water with the Roos ionisation chamber at a fixed position from the cobalt-60 source. Measurements were normalised to the value obtained at a depth of 10 cm.

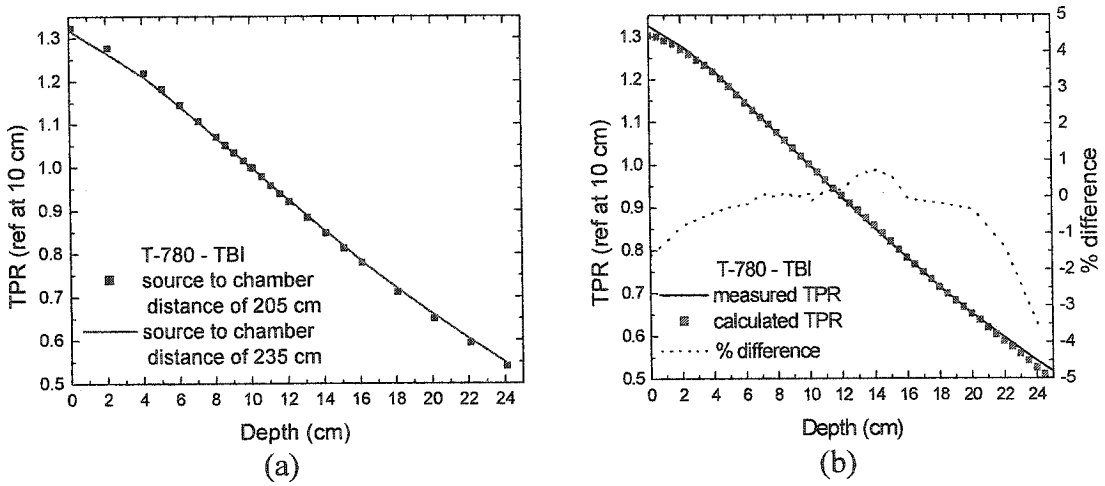


*Figure 6.17* Tissue phantom ratio: (a) in solid water with source to chamber distances of 205 and 235 cm, (b) measured and calculated from PDD data as well as the % difference between the two.

In *Figure 6.17*(a), the tissue phantom ratios obtained at a source to chamber distances of 205 and 235 cm from the source were compared. The two curves were essentially identical and led to the conclusion that the tissue phantom ratio was independent of SAD distance in the region where the patient is positioned for treatment. This was expected since it has been already shown that PDD in this SSD range was independent.

The choice of a reference depth of 10 cm was based on the fact that the absolute output of the unit was determined at a depth of 10 cm in water. This depth was meaningful since the thickness of an average patient is roughly 20 cm, with the mid-separation at 10 cm.

*Table 6.8* TPR values measured for the modified cobalt-60 TBI technique with a Roos ionisation chamber in solid water.

| DEPTH | TPR | DEPTH | TPR | DEPTH | TPR |
|---|---|---|---|---|---|
| 0.1 | 1.323 | 9.6 | 1.015 | 15.1 | 0.812 |
| 2.1 | 1.277 | 10 | 1 | 16.1 | 0.779 |
| 4.1 | 1.219 | 10.1 | 0.998 | 18.1 | 0.711 |
| 5.1 | 1.182 | 10.6 | 0.978 | 20.1 | 0.65 |
| 6.1 | 1.144 | 11.1 | 0.958 | 22.1 | 0.593 |
| 7.1 | 1.107 | 11.6 | 0.939 | 24.1 | 0.54 |
| 8.1 | 1.071 | 12.1 | 0.921 | 26.1 | 0.489 |
| 8.6 | 1.051 | 13.1 | 0.884 | 28.1 | 0.445 |
| 9.1 | 1.034 | 14.1 | 0.847 | 30.1 | 0.402 |

In section 2.4, a relationship between the TPR and PDD was presented. Applying this relationship to TPR data and comparing with measured PDD data, we obtained *Figure 6.17* (b). The measured and calculated TPR's agree within 4% of one another, even though the peak scatter factor ratio was neglected, confirming the validity of the derived equation.

## 6.12 PHANTOM SIZE EFFECTS

To study the effect of phantom size on dose deposition throughout the phantom, a series of tissue phantom ratios and relative output measurements were conducted with different size, shape and thickness of solid phantoms. In *Figure 6.18*, it can be seen that the various phantoms lead to the same tissue phantom ratio. The results were thus clinically independent of phantom thickness or size.

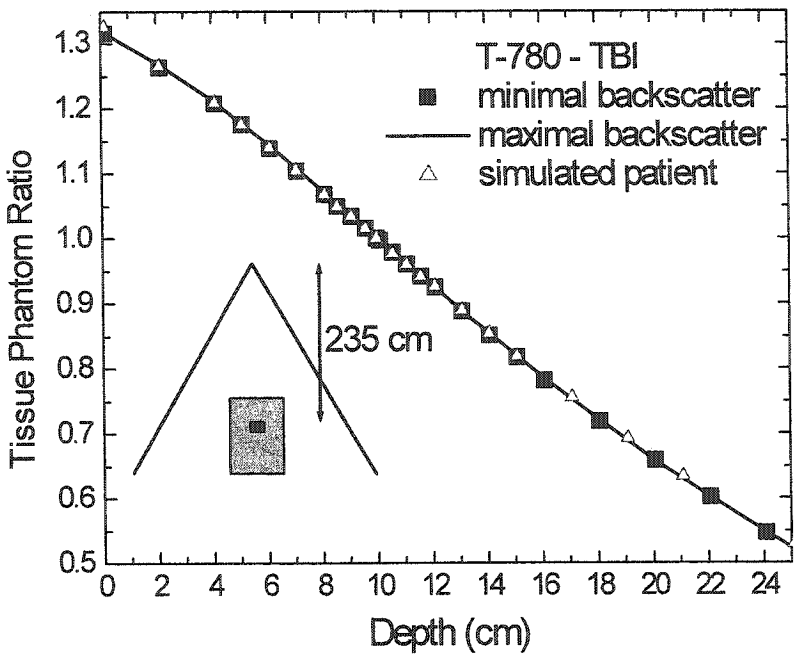


*Figure 6.18* Tissue phantom ratios measured at 235 cm from the source, with minimal and maximal back-scatter conditions and with a simulated patient of solid water and bolus on a stretcher.

Relative output measurements corrected by the inverse square law to maintain a constant source to surface distance, do suffer from lack of backscatter, as shown in *Figure 6.19*. The results show that for a phantom thickness beyond 10 cm, there is no phantom thickness effect, but that below this thickness, a lower dose is measured leading to a discrepancy up to 1.5% for a 3 cm thick phantom.

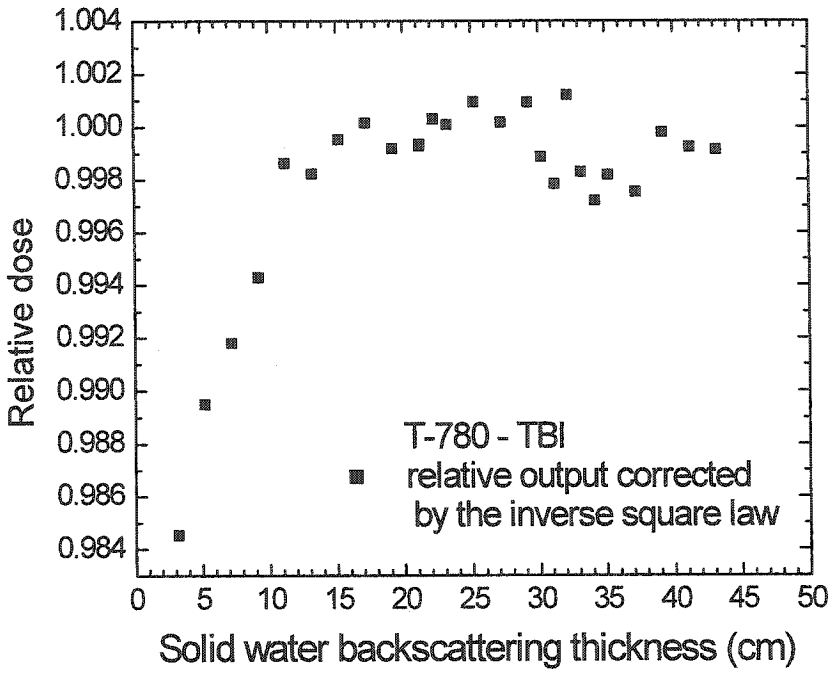


*Figure 6.19* Relative output measured in solid water with the Attix ionisation chamber corrected by the inverse square law due to the varying SSD of phantom.

Another measurement to determine effects from phantom thickness was conducted by keeping the chamber in the same spatial position, but substituting solid water below the chamber by Styrofoam (see *Table 6.9*). In this situation, no correction such as the inverse square law was needed since the chamber position did not change. The results presented in *Table 6.9*, confirm that a phantom thickness that varies between 30 and 12.5 cm does not suffer from a lack of backscattered radiation.

*Table 6.9* Measurements with PTW-Freiburg Farmer ionisation chamber at a depth of 3 cm in a 30x30 $cm^2$ solid water phantom with varying thickness of solid water backing.

| Thickness of solid water (cm) | Measurement (nC) | Normalised measurement |
|---|---|---|
| 30 | 1.678 | 1 |
| 22.5 | 1.681 | 1.0018 |
| 17.5 | 1.682 | 1.0024 |
| 12.5 | 1.683 | 1.0030 |

## 6.13 DOSE TO SOLID LUNG DETERMINED WITH TLD CRYSTALS

The use of thermoluminescent crystals for dosimetry required extensive calibration of the TLD crystals prior to use. Irradiating the crystals with a known dose and then reading the light production with the Harshaw 3500 TLD reader provided the calibration. This was repeated to verify the reproducibility of the reading. Once the TLD crystals were calibrated, they could be used to take measurements. One of the measurements was in solid lung, a solid phantom with a density close to that of healthy lung. TLD-700 crystals were placed at the mid-separation of the solid lung phantom and solid water phantom. The solid lung and solid water phantom was arranged to mimic the human thorax, with two solid lung regions separated and surrounded by solid water (as shown in *Figure 5.8*). The mean dose to TLD-700 crystals in solid lung was 18% higher than to that in the surrounding solid water. To reduce the dose to the solid lung to that received by solid water, attenuators must be used. Two methods were used to determine attenuator thickness. The first was to use the previously measured attenuation curve for lead measured in solid water for lead placed near the patient (see *Figure 6.1*). With this method, the attenuator lead thickness corresponds to the thickness able to attenuate the beam by 18%. The second method was to use TLD's inside the thorax model and place lead above the solid lung on the Lucite support tray and determine what thickness was necessary to equalise the dose to both the solid water and solid lung. Since scattered radiation from the solid water to the solid lung may affect the measurement, it was determined that the results from the thorax model (see *Figure 5.8*) using TLD's were more reliable than the chamber measurements in solid water. Results from the TLD's used with the thorax model produced the attenuation curve presented in *Figure 6.20*.

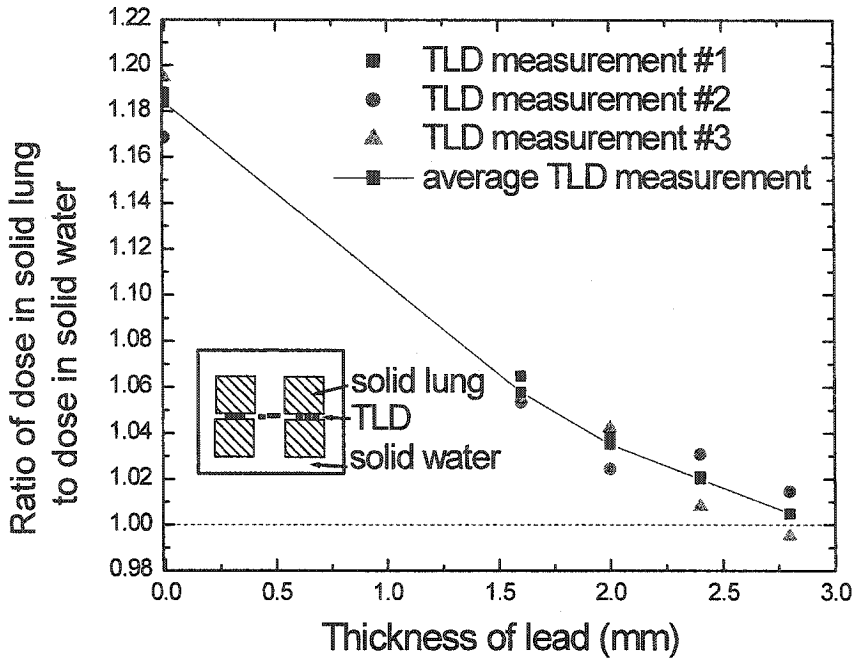


*Figure 6.20* Attenuation from lead placed on a Lucite support tray above solid lung in a solid lung-solid water phantom. The three TLD measurements as well as the average is shown.

From *Figure 6.20*, with 2.8 mm of lead above the solid lung, the ratio between dose to solid lung and solid water is near 1. With this result, the attenuator thickness that is determined with the thorax model is 2.8 mm of lead. If we use the attenuation data previously collected in solid water, a reduction in dose of 18% is obtained with 3.1±0.3 mm of lead (insert y = 0.82 in equation 6.4). As expected, the TLD measurements in a solid lung-solid water phantom led to an attenuator thickness lower than when measured in only a solid water phantom. A complete TLD study using an anthropomorphic phantom is presented as a complement to these results in chapter 7.

## 6.14 ABSOLUTE OUTPUT

The absolute output of the modified cobalt-60 unit varies with time due to the decay of the cobalt-60. Since the half-life of cobalt-60 is known to be 5.26 years, it is possible, once the absolute output is measured, to calculate it any point in time from then on by using the exponential decay law. In clinical practice, this is confirmed every 6 months. A series of readings were measured at different source to surface distances with a calibrated ionisation

chamber at a depth of 10 cm in water. Once the measurement M is corrected for standard air temperature, pressure and other effects described in chapter 4, dose is determined with:

$$D_w = M^C N_{D,w}^{Co} k_Q . \tag{6.8}$$

With the calibration factor for absorbed dose in water, $N_{D,w}^{Co}$, traceable to the NRCC standard and a value for $k_Q$ for cobalt-60 of 1, dose to water can be determined [5]. This dose serves as an absolute output for the modified cobalt-60 unit. A typical dose rate at a prescription distance of 230 cm from the source and at a depth of 10 cm in water is of the order of 6-7 cGy/min.

## 6.15 SUMMARY

It was found that the vault housing the modified cobalt-60 unit was safe and a Canadian Nuclear Safety Commission (CNSC, Ottawa, ON, Canada) operating license was obtained. Dose rates in areas outside the treatment room were below the legal limits and in most cases, below the limits when the ALARP principle was applied. When considering the radiation beam itself, measurements made to determine the attenuation of the beam by lead below the source, and just above the patient, yielded different HVL's as expected due to the different geometry. The beam profiles of the open beam confirmed the radial symmetry of the source emission and the necessity to only do measurements in one quadrant of the field. With the flattening filter built and in place below the source, additional beam profiles were measured to verify proper beam flatness. The shutter error was then measured and an interesting effect was observed whereby the distance between the source and the dosimeter had an impact on the measured shutter error. This was explained as a variation in the solid angle view of the source by the dosimeter. Also, a study of the inverse square law concluded that within the range of clinically relevant SSD's, the output can be corrected for by the inverse square law. This did not apply to measurements in air due to the collimator and floor scattering. A similar result was also obtained when comparing the percent depth-dose measured within the range of the patient SSD compared to that obtained at an SSD of 80 cm. The Mayneord factor was able to reduce the difference between the PDD measured at an SSD of 80 and 210 cm to within 5%. Tissue-phantom ratios showed that the SSD could vary by 30 cm without a

clinically relevant difference. This was expected since TPR's are independent of SAD. It was also shown that a correspondence between TPR and PDD could be achieved. Finally, the TPR was not significantly affected by phantom size and thickness. Inverse square law corrected output measurements did show a small effect from a phantom thickness under 10 cm. Attention to inhomogeneities in the patient such as lung showed that in an average patient, dose to lung would be 18% higher than the dose to surrounding soft tissue. Lead attenuators of 2.8 mm limited the dose to the lung to the same level in soft tissue. Absolute measurements in water provided the final calibration information for the modified cobalt-60 unit. Further measurements in patient-like conditions, such as in the Alderson-Rando anthropomorphic phantom, are presented in the following chapter verifying these results.

## 6.16 REFERENCES

[1] H.E. Johns and J. R. Cunningham, *The Physics of Radiology*, 4th ed., Charles C Thomas, Springfield, IL, USA, 1983.

[2] J. Van Dyk, P.M. Leung and J.R. Cunningham, "Dosimetric considerations of very large cobalt-60 fields", Int. J. Radiat. Oncol. Biol. Phys., 6 (6), 753-759, 1980.

[3] E.G.A. Aird et al., *British Journal of Radiology Supplement 25: Central Axis Depth Dose Data for Use in Radiotherapy*, British Institute of Radiology, Volume 25, London, England, 1996.

[4] M. Pla, S.G. Chenery and E.B. Podgorsak, "Total body irradiation with a sweeping beam", Int. J. Radiat. Oncol. Biol. Phys., 9 (1), 83-89, 1983.

[5] P.R. Almond et al., "AAPM's TG-51 protocol for clinical reference dosimetry of high-energy photon and electron beams", Med. Phys., 26 (9), 1847-1870, 1999.

# Chapter 7

# Treatment verification



## 7.1 ALDERSON-RANDO ANTHROPOMORPHIC PHANTOM

The Alderson-Rando anthropomorphic phantom is a solid water phantom representing a 175 cm tall, 73.5 kg male. Arms and legs are absent and the phantom is built from a succession of 2.5 cm thick slices. The phantom is made to reproduce a male patient as closely as possible, with soft tissue, bone, lung and air cavities. Holes drilled into each slice enable the use of thermoluminescent crystals for dosimetry. It is the Alderson-Rando anthropomorphic phantom and TLD-100 thermoluminescent crystals that were used to verify proper patient treatment planning and dose deposition.

## 7.2 TREATMENT PLANNING

During the stages of set-up and treatment planning, the anthropomorphic phantom was first laid in a supine position and its separation at the umbilicus was measured. The phantom was then turned to lie in a prone position and its separation was again measured at the level of the umbilicus. The patient was placed with the central axis of the stationary TBI beam centred at the umbilicus, and in the prone position this was referenced to the anal verge in a manner analogous to the supine position patient set-up procedure. Appendix A presents sample

planning and treatment sheets used with the Alderson-Rando anthropomorphic phantom. In each treatment position (supine and prone), a chest radiograph was taken of the phantom using PP-L portal film (Eastman Kodak Inc., Rochester, NY, USA) in a cassette positioned under the phantom on the floor. From the radiograph shown in *Figure 7.1*, the outline of the desired lead lung compensator placed on the Lucite support tray above the patient was drawn. The shape of the lung on the radiograph must be de-magnified by a factor of 0.83 to be the proper size on the Lucite support tray above the patient. With this template, a 2.8 mm thick lead compensator was built.

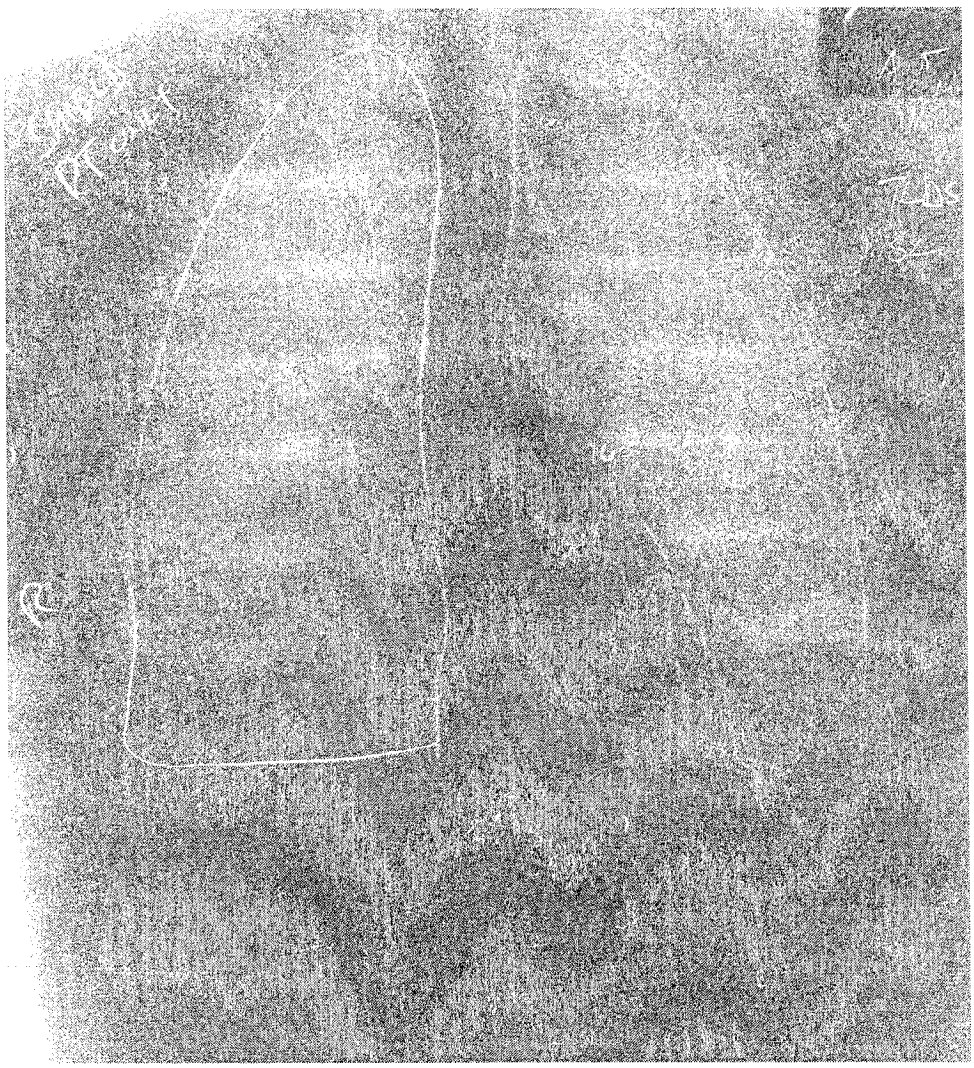

*Figure 7.1* Planning film taken of the Alderson-Rando anthropomorphic phantom with drawn lung outline. The phantom was supine on the stretcher. Two registration lead crosses are seen inferiorly and centrally.

Three lead registration crosses were placed on the phantom to help align the phantom and lung compensators during treatment. Two of these crosses are visible in *Figure 7.1.* A cross was placed on the sternum, corresponding to slice 16 of the phantom, another cross was placed on slice 21 and the other cross, not visible on the film, was placed at the umbilicus at slice 25.

To determine the time of exposure to deliver 50 cGy to the mid-separation of the phantom, the results presented in chapter 6 were used. The phantom thickness at the umbilicus and at the anal verge was 20 cm, and the distance from the floor to the incident surface of the phantom was 32 cm. The source to surface distance was therefore 219.2 cm. The absolute output at the time of the experiment was 6.644 cGy/min at a depth of 10 cm in muscle. Since the thickness of the patient was 20 cm, the depth to the mid-separation was 10 cm. The value of the TPR at a depth of 10 cm is 1.00. Therefore, to deliver 50 cGy, the beam on time is calculated to be:

$$\text{beam time} = \frac{50\ \text{cGy}}{6.644\ \text{cGy/min} \times TPR(10\ \text{cm})} = 7.53\ \text{min} \qquad (7.1)$$

Taking into consideration the shutter error, -0.02 min, the treatment time for the Alderson-Rando anthropomorphic phantom was 7.51 minutes in both the supine and in the prone positions. The total dose was therefore expected to be 100 cGy to the mid-line of the umbilicus.

## 7.3 DOSE DELIVERY VERIFICATION

*Figure 7.2* The Alderson-Rando anthropomorphic phantom in treatment position with lead compensator over right lung.

To verify proper dose deposition throughout the phantom, TLD-100 crystals were used. The anthropomorphic phantom was prescribed 100 cGy at the mid-line at the level of the umbilicus with AP-PA dose delivery. *Figure 7.2* shows the anthropomorphic phantom in treatment position with the lead compensator placed above the right lung. The left lung was left unprotected to receive an uncompensated dose. Three TLD-100 crystals were placed in the centre of slice 25, corresponding to the umbilicus of the phantom, to verify delivery of the prescribed dose. Another twenty TLD-100 crystals were placed in a star pattern in slice 15. Within slice 15, lung and soft tissue-like media serve to verify proper dose attenuation in the lung from the lead compensator. Another set of measurements was repeated with the TLD-100 crystals distributed along the longitudinal axis of the anthropomorphic phantom. Three TLD-100 crystals were placed in slice 25 (the umbilicus) to again verify prescribed dose delivery. The remaining TLD-100 crystals were distributed two per slice in slices 34, 30, 22, 18, 15, 11, 9, 8, 6 and 2, corresponding to positions from the head through to the most inferior slice available in the groin region. A diagram depicting exact location of each TLD-100 crystal as well as the dose they received is presented in *Figure 7.3* and *Figure 7.4*.

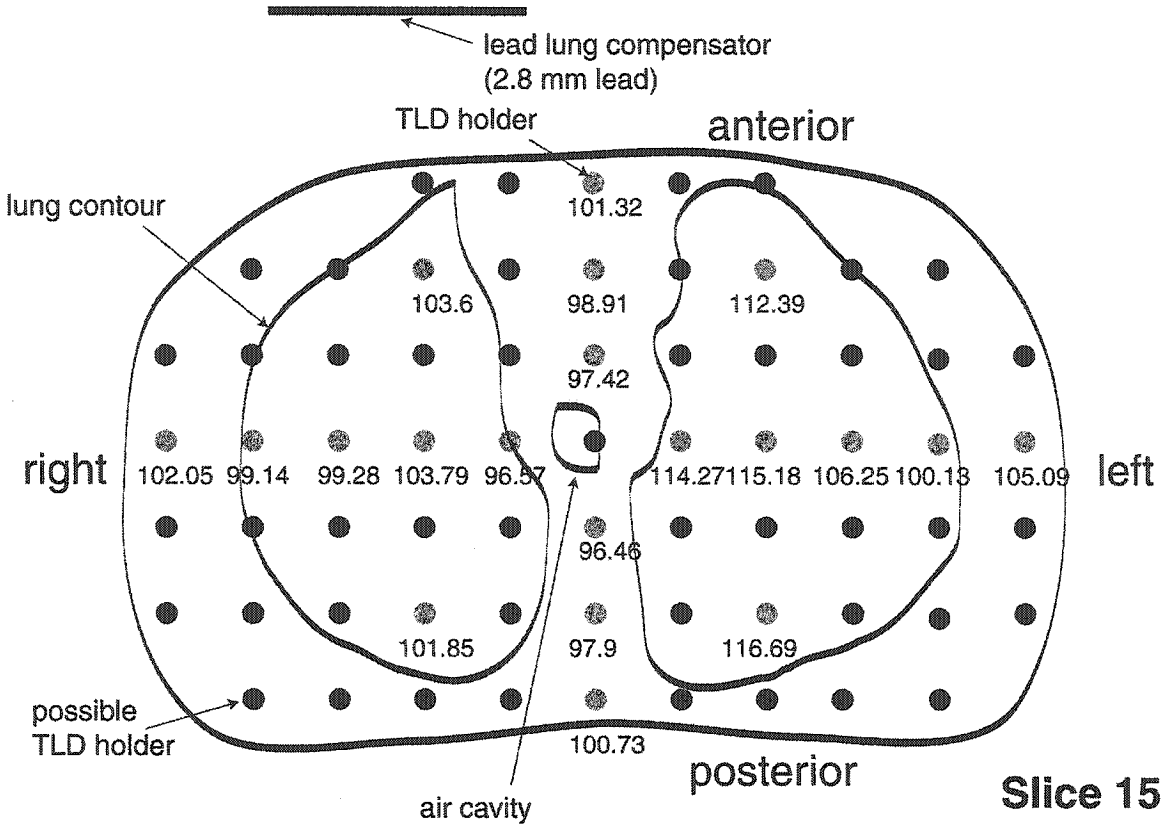


*Figure 7.3* Dose in cGy received by the TLD-100 crystals in slice 15 of the Alderson-Rando anthropomorphic phantom, viewed from feet to head.

To obtain the measurements presented in *Figure 7.3* and *Figure 7.4*, TLD-100 crystals were irradiated 5 times with 100 cGy, using a 10 MV photon beam to determine a calibration factor. Day to day variation was corrected with a standard set of five TLD's receiving 100 cGy from a calibrated 10 MV linear accelerator photon beam. The corrected relative doses are presented in *Figure 7.3* for slice 15 and in *Figure 7.4*. Slice 15 is representative of the thorax region with lung and soft tissue components. 100 cGy was prescribed to the mid-line at the level of the umbilicus at slice 25 of the Alderson-Rando phantom. The results from the three TLD's placed in the centre of slice 25 are 101.98, 103.75 and 100.73 cGy respectively, giving an average dose of 102.2 cGy. An error in dose determination of up to 3% is expected with TLD's and a 2% error in the administration of the prescription is expected.

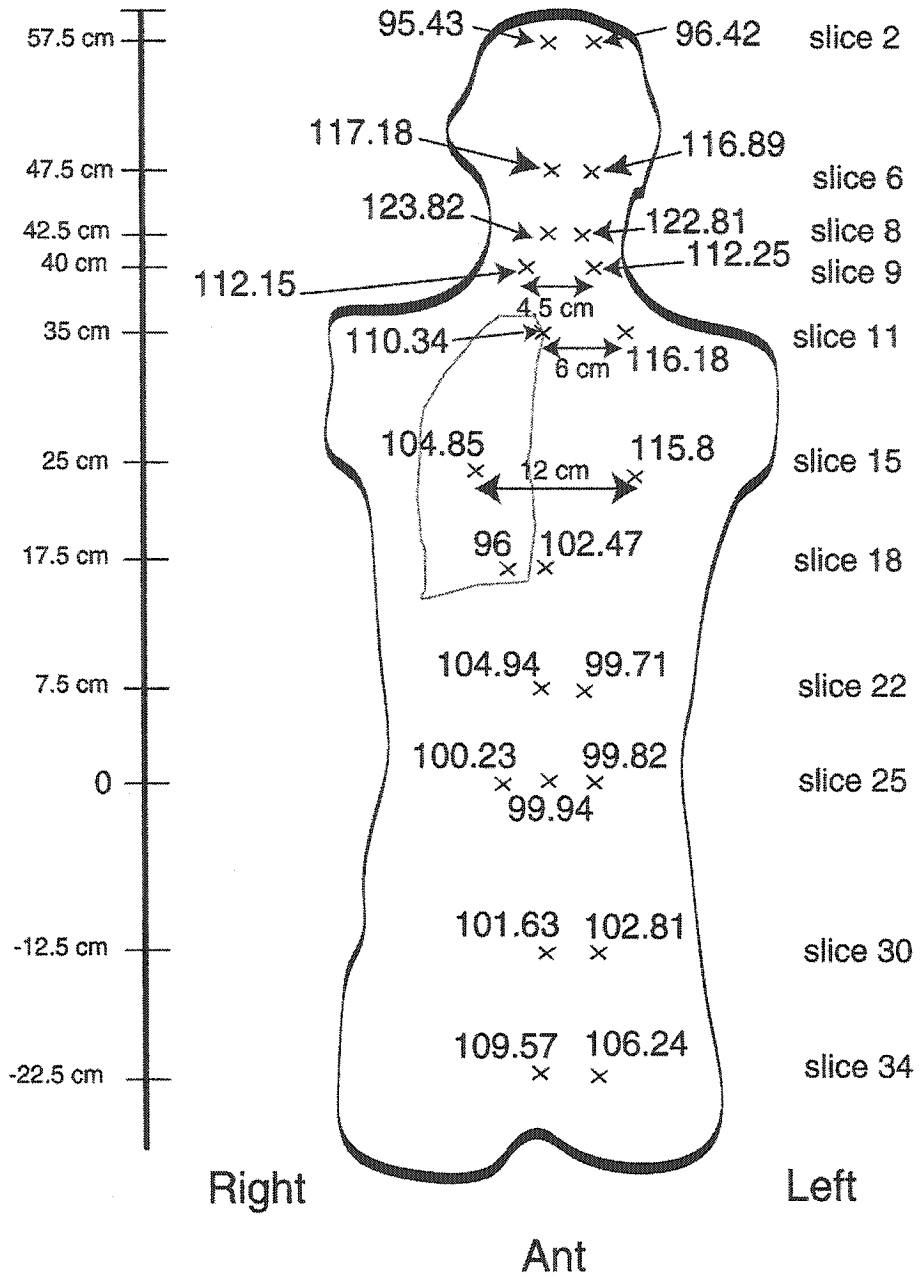


*Figure 7.4* Outline of the Alderson-Rando anthropomorphic phantom with the dose in cGy received by the TLD-100 crystals. To the left of the phantom, distance from the umbilicus is shown while to the right, the slice number is indicated. If no distance is indicated between two measurements of one slice, the distance is 3 cm.

The left lung on slice 15 received the highest dose (up to 116.69 cGy) due to its low density, and this is in agreement with the 18% prediction of overdosage to the lung as determined from earlier measurements in chapter 6. The maximum variation within the lead compensated lung

on slice 15 was between 96.46 and 103.79 cGy; that is within ±4% of the mid-line dose at the prescription point in slice 25.

Another set of measurements was carried out to observe the variation in dose longitudinally along the patient. The results are shown in *Figure 7.4*. The average of the measurements at the prescription point was 99.5 cGy. Comparing doses received in slice 15 with repeated measurements, we obtain in the open lung 115.8 and 115.18 cGy and in the compensated lung, 104.85 and 103.79 cGy. TLD measurements therefore agreed very well within the intrinsic error of each TLD of ±3%.

These results were compared with the technique previously used at the McGill University Health Centre (MUHC, Montréal, Québec, Canada) based on a sweeping beam from a column mounted 4 MV linear accelerator [1]. The uncompensated lung would receive up to a 13% higher dose and the compensated lung would receive up to a 4% higher dose than the prescription. These results are similar to the uniformity obtained with the modified cobalt-60 technique.

Over a 10% increase in dose in the neck area of the phantom was observed. Since this area is not as thick as the rest of the body, an increase in dose is expected. A simple model to predict the expected dose in slices 8 and 9 was based on the average thickness of the phantom at each TLD position. The right TLD of slice 9 was within an average thickness of 12 cm, referring to a mid-line depth of 6 cm. The left TLD was within an average thickness of 12.6 cm, with a mid-line depth of 6.3 cm. In slice 8, the right TLD was within an average thickness of 14.2 cm and the left TLD was within a phantom thickness of 14.3 cm. The presence of air cavities complicated the situation. If the air cavities were subtracted from the total thickness, a 10.6 cm thickness surrounding the right TLD and 10.2 cm thickness surrounding the left TLD was estimated. The expected dose to the neck area is presented in *Table 7.1*. These doses were calculated with the tissue phantom ratios corresponding to the depth of the mid-plane $x$ and were based on a dose deposition of 100 cGy for a phantom thickness of 20 cm. To calculate the expected dose, the off-axis ratio at this level was 1.00 with respect to the central axis. To calculate the dose off-axis, the following simple relationship was used:

$$\text{expected dose}(x) = \frac{100\,cGy}{TPR(10\,cm)} TPR(x)\,OAR(x) \qquad (7.2)$$

*Table 7.1* Expected doses to slices 8 and 9 of the Alderson-Rando phantom

| TLD position | Phantom thickness (cm) | Tissue-phantom-ratio | Expected dose | Observed dose | Difference (%) |
|---|---|---|---|---|---|
| Slice 9: right | 12 | TPR(6)=1.15 | 115 cGy | 116.61 cGy | 1.4% |
| Slice 9:left | 12.6 | TPR(6.3)=1.14 | 114 cGy | 116.32 cGy | 2.0% |
| Slice 8 right | 10.6 | TPR(5.3)=1.17 | 117 cGy | 123.21 cGy | 5.0% |
| Slice 8 left | 10.2 | TPR(5.1)=1.18 | 118 cGy | 122.21 cGy | 3.4% |

## 7.4 CONCLUSIONS

It was clearly shown that the use of lead lung compensators are necessary when treating the anthropomorphic phantom since the dose deposited in the uncompensated lung is up to 18% higher than in the surrounding soft tissue. The dose received by the neck area is also of some concern due to the presence of airways and its smaller thickness. It was shown in *Table 7.1* that a simple model of phantom thickness with the dimensions of the airways subtracted was capable of calculating the expected dose to the throat area within 5% of the actual deposited dose, with higher accuracy when no airways are present. This suggests the possibility of the use of lead compensators to reduce the dose to the off-axis areas of the anthropomorphic phantom. In general the dose uniformity throughout the compensated anthropomorphic phantom is well within ±10%, reaching the goal established in chapter 1, and similar to the technique previously used at the MUHC. The accuracy in delivery of the prescribed dose is within the error associated with TLD measurements, indicating successful planning and positioning of the Alderson-Rando anthropomorphic phantom.

## 7.5 REFERENCES

[1] M. Pla, S.G. Chenery and E.B. Podgorsak, "Total body irradiation with a sweeping beam", Int. J. Radiat. Oncol. Biol. Phys., 9 (1), 83-89, 1983.

# Chapter 8

# Conclusions and future work

An isocentric teletherapy cobalt-60 unit was successfully modified to produce large fields for total body irradiation treatments. The original collimator of the source was removed and the sourcehead was installed at a height of 251.2 cm above the floor with a 5-cm thick lead secondary collimator added below the sourcehead to define a 277×132.6 $cm^2$ radiation field at floor level. Below this collimator, a custom-made lead filter flattened the central 90.8×181.6 $cm^2$ of the field to within ±3% of the central axis dose as measured at 10 cm in water. No patient is expected to be wider than the flattened field, set at over 90 cm. The patient is treated lying supine then in the prone position on a stretcher so as to obtain an anterior-posterior posterior-anterior (AP-PA) dose deposition. Films placed below the stretcher are used to verify that the custom lung attenuators are properly positioned during treatment.

Measurement of a high surface dose (85%) and a depth of dose maximum situated at a depth of 0.2 cm instead of 0.5 cm for the classical cobalt-60 unit suggested electron contamination in the radiation field of the modified cobalt-60 unit. Addition of a sheet and blanket, normally used for patient comfort, increased the surface dose to nearly 100% of the dose normalised to a depth of 0.5 cm. There was therefore no need to add any additional bolus or to spoil the beam to increase the surface dose since a high surface dose is a requirement for total body irradiation. Other dosimetric parameters investigated during the implementation of this technique included the percent depth-dose, tissue-phantom ratio, inverse square law, scattering effects and the measurement of absolute output. The Mayneord factor was able to transform a percent depth-dose curve measured at an SSD of 80 cm to that of a percent depth-dose curve for an SSD of 210 cm with an accuracy of 5%. Tissue phantom-ratios calculated from

percent depth-dose data also favourably compared with measured data with an error less than 4%.

Other factors affecting dose uniformity depend on the patient's thickness and on the presence of inhomogeneities such as airways or lung tissue. Dose variation is seen to increase with patient separation and is expected to be ±1% for a 20 cm thick patient and ±6% for a 30 cm thick patient. Inhomogeneities cause an increase of up to 18% in dose deposited to lung tissue phantom as compared to dose deposited in Solid Water® phantom. This dose increase was compensated for by a 2.8 mm lead compensator placed above the lung, of which the outline was determined with a chest radiograph of the patient in treatment position.

Verification of dose uniformity performed with the Alderson-Rando anthropomorphic phantom and thermoluminescent crystals confirmed the use of a 2.8-mm thick lead compensator to reduce dose variation within the lung to 4% of the prescribed dose. The measured dose at the mid-separation point of the phantom slice used for prescription was within 1% of the expected dose. Measurements made in the neck area of the phantom identified a small high-dose region receiving up to 24% more than the prescribed dose. The increase in dose was due to the small thickness of the phantom in that area and to the presence of airways. A simple model based on tissue-phantom ratios and soft tissue thickness within the patient was able to predict the elevated doses to better than 5% of their measured value, suggesting this model could be used to determine necessary additional or more elegant compensation. Otherwise, dose deposition in the Alderson-Rando anthropomorphic phantom used to verify proper dose planning and delivery was within the ±10% of the prescribed dose; the goal set forth at the beginning of this work. The dose uniformity measured in the phantom was comparable to that observed with the technique previously used on site at the McGill University Health Centre (MUHC, Montréal, Qc, Canada) and based on a 4 MV photon sweeping beam.

Of the 441 patients treated since 1980 with TBI, 19 patients have received a whole body dose of 1200 cGy using the modified cobalt-60 unit between November 2001 and August 2002. Of these patients, 16 were paediatric cases. Future work will have the goal of further improving dose uniformity, principally by predicting the dose throughout the patient, not only at the

umbilicus. A simple model was proposed in chapter 7 based on patient thickness that accounts for inhomogeneities and TPR. This model was able to predict doses at the mid-line and off-axis to within 5% accuracy. Density information available from CT scans would prove useful to further improve this model. Other future work might be directed towards the development or modification of a treatment planning system with built-in inhomogeneity corrections to determine dose distributions throughout the entire patient. With additional knowledge on the dose distribution for each patient, a further refinement to the cobalt-60 total body photon irradiation technique would be to develop a system by which whole body custom compensation can be determined to improve dose uniformity, thus allowing for patient specific TBI treatments.

# Appendix A

## Sample planning and treatment sheets

The following sheets are used in clinical practice when planning and treating a patient with the modified cobalt-60 total body irradiation technique.

# T-780
# MUHC-MGH
McGill Medical Physics
Total Body Irradiation

Patient Name SAMPLE PLANNING SHEET Date FEB 6/2002

Hospital ☐ MUHC ■ St. Justine Other: Age 17 MONTHS

Diagnosis AML Sex M

Tumour Dose: 150 cGy x 2 fr/day x 4 days = 1200 cGy (total dose)

Average separation at centre (umbilicus): AP 12 cm PA 11 cm AP/PA average 11.5 cm

Floor-surface distance (cm): AP 23.5 cm PA 22.5 cm average 23 cm

| | AP Separation (cm) | Distance from centre (cm) | Total Dose (cGy) |
|---|---|---|---|
| A- Head | LAT 12 AP 16.5 | 31 | |
| B- Neck | | | |
| C- Shoulder | 8 | 17 | |
| D- Mid-mediastinum | 11 | 14 | |
| E- Hip | 8 | 10 | |
| F- Knee | 6 | 22 | |
| G- Ankle | 4 | 36 | |

Average separation for prescription (HEAD LAT+UMBILICUS)/2=(12+11.5)/2=11.75 cm

Film ■ PPL Other: _____ Beam time (min) 0.15

Tray position ■ A Other:

Radiation Oncologist Freeman

Physicist ME/SO

Radiation Therapist NR/FP

SO/ME/MO 20 Feb 2002

# T-780

MUHC-MGH

McGill Medical Physics

Total Body Irradiation

| | |
|---|---|
| Patient Name: | SAMPLE QA SHEET |
| Patient Number: | 1111111 |
| Physicist: | SO |
| Date: | 06-Mar-02 |

## Time and Dose Rate Calculation

| | |
|---|---|
| $t$ =separation at centre of field=(AP+PA)/2 (cm) | 11.5 |
| Average separation for prescription (cm) | 11.75 |
| Rx depth=(Average separation for prescription)/2 (cm) | 6 |
| Floor-to-surface distance (fSD) (cm) | 23 |
| Source-to-Rx distance* (cm) $= \left(251.2\text{ cm} - \text{fSD} + \frac{t}{2}\right)$ | 234 |
| $\dot{D}$(Source - to - Rx distance, depth = 10 cm) (cGy / min to muscle) | 6.6566 |
| TPR(Rx depth) | 1.148 |
| $\dot{D}$(Rx depth) (cGy / min to muscle) $= \dot{D}$(source - to - Rx distance, d = 10 cm) × TPR(Rx depth) | 7.642 |
| Prescribed Dose, D (cGy) | 1200 |
| Number of fractions, N | 8 |
| Dose per fraction per side (cGy), $D_{side} = (D / N) \div 2$ | 75 |
| Time (min) = $D_{side} \div \dot{D}$(Rx depth) | 9.81 |
| Set timer to: [time + (-0.02)] (min) | 9.79 |

* 251.2 cm=source-to-floor distance

## Measured Dose Rate

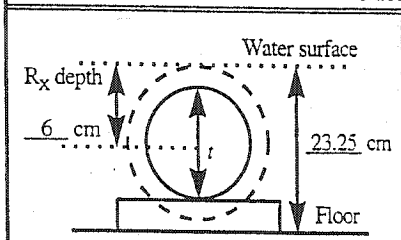


| | |
|---|---|
| Temperature (water) (° C) | 20.75 |
| Pressure (Torr ) | 750.8 |
| Electrometer SN | KEITHLEY 6517A |
| Chamber SN | EXRADIN 309 |
| $(\mu_{en} / \rho)^{\text{muscle}}_{\text{water}}$ | 0.99 |
| $N_{DW}$ (cGy / nC) | 4.930 |
| Depth of measurement (Rx depth) (cm) | 6 |
| Floor-to-water surface distance (cm) $= \left[\text{fSD} - \frac{t}{2} + (R_X \text{ depth})\right]$ | 23.25 |
| Readings, R (nC)/0.98 min set time | 1.440, 1440, 1440 |
| Average reading (nC )/0.98 min set time | 1.440 |
| $\dot{D}$(source - to - Rx distance, d = Rx depth) (cGy / min to muscle) $= \bar{R} \times \frac{760}{P} \times \frac{T+273}{295} \times N_{DW} \times \left(\frac{\mu_{en}}{\rho}\right)^{\text{muscle}}_{\text{water}}$ | 7.566 |

**Comments:**

Calc 7.642 cGy / min to muscle VS Meas 7.566 cGy / min to muscle = 1% Dose rate ok ME / SO

SO/ME/MO 23 April 2002

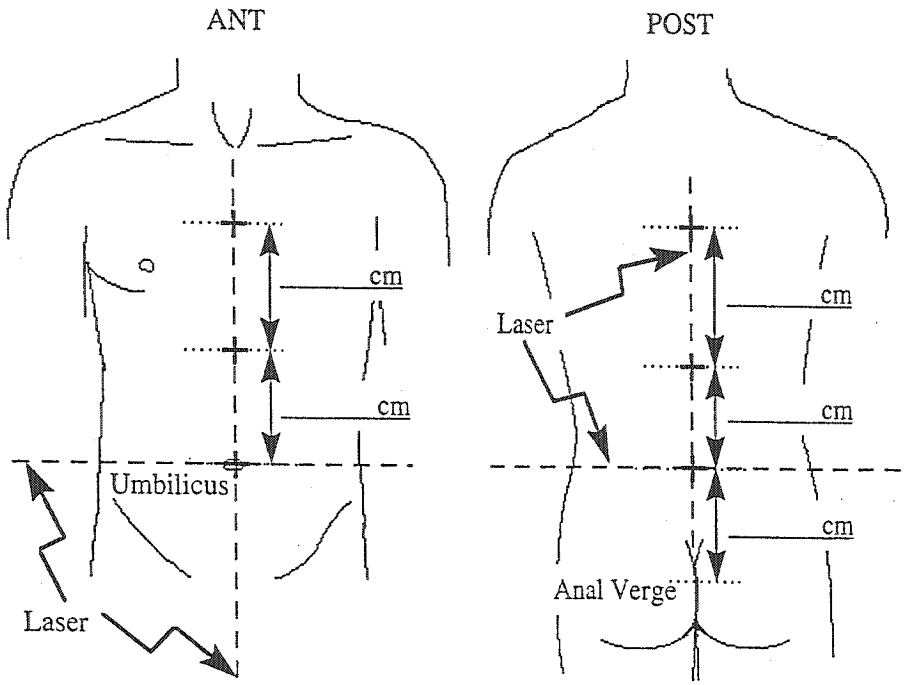


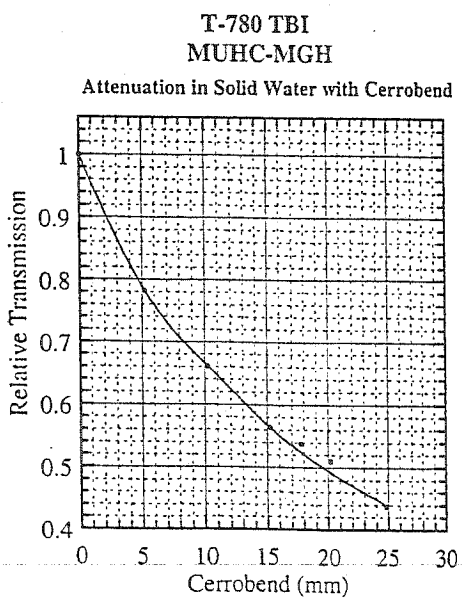


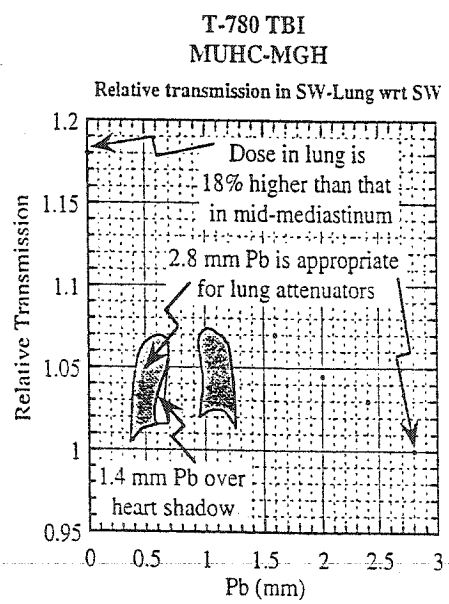


SO/ME/MO Jan 31/2002

# T-780

MUHC-MGH
McGill Medical Physics
Total Body Irradiation

Patient Name: _____

Patient Number: _____

Prescription Dose: _____cGy

| FR | Date | Position | Treatment Time (min) | Time Given (min) | Start Time | Stop Time | Dose (cGy) | Cumulative Dose (cGy) | Physicist |
|---|---|---|---|---|---|---|---|---|---|
| 1 | AM | POST | | | | | | | |
| | | ANT | | | | | | | |
| 2 | PM | POST | | | | | | | |
| | | ANT | | | | | | | |
| 3 | AM | POST | | | | | | | |
| | | ANT | | | | | | | |
| 4 | PM | POST | | | | | | | |
| | | ANT | | | | | | | |
| 5 | AM | POST | | | | | | | |
| | | ANT | | | | | | | |
| 6 | PM | POST | | | | | | | |
| | | ANT | | | | | | | |
| 7 | AM | POST | | | | | | | |
| | | ANT | | | | | | | |
| 8 | PM | POST | | | | | | | |
| | | ANT | | | | | | | |
| 9 | AM | POST | | | | | | | |
| | | ANT | | | | | | | |
| 10 | PM | POST | | | | | | | |
| | | ANT | | | | | | | |
| 11 | AM | POST | | | | | | | |
| | | ANT | | | | | | | |
| 12 | PM | POST | | | | | | | |
| | | ANT | | | | | | | |
| 13 | AM | POST | | | | | | | |
| | | ANT | | | | | | | |
| 14 | PM | POST | | | | | | | |
| | | ANT | | | | | | | |
| 15 | AM | POST | | | | | | | |
| | | ANT | | | | | | | |
| 16 | PM | POST | | | | | | | |
| | | ANT | | | | | | | |

SO/ME/MO Jan 31/2002

# List of Figures

## Chapter 1



## Chapter 2

## Chapter 3



## Chapter 4

## Chapter 5



## Chapter 6

## Chapter 7

# List of Tables

## Chapter 6



## Chapter 7

# Bibliography

"0.6 $cm^3$ Farmer-Type Ionization Chambers", PTW-Freiburg, Freiburg, Germany, 2000. .....(49)

E.G.A. Aird et al., *British Journal of Radiology Supplement 25: Central Axis Depth Dose Data for Use in Radiotherapy*, British Institute of Radiology, Volume 25, London, England, 1996 .....(23, 26, 70, 71, 93)

AECL, "Service Manual Theratron-780 Cobalt-60 Teletherapy Unit", 1st ed., Atomic Energy Canada Limited, Ottawa, ON, Canada, 1973 .....(32, 34)

P.R. Almond et al., "AAPM's TG-51 protocol for clinical reference dosimetry of high-energy photon and electron beams", Med. Phys., 26 (9), 1847-1870, 1999.

.....(26, 43, 47, 51, 57, 105)

F. H. Attix, *Introduction to Radiological Physics and Radiation Dosimetry*, John Wiley and Sons, John Wiley and Sons, Madison, WI, USA, 1986..... (16, 21)

"Attix Plane-Parallel Ionization Chamber: Model 449 – User's Guide", Gammex/RMI, Middleton, WI, USA, 1993..... (52)

A. Barrett, "Total Body Irradiation", Reports on practical Oncology and Radiotherapy, 4(3), 47-64, 1999..... (3)

M. Boutillon and A.M. Perroche-Roux, "Re-evaluation of the W value for electrons in dry air", Phys. Med. Biol., 32, 213-219, 1987..... (16, 43)

"Canadian Cancer Statistics 2001", National Cancer Institute of Canada, Toronto, ON, Canada, 2001..... (1)

M. Chrétien et al., "A variable speed translating couch technique for total body irradiation", Med. Phys., 27(5), 1127-1130, 2000..... (7)

R. Corns et al., "Designing attenuators for total-body irradiation using virtual simulation", Med. Dosim., **25** (1), 27-31, 2000 ..... (64)

J.R. Cunningham and D.J. Wright, "A Simple Facility for Whole-Body Irradiation", Radiology, **78**, 941-949, 1962 ..... (7)

D.R. Dance, "Diagnostic Radiology with X-rays" in *The Physics of Medical Imaging*, Institute of Physics Publishing, Philadelphia, PA, USA, 1988 ..... (57)

J.A. del Regato, "One hundred years of radiation oncology" in *Current Radiation Oncology*, Oxford University Press Inc., New York, NY, USA, 2000 ..... (3)

C. Dominique et al., "A modified $^{60}$C teletherapy unit for total body irradiation", Int. J. Radiat. Oncol. Biol. Phys., **33**(4), 951-957, 1995 ..... (10)

G.P. Glasgow, "Cobalt-60 teletherapy" in *The Modern Technology of Radiation Oncology: A compendium for Medical Physicists and Radiation Oncologists*, Medical Physics Publishing, Madison, WI, USA, 1999 ..... (29)

E.J. Hall, *Radiobiology for the Radiologist*, Medical Department Harper and Row, New York, NY, USA, 1973 ..... (2)

A.C. Heublein, "A preliminary report on continuous irradiation of the entire body", Radiology, **18**(6), 1051-1062, 1932 ..... (4)

A. Ho, S. Kishel, and G. Proulx, "Partial lung shield for TBI", Med. Dosim., **23**(4), 299-301, 1998 ..... (9)

S. Hussein and E. el-Khatib, "Total body irradiation with a sweeping $^{60}$Cobalt beam", Int. J. Radiat. Oncol. Biol. Phys., **33**(2), 493-497, 1995 ..... (8)

ICRU, "Measurement of absorbed dose in a phantom irradiated by a single beam of X of gamma rays", ICRU Report 23, International Commission on Radiation Units and Measurements, Bethesda, MD, USA, 1973 ..... (2)

ICRU, "Tissue Substitutes in Radiation Dosimetry and Measurements", ICRU Report 44, International Commission on Radiation Units and Measurements, Bethesda, MD, USA, 1989 ..... (58)

H.E. Johns and J. R. Cunningham, *The Physics of Radiology*, Charles C Thomas, 4th ed., Springfield, IL, USA, 1983 ..... (19, 28, 66, 81)

F.M. Khan, *The Physics of Radiation Therapy*, 2nd ed., Lippincott Williams and Wilkins, New York, New York, U.S.A., 1994 ..... (26, 53, 55, 57)

T.H. Kim, B.J. Gerbi and J.N. Lo, "Total body irradiation for bone marrow transplantation" in *Levitt and Tapley's Technological Basis of Radiation Therapy: Practical Clinical Applications*, Lea and Ferbiger, Philadelphia, PA, USA, 1992 ..... (2)

G.F. Knoll, *Radiation Detection and Measurement*, 3rd ed., John Wiley and Sons, Inc., Toronto, ON, Canada, 2000 ..... (42, 44)

"Kodak X-Omat V Film", Eastman Kodak Company, Rochester, NY, USA, 1994 ...(59)

K.S. Krane, *Introductory Nuclear Physics*, John Wiley and Sons, Toronto, ON, Canada, 1988 .....(44)

P.M. Leung et al., "Cobalt-60 therapy unit for large field irradiation". Int. J. Radiat. Oncol. Biol. Phys., 7(6), 705-712, 1981 ..... (10)

MDS Nordion, "Sources: Integrity in the Product, the Process, the Company" MDS Nordion, Kanata, ON, Canada, 2001 ..... (29)

R. Miralbell et al., "Can a total body irradiation technique be fast and reproducible?", Int. J. Radiat. Oncol. Biol. Phys., 29(5), 1167-1173, 1994 ..... (9)

L.J. Peters et al., "Radiobiological considerations in the use of total-body irradiation for bone-marrow transplantation", Radiology, 131, 243-247, 1979 ..... (6)

M. Pla, S.G. Chenery and E.B. Podgorsak, "Total body irradiation with a sweeping beam". Int. J. Radiat. Oncol. Biol. Phys., 9(1), 83-89, 1983 ..... (8, 97, 113)

E.B. Podgorsak and M. Podgorsak, "Special Techniques in Radiotherapy" in *The Modern Technology of Radiation Oncology: A compendium for Medical Physicists and Radiation Oncologists*, edited by J. Van Dyk, Medical Physics Publishing, Madison, WI, USA, pp. 641-662, 1999 ..... (2)

O.D. Sahler, "Development of a Room Specifically Designed for Total-Body Irradiation", Radiology, 72, 266-267, 1959 ..... (6)

H. Smith, "Evolution of the ICRP System of Protection" in *Radioprotection et droit nucleaire: Entre les contraintes économiques et écologiques, politiques et éthiques*, Georg Editeur, Geneva, Switzerland, 1998 ..... (4)

W.H. Tait, *Radiation Detection*, Butterworths, Toronto, ON, Canada, pp. 224-226, 1980. ..... (52, 53)

Task Group 29 of the Radiation Therapy Committee, American Association of Physicists in Medicine (AAPM), "The Physical Aspects of Total and Half Body Photon Irradiation", published for the American Association of Physicists in Medicine by the American Institute of Physics, New York, NY, USA, 1986 ..... (2)

E.D. Thomas et al., "Marrow transplantation for patients with acute lymphoblastic leukemia in remission", Blood, 54, 468-476, 1979 ..... (6)

E.D. Thomas, "Bone Marrow Transplantation — Past, Present and Future" in *Les Prix Nobel 1990*, Almqvist & Wiksell International, Stockholm, Sweden, 1991 ..... (3)

J. Van Dyk, P.M. Leung, and J.R. Cunningham, "Dosimetric considerations of very large cobalt-60 fields", Int. J. Radiat. Oncol. Biol. Phys., 6(6), 753-759, 1980 ..... (92)

E.W. Webster, "Physical Considerations in the Design of Facilities for the Uniform Whole-Body Irradiation of Man", Radiology, 75, 19-33, 1960 ..... (4, 5)

M. Wise and D. Markwick, "Operator's Manual for the Theratron 780-2 cobalt-60 teletherapy unit", Atomic Energy of Canada Limited: Commercial Products, Ottawa, ON, Canada, 1977 ..... (31, 34)

"WP 700 and WP 700s: Operating Instruction for IBM-AT compatible computers", Wellhofer Dosimetrie, Schwarzenbruck, Germany, 1994 ..... (50)